ON THE MODELING OF OROGRAPHIC RAIN USING THE SEEDER-FEEDER MECHANISM

by

Alain Robichaud

A thesis submitted to the Faculty of Graduate Studies and Research in partial fulfilment of the requirements for the degree of Master in Sciences.

Departement of Meteorology
McGill University
Montreal, Canada

September 1986

ISBN 0-315-38144-2

A ma meilleure amie

Itandéhui Sánchez

Abstract

The first two chapters of this thesis review the problem of orographic rain. They consist of a general survey containing several references to observational studies (using raingauges and radar observations) in different regions of the world.

A two-dimensional model of the seeder-feeder mechanism of orographic rain is then presented in the following chapters and comparisons are made both with other models found in the literature and available observations. The modeling approach is based on the principle of continuity for the water substance and on the 2-D theory of small adiabatic perturbation of airflow over topographical ridges of modest dimensions.

The model, which utilizes the formulation of the seeder-feeder mechanism, satisfactorily reproduces observed rainfall rate distribution due to topography. Such a model is also helpful in studying some aspects of the physics of orographic rain.

RESUME

Les deux premiers chapitres de cette thèse constituent une revue générale du problème de la pluie orographique. Plusieurs références relatives aux études d'observations (pluviométriques et par radar) dans différentes parties du globe y sont mentionnées.

Dans les chapitres suivants, un modèle bi-dimensionnel pour la pluie orographique utilisant le mécanisme "seeder-feeder" est présenté et comparé à d'autres modèles existant dans la littérature ainsi qu'aux observations disponibles. L'approche adoptée lors de la modélisation est basée sur les principes de continuité pour la substance aqueuse et sur la théorie linéaire des petites perturbations adiabatiques pour l'écoulement de l'air au dessus d'une crête orographique de dimension modeste.

Le modèle reproduit d'une façon satisfaisante l'augmentation de la précipitation causée par l'orographie. De plus, un tel modèle sert à l'étude de certains aspects concernant la physique de la pluie orographique.

ACKNOLEDGMENTS

I am thankful to Dr. G.L. Austin, my thesis supervisor and director of the McGill Radar, for his support and for his numerous encouragements and interest in the course of this investigation. Special acknowledgement is made to Dr. A. Bellon who has checked the final versions of the text.

Thanks are also due to the "Instituto Nacional de Meteorología" of Spain for their hospitality and help in providing the data necessary to one of the case studies.

TABLE OF CONTENTS

LIST OF FIGURES

LIST OF TABLES

CHAPTER I: INTRODUCTION

It has been recognized for a long time that precipitation usually increases with ground elevation. A huge amount of information throughout the world has been collected concerning the distribution of precipitation in mountainous area. The following statistical correlation is a first attempt to express the distribution of annual rainfall with respect to elevation:

$$R(Z_g) = R_o + AZ_g \qquad (1.1)$$

where $R(z_g)$ is the annual rainfall (mm/year) at ground level above a reference level z=0 (e.g. at sea level), Ro is the rainfall rate at the reference level and A , the coefficient which describes the rate of increase of annual precipitation with ground elevation. Finally, z_g expresses the height of the ground.

Table 1.1 shows specific examples for values of A and B, the latter being defined by the percentage increase of precipitation with ground elevation (e.g. $B = A/R_o$).

	A (mm/year/100m)	B (%/100m)
United kingdom		
Hill,Browning (1980)		
(South Wales)	325	30
Chuan and Lockwood (1974)		
(East Pennies)	200	40
(West Pennies)	190	25
Canada		
Storr,Ferguson (1972)		
(Marmot Creek,Rockies)	60	10
Sweeden		
Ryden (1972)	7	6
Bergeron (1960)	350	-

Table 1.1: Specific examples of values for A and B. (adapted from Smith,1979)

The linear relation (1.1), however, is of little use for the operational meteorologist trying to determine an enhancement factor of the rainfall rate for a rainband crossing a mountainous area as well as for the scientist trying to understand the causes of such enhancement. The reason is that there is a considerable scatter about the linear relation (1.1) and also because A and B are far from being fundamental constants and greatly vary from case to case as suggested in table 1.1. More precisely, since the distribution of orographic rain depends on many factors other than only the elevation such as the size and profile of topography, air mass characteristics, vertical profile of temperature, wind, humidity , etc., it becomes obvious that one cannot forecast the rainfall distribution by a simple relation as (1.1).

Moreover, relation (1.1) fails to describe the actual profile of rainfall rate most often observed; that is a maximum on the windward side near the crest of the mountain and a sharp decrease on the lee slopes (rainshadow effect) which is known to be important for medium and broad mountains. Finally, (1.1) is totally unable to account for the important exception that rainfall may increase up to a certain height and then decrease (especially true for the case of very high mountains).

The dependence of rainfall on topography on the climatological time scale is often a sum of single rainfall events where the maximum rainfall occurs near or slightly upwind of the steepest surface slope. At the divide, the rainfall is a fraction of the upslope maximum and the lee side is remarkably dry. Again, there are important exceptions to this picture and some are sumarized in Smith (1979) who further points out that the size of the mountain determines whether the orographic rain maximum will occur on the upwind slope or not. He suggests that for large mountains (mean width a > 100 km), the maximum will occur on the upwind slope with a rain shadow on the lee whereas for small mountains (a < 20 km), the maximum tends to be more nearly centered on the mountain.This seems to be supported independently by many workers in the field such as Sawyer (1956) who noted that the time taken for a strong airflow to cross a hill of small or even moderate dimension can be short compared with the time taken for precipitation growth. More recently, Gocho (1978) uses the above argument to explain that many drops of the orographic rain would consequently fall on the lee side of Suzuka mountains (in Japan) which helps explaining the lee rainfall maximum there (mountain half width is about 4 km).

Bergeron (1965) concludes that very small orographic features (height less than 60 m) significantly influences the rainfall distribution. He showed a close correlation between rainfall and elevation; for example, between two locations, one 60 m higher and 5 km apart, the rainfall enhancement is 50 %. Accordingly, a new mechanism must be proposed for explaining this type of results. The differential evaporation between the bottom of the hill and the top is not sufficient in explaining the phenomenon. Bergeron (1965) presents a conceptual model called the <u>seeder-feeder mechanism</u> which consists of natural seeding of raindrops through a feeder cloud (e.g. pannus cloud) generated by the condensation of the humidity contained in the upslope flow. This mechanism will be described in greater details later.

In general, terrain influences on the distribution of rain can be broken down into three mechanisms;

1) thermal effect of orography; that is triggering of convective showers by elevated heat sources and by organized mesoscale circulation (such as the mountain valley wind system)

2) frictional effects of orography;
different surfaces having different friction factor can produce a local boundary layer convergence which leads to enhanced rain at low levels and

3) forced upslope flow;
when a moist flow impinges a mountain at right angle, vertical motion is produced (typically of the order of 10-50 cm/s), condensation takes place and a rainfall enhancement occurs.

Although, the three effects can simultaneously occur, only the third mechanism is examined in this thesis and we will simply refer to it, in the future, as orographic rain. Therefore, since no attempt will be done here to simulate the first two phenomena, we shall restrict our study - along with any possible conclusions - to stratiform (steady-state) precipitation[a] and to situations where the flow is approximately perpendicular to the mountain.

[a]closely packed convective cells found in quasi-steady state monsoon situations are also included in this definition.

Moreover, no change of direction in the airflow will be assumed due to topography ignoring the fact that an actual incoming airstream while passing over a mountain will slow down, turn aside, flow completely around or pass over. Any of the above possibility would surely give different rainfall distribution but in cases of airflow crossing a range of very large extent in the perpendicular direction ,a useful approximation is to consider the flow lifted entirely over the mountain.

It is very important to explain quantitatively observed rainfall distribution in any mountain range. This represents a crucial operational requirement since orographic rain due to upslope flow contributes in many countries to a large proportion of the water supply. Browning (1980) reports that for the British Isles most of the orographic rain is not as intense as showers or thundershowers but by falling fairly steadily at rates of typically 2 to 8 mm/h for periods of many hours, daily accumulations can be very large.

In northern Spain, the same phenomenon occurs in connection with winter baroclinic system (Rivera,1986). Finally, Gocho (1978) mentions tremendous daily accumulations (over 200 mm) falling out from stratiform clouds associated with the flow set up by a distant approaching typhoon in Japan.

Not only the meteorologist is interested in predicting rainfall in mountainous area, but also the hydrologist must foretell possible floods which can occur from heavy rainfalls whose waters concentrate in nearby valleys.

Measuring orographic rain is a very difficult task. Because of the complex form of mountainous regions, local measure by raingauges can give a very different picture compared with the average rainfall measured in the neighborhood (if, for instance, the gauge happens to lie in a very deep isolated valley or at the top of a mountain peak). Another problem with gauges is that horizontal rainfall gradients tend to be large in connection with orographic rainfall such that a rainfall maxima or minima can easily lie between two raingauges.

On the other hand, the use of radars also presents difficulties in measuring orographic rain due to the important problem of ground echoes and hence the tendency of the radar beam to be above the shallow zone of rainfall enhancement[3].

The presence of strong vertical gradients of orographic rainfall intensity implies that at large ranges, the radar may significantly underestimate the surface rainfall intensity in hilly regions according to Browning (1980). He gives the example that, at 75 km, a narrow 1 degree beam would extend from 400 to 1600 m above the height of the radar, over which interval, the rainfall intensity may decrease by a factor of 2 giving an underestimation of the surface rainfall by 25 %.

[3] orographic rainfall enhancement usually takes place in the first one km or two (see chap. 2 and chap.5)

The major challenge of this research project will be to provide a simple numerical model which will evaluate the horizontal and vertical distribution of rainfall rate for an idealized (smoothed) topography. This model is required to be inexpensive to run, simple, and is also expected to contain the physics essential to the generation and distribution of rain. In fact, such model could be made operational and be a key part of a combined approach to the forecasting of orographic rain (see Browning,1980).

Another important aspect of the present study will be to investigate the effect of mountain size on the nature of orographic rain. In the case of small hills, for instance, it seems that the seeder-feeder mechanism plays a major role in causing a rainfall enhancement like suggested by Bergeron (1965) whereas when the size of the topography is sufficiently increased ,a new regime is set up where the above mechanism has less importance (see subsequent chapters).

Finally, the last objective of this thesis is to make clearer the mechanisms of orographic rain and the relative importance of the factors influencing orographic enhancement through the use of a numerical model.

CHAPTER 2: CAUSES, MECHANISMS AND DISTRIBUTION OF OROGRAPHIC RAIN

2.1 FACTORS DETERMINING OROGRAPHIC RAIN

If we consider only the forced upslope flow (the third category of terrain influences described in chapter 1) as being predominant, it is then possible to subdivide it further into three classes. That is;

a) orographically forced vertical motion (stable upglide)

b) increase of precipitation by washout of cloud droplets of low level clouds by the rain falling from upper larger scale clouds (seeder-feeder mechanism)

c) triggering of orographic precipitation due to lifting of potentially unstable layers.

These three independent mechanisms of orographic rain are now examined in greater details here;

a) Orographically forced vertical motion:

We will derive a simple expression for the rate of condensation (COND) of a flow lifted by orography to illustrate the most important factors involved in the increase of rain due to topography. This simple relation can be written as;

$$\text{COND} = -\frac{D}{Dt}\left(\rho_o r_s\right) \tag{2.1}$$

where ρ_o is the density of the air and r_s, the saturated water vapor mixing ratio. Relation (2.1) expresses the rate at which the saturated water vapor density, $\rho_{vs} = \rho_o r_s$, decreases following the motion over topography.

The condensation rate COND (in kg/m³ · sec) can be further expressed as (see chapter 3);

$$\text{COND} = -\frac{D}{Dt}\left(\rho_o r_s\right) = -\frac{d}{dz}\left(\rho_o r_s\right)\frac{dz}{dt}$$

$$= \left(\rho_o^2 g \left.\frac{\partial r_s}{\partial p}\right|_{sat} - r_s \frac{\partial \rho_o}{\partial z} \right) w \tag{2.2}$$

where w in (2.2) is the vertical velocity. The condensation rate is thus proportional to the vertical velocity and to a term which includes the decrease with altitude of the saturated water vapor mixing ratio (following a moist adiabatic curve) and another term which is due to the decrease of density with z. Let us consider w, one of the main factor of equation (2.2); we can see that the condensation rate is proportional to the forced vertical velocity w which is due to upslope flow. In first approximation, w can be taken as order of magnitude of $w = U \cdot \nabla h$ where U is the average low level wind velocity perpendicular to the mountain range and ∇h, the gradient of topography. It is then clear that strong value of the wind at low levels combined with a steep slope of the topography will tend to give a strong rainfall enhancement. For a given topography, the strength of the low level wind plays a major role. As a matter fact, the dependence of the mean low level wind speed on the orographic enhancement (P - Po) has been found by Hill and Browning (1980) to be quite sensitive and of the form;

$$P - Po = 6.5 \times 10^{-4} \cdot U^{2.8} \qquad (2.3)$$

where P is the precipitation rate (mm/h) at the top of South Wales hills (England) , Po, the radar derived rainfall rate at the coast and U , the 600 m wind speed oriented at right angles of the hills (in m/s).The above relation expresses,of course, indirectlty a strong relation between the vertical motion and the condensation rate.

One of the problem of orographic rain is to determine not only the vertical motion (from the the wind speed) but also its vertical profile which is essential in computing the total water condensed. A first approach to the problem is to assume the vertical motion zero at some height ,z_N ,so-called the " nodal surface " (fig 2.1). Near the ground (say at 10 m above it),the value of w is simply $U \cdot \nabla h$ which is obtained by applying the no-slip condition (e.g. the airflow follows the topography near the ground).

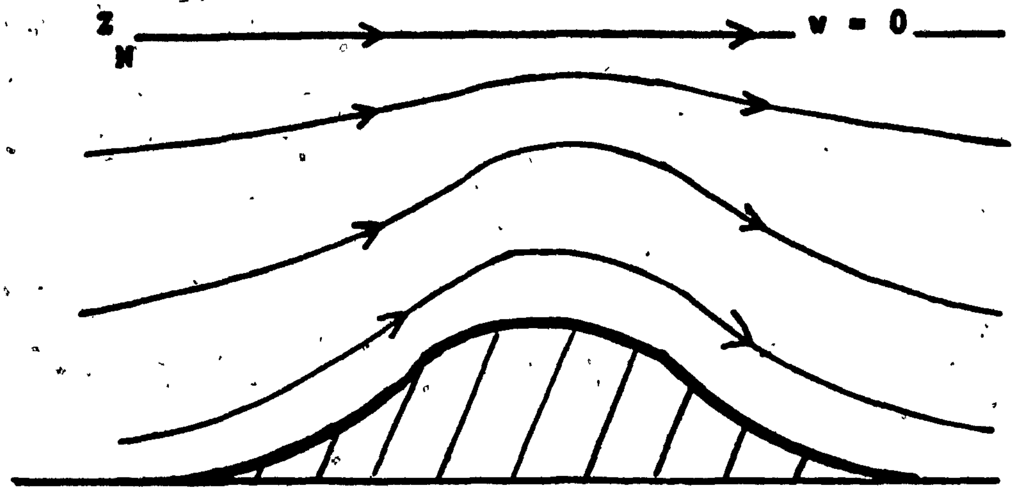

Fig. 2.1 A simple representation of airflow over topography.

Therefore, fig.2.1 implies a linear decrease of w in the vertical which is typical in the troposphere. Myers (1962) argued that such a vertical profile can be derived from hydraulics principles. But according to Smith (1979,p 186) the arguments are not applicable to the continuously stratified atmosphere and such an airflow pattern would probably not occur. Moreover, it is not known whether the use of such a model would introduce appreciable error in the computation of total condensation. Nevertheless, it provides with a first approximation to modelize the airflow which passes smoothly and stably over the topography and it is given here for completeness.

A more general theory will be presented, however, in chapter 4 (two dimensional theory of airflow over mountains) which provides a more theorical answer for the vertical as well as the horizontal variation of w. It then turns out, as we will see, that the vertical profile depends not only on topography and wind speed and direction but as well as on the vertical structure of temperature and wind. This aspect is discussed by Scorer (1949) and by Sawyer (1956).

The possibility of the blocking of the flow over the topography is not considered here. Several other phenomena are possible in connection with the airflow over topography (e.g. funneling, drainage, forced convergence etc.). However, in evaluating the vertical velocity ,w, we have to ignore many local effects and keep only those which are the most appropriate to a specific situation.This is necessary since no complete theory seems to exist which is capable to take into account how rainfall is modified by the airflow over mountains.

So far, we have examined only the effect of w. In the following we will look at the first factor in the bracket in equation 2.2; the rate of decrease of the saturated water vapor mixing ratio with altitude; drs/dp) sat.

For a non-saturated flow, lower is the relative humidity, more orographic lifting distance it takes to reach saturation and hence give a non-zero value to the condensation rate COND. Therefore, it clearly appears that the relative low level humidity is an important factor in orographic rainfall enhancement. This is, in fact, strongly supported by observations; Bergeron (1965) reports that in situations of strong orographic enhancement, the low level air is almost saturated.Furthermore, Douglas and Glasspoole (1947) point out the importance of strong moist low level flow for producing heavy orographic rain in Western Britain. The same point applies to the Western Ghats mountains in India during the monsoon (Sarker,1966).

On the other hand, Holgate (1973) found that heavy orographic rain is associated not only with high relative humidity at low levels but also with a moist layer of considerable depth. However, Browning et al. (1975), have observed heavy orographic rain with a dry capping layer at 3 km. Similarly, Woodcock (1975) reports moderate orographic rain with the top of the moist layer as low as 2.1 km in Hawaii.

Once the airflow has been saturated by orographic lifting , the condensation starts and COND in equation (2.2) becomes proportional to drs/dp (sat). As the temperature T increases, $dr_s/dp)_{sat.}$ increases as well. Saturated air mass having high temperature will then give a high condensation rate in equation 2.2 and vice versa. This is clearly illustrated if we look at a tephigram; $drs/dp)_{sat.}$ is stronger for a high temperature than for a low one. If we represent the characteristic airmass temperature by θ_w, the wet bulb potential temperature, then the orographic enhancement should increase as θ_w increases. The second term in the bracket of equation 2.2 represents the effect of compressibility. The importance of neglecting or not this term will be assess in chapter 5.

b) <u>increase of precipitation by washout of the orographic cloud droplets (seeder-feeder mechanism).</u>

From radar observations, Hill et al.(1981) concludes that the effect of hills of low or moderate dimensions is to intensify existing rain areas rather than to produce major new areas of rain.

For small hills, using a very dense gauge network, Bergeron (1965) points out that unexpectedly small orographic features (hills a few tens of meters high) can produce an orographic enhancement of 50 %. Since observations were done in autumn at latitude 60° N (Uppsala region, Sweeden), local convection is rather weak and the observed excess is truly orographic. According to Bergeron, the theory of mountain waves alone cannot explain the close relation between the topography and the rainfall distribution in the case of very small orographic obstacles. Moreover, he suggests that the main "modeling" of the rainfall distribution must occur within the lowest air layer of 0.5 to 1 km depth. This seems in agreement with Browning's observations and consistent with Holgate (1973) who found that orographic enhancement occurs at low levels.

In order to explain the regular occurence of these rainfall anomalies , the vertical distribution of the rainfall rate associated and the local character of the precipitation increase, Bergeron (1965) postulates the mechanism of seeder-feeder. It consists basically of a so-called feeder cloud which is produced by forced uplift of moist low-level air over topography and a so-called seeder cloud which is supposed to exist independently of the hills and having the function of washing out (or scavenging) the cloud droplets of the feeder cloud (fig 2.2).

The background rainfall rate Po, hence defined is the mean rainfall rate falling from the pre-existing seeder cloud and dependent of the larger scale ascent (i.e not related to topography).

It seems,a priori, that a high background rainfall rate will be more efficient in increasing the rainfall rate. This hypothesis is verified in chapter 5.

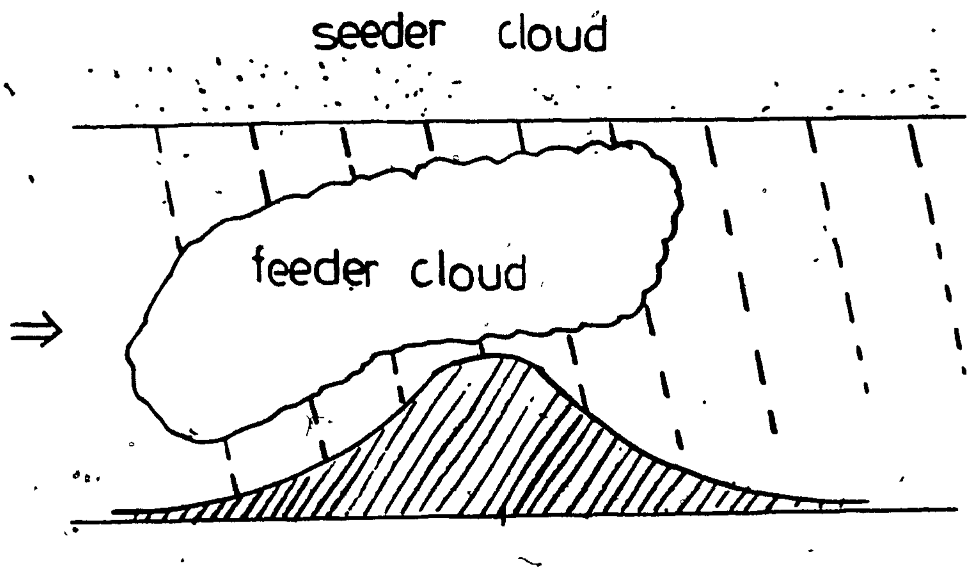

Fig 2.2. The seeder-feeder mechanism. The upper releaser or seeder cloud formed by large scale ascent of moist air is supposed independent of small scale topography. The low-level feeder or spender cloud formed by local topographical features is scanvenged by precipitation elements from the releaser cloud.

Browning (1980) gives some arguments, following Sawyer (1956), that orographic rain is not simply the result of cloud particles growing from " nothing " and that the pre-existing rain could play a major role. He claims that the time required for precipitation growth is rather comparable and even greater than the time taken for a strong airflow to cross a hill of moderate dimension. In other words, no orographic enhancement will take place if there is no seeding from above. To fix ideas, let us review a typical example; for a hill having a mean width of 30 km, the time taken for an airflow to cross the hill is approximately 1500 sec (assuming cloud droplets follow the mean air motion, that is about 20 m/s). A typical time scale often given for precipitation growth is 20 minutes or 1200 sec and even less under special circumstances. Based on observations on the island of Oahu, Hawaii, Woodcock (1975), for example, estimates that rain can form within and fall continuously from a shallow layer of warm low level cloud in about 5-13 minutes. Therefore, this suggests that precipitation can have time to form in orographic lifting and is not really starting from " scratch " like mentioned above. For small hills, however, Browning's argument is quite appropriate. On the other hand, it is thought that the time required for precipitation to form may be variable from case to case and it is rather suggested to use the cloud liquid water content of the feeder cloud as a threshold to decide if rain can form independently of the seeder-feeder mechanism in the orographic cloud.

Nevertheless, the above concept is useful in that it may be generalized through a non-dimensional number; $T_s \bar{U}/a$, where T_s is a typical time scale for precipitation growth, $\bar{U}$, the mean wind speed in the lower troposphere and a, the mean mountain width. If this non-dimensional number is greater than 1, then we should expect no rain formation in the feeder cloud and orographic enhancement determined to a great extent by the seeder-feeder mechanism. Conversely, if it is less than one, the seeder-feeder mechanism does not play the major role in orographic enhancement.

This important point will be further discussed in subsequent chapters.

The concept of time available for growth, on the other hand, seems related to the efficiency of release of precipitation. Elliot and Hovind (1964) in a study over mountains of California concluded that the efficiency (e.g. observed rainfall/computed condensed water) tends to increase with mountain size. This is consistent with the fact that for large mountains, droplets embedded in a strong flow have plenty of time to grow before reaching the lee side where evaporation is expected to take place whereas for very narrow mountains,the time available for growth is not sufficient and consequently precipitation efficiency is very low in absence of any seeder rain. Also, Elliot and Hovind found a slight increase in efficiency for unstable flow which can be explained by an improved release mechanism due to the generation of convective cells.

Myers (1962) computed an efficiency of 70 % for the large Sierra Nevada (130 km wide). However, efficiency of precipitation does not only depend on the mountain width or the presence of convection but also is closely link to the assumed field of lifting and on the microphysical processes leading to the formation of hydrometeors (Smith ,1979 p 77). It appears that when conditions are favorable for heavy orographic rain, the efficiency is nearly 100 % (Sawyer,1956).But the efficiency can be very small as point out by Browning et al. (1975) who found values of 10 % and 30 % respectively for 2 cases where the airmass was unsaturated and therefore air requiring some finite ascent before condensation begins. This suggests that a decreased moisture content can lead to a decrease efficiency.

Young (1974) in a numerical simulation of wintertime orographic precipitation computed an incredibly low value for efficiency (0.04 %) for the Front Range mountains of Colorado. This is believed to be a very abnormal case and some atempts to explain this anomaly is given by Smith (1979, p 177) who concludes with the following;

> " Possibly , by considering narrower mountains such as the front range we have stepped into a new regime where the time for hydrometeor formation and fallout is the same or longer than the time for the air to pass over the mountain....The narrower mountains can cause precipitation only by introduction of seeding, either natural or artificial. "

He further adds that high values for efficiency obtained by Sawyer and Myers are questionable and proposed that the vertical motion used in these works might underestimate the real vertical displacement. Moreover, he suggests the possibility that orographic lifting might trigger deep convection. Both effects would increase considerably the computed condensed water and accordingly reduce the efficiency.

In any case , it appears that a wide range of precipitation efficiency has been obtained from independent workers for more or less the similar mountain ranges which probably reflect the fact that precipitation mechanisms are quite complicated especially when we deal with orographic precipitation. Nevertheless, for the special case of warm stratiform rain, the efficiency of precipitation is expected to be large (see Wexler and Atlas,1958).

In summary, enhancement of orographic rainfall depends on formation of precipitation due to forced upward motion over topography (process which creates condensation) and also on the seeder-feeder mechanism. The importance of the former with respect to the latter is linked to the concept of efficiency (and also to mountain width) and will be again discussed in the next chapters.

Another factor can be important in enhancing precipitation; release of potential instability which is discussed below.

c) Triggering of orographic precipitation due to release of potential instability:

Browning (1980) points out that situations responsible for most large falls of orographic rain in Britain are not normally associated with deep convection. In many of these cases, the lower troposphere were rather highly stable. On the other hand, in a study of the water balance of orographic clouds, Elliot and Hovind (1964) did not find significantly higher precipitation efficiency with convection (from case studies for a numerous amount of winter storms during a four year period in California). This seems consistent with the case of a relatively drier layer lying above a low level moist layer where mixing of moist convection columns with the drier air above can reduce the efficiency of precipitation.

However, potential instability aloft is often detected in connection with orographic rainfall enhancement in warm sectors (Browning et al. 1975) but what is not clear is whether the convection aloft is a major cause in enhancing orographic precipitation. Most of the orographic rain, Browning adds, is generated in the low-level cloud and if convection aloft plays a role it would be as a result of more effective seeding of the low level feeder cloud. Such a possibility, nevertheless, seems to lack observational support according to Gocho (1978) who did not encounter such phenomenon during very heavy orographic rainfall in Japan. In any cases, a controversy seems to exist concerning stable versus unstable upslope rain and is described in greater detail by Smith (1979, p178-183).

Spinnångr and Johansen (1955) and in a similar way, Douglas and Glasspoole (1947) and Sawyer (1956), show that observed intense rainfall in the Western Europe coast can be explained by stable uplift if 100 % efficiency of precipitation is assumed. But one can ask oneself if it is possible to convert such a high fraction of the condensed water into precipitation. If not, then the empirical vertical velocity profile (such as the one in fig 2.1) must be in error or orographic lifting triggers deep convection.

We will try in this thesis to clarify the above point by using the mountain wave theory to derive a better 2-D field of vertical velocity (see chap 4). Concerning the role of potential instability, we will assume that it does not play a major role in orographic rain.

2.2 VERTICAL AND HORIZONTAL DISTRIBUTION OF OROGRAPHIC RAIN

On a climatological time scale, we have seen that surface precipitation increases with elevation for a given topography (table 1.1). From case to case, this pattern is also reproduced in many occasions in connection with frontal systems impinging the coast of Western Europe. Fig 2.3 shows the horizontal distribution across Snowdonia in a warm sector (west southwesterly flow at low levels); the rainfall maximum lies very sligthly upwind of the crest with a general increase of precipitation from the coast up to the top and a decrease on the lee side. Radar observations over South Wales hills in Britain associated with baroclinic systems also shows a general tendency of orographic enhancement on windward slopes (Hill and Browning,1980). Figure 2.4 reproduces results from an unpublished paper by Nash and Browning (1977) which illustrates 24 h rainfall distribution along the orography. Notice that the peak of the distribution is slightly localized on the lee of such hills. The small width of these particular hills is certainly a factor explaining the displacement of the peak. Gocho (1978) presents evidence of a strong maximum in the lee of Suzuka mountains (half width is 4 km) in situations of strong southeasterly flow (perpendicular to the range) associated with distant moving typhoon.

To examine, on the other hand, the vertical structure of orographic rain, we need to look at radar data. Yet, Bergeron (1965) had argued that from the close link between the rainfall maxima and the terrain height, one can deduce a very low level origin of orographic rain (in the first 1500 m). For higher hills, however, such as South Wales, the layer of orographic enhancement is deeper (may be about 2.5 km) but still confined to the very lower troposphere as it can be observed from fig 2.5.

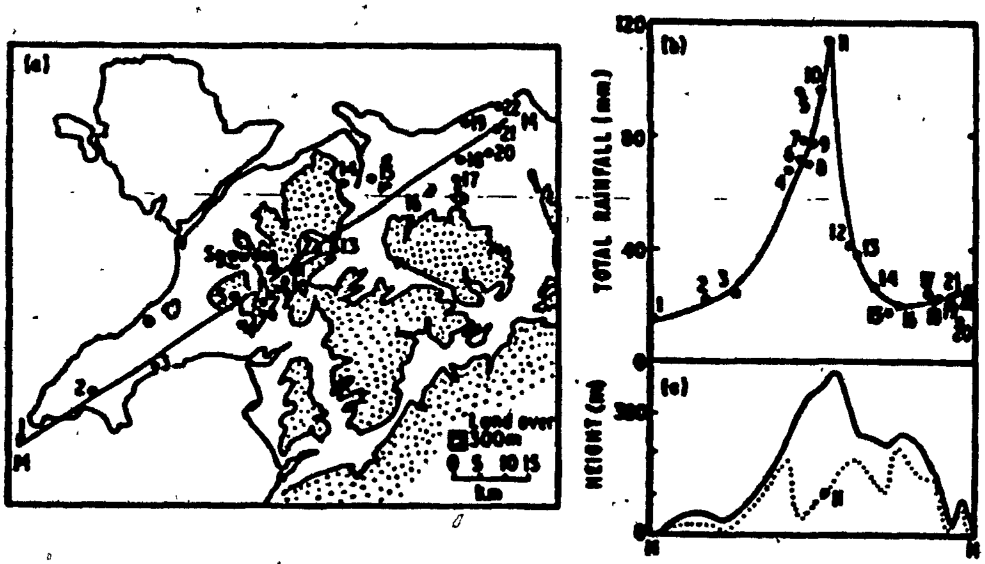

Fig.2.3. a) Map showing the topography of Snowdonia and the locations of 22 raingauges whose data are plotted in b.
b) distribution of rainfall (in mm) along the line MM in a) which is mainly in the period 1530 GMT of June 26 up to 1220 GMT, June 27 1966.
c) altitude of the raingauge sites. The height of gauges is indicated by the dotted curve. The full curve is a profile obtained by taking the average height within 3 km of each raingauge site (after Pedgeley, 1970).

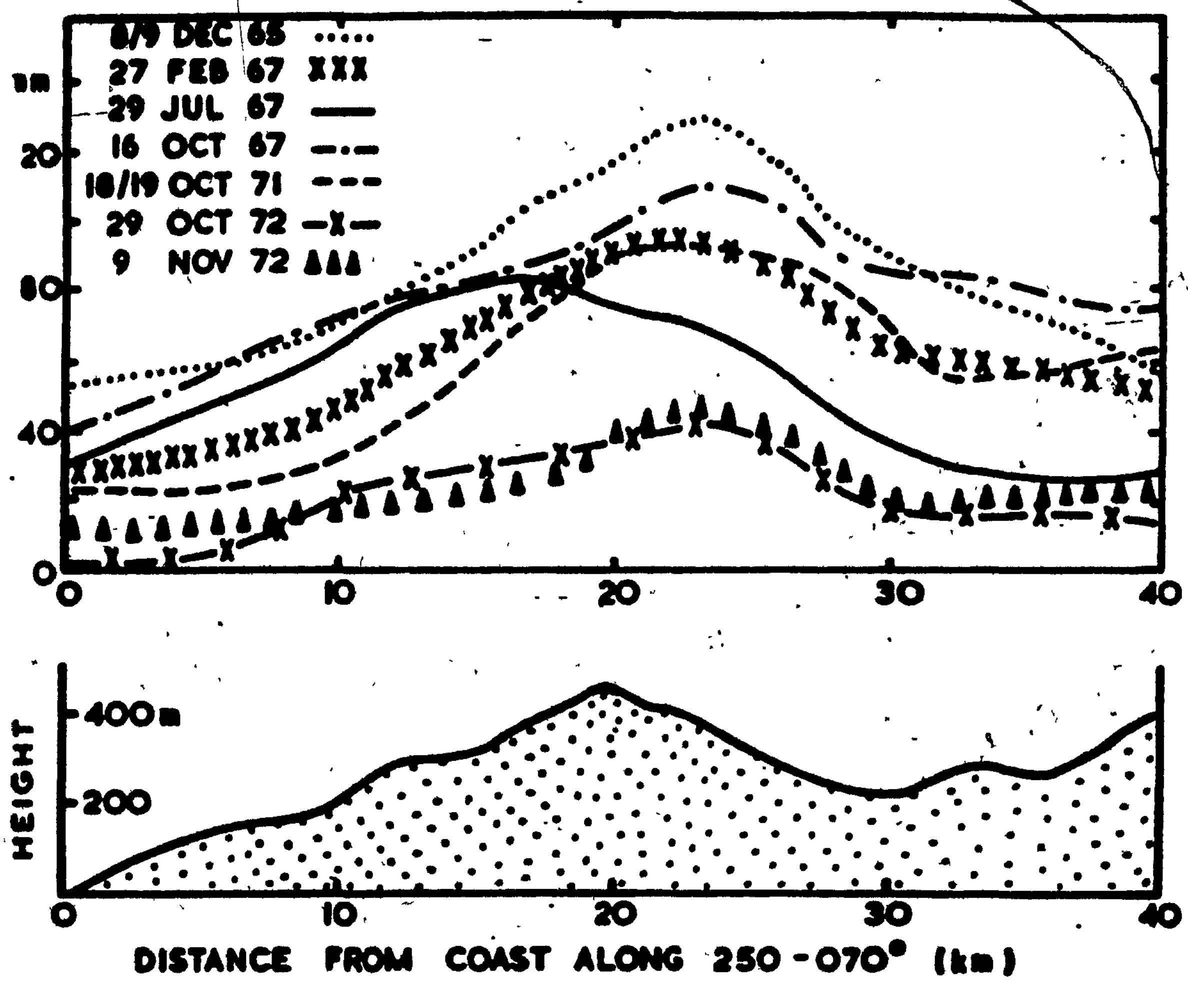

Fig.2.4 a) Distribution of 24h rainfall within sections 10 km wide across the hills in South Wales for 7 cases of prolonged orographic rainfall. In each case, the winds were persistently from about 250 degrees and a profile of the hill along this direction is shown in b). (After Nash and Browning, 1977).

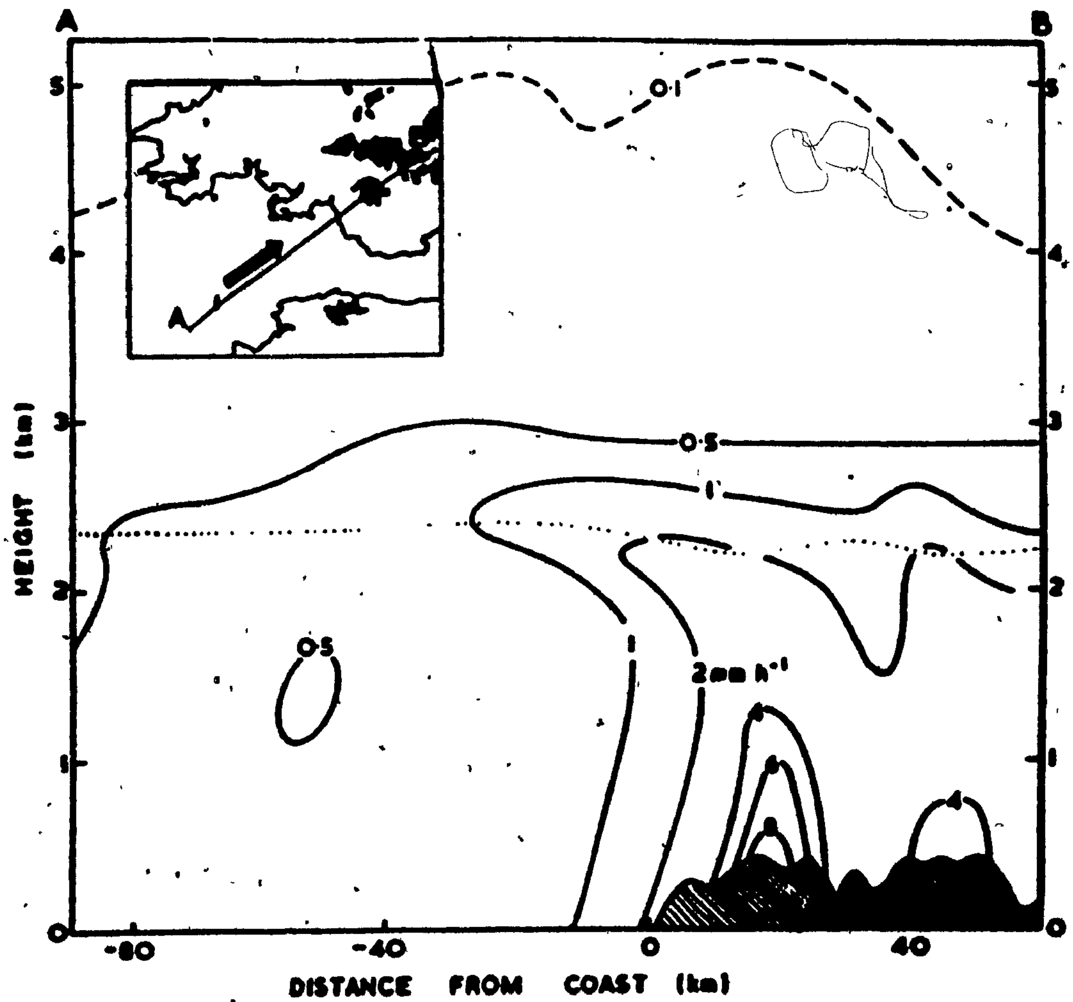

Fig.2.5 . Vertical structure of time-integrated rainfall pattern over Glamorgan Hills (England). The mean flow is perpendicular to the range. (After Hill and Browning, 1980).

2.3 SYNOPTIC ASPECTS OF OROGRAPHIC RAIN

From synoptic studies of Douglas and Glasspoole (1947) and Sawyer(1956) in the Bristish Isles, we can list features of the synoptic situation which are associated with large orographic rainfall;

1) a strong low level flow perpendicular to an extensive topographical ridge
2) an almost saturated airmass having an extensive depth
3) a lapse-rate without markedly stable layers or inversions (preferably near neutral stability)
4) a vertical wind-profile with $\partial^2U/\partial z^2$ negative,which is often found associated with a low level jetstream (LLJ).
5) an existing upper cloud layer with the function of seeding the low level cloud

Conditions 1,2 and 5 have already been discussed in some details earlier. Condition 3 and 4 are less obvious but often found in connection with large rainfalls (according to the above authors). The relative importance of each of theses conditions is not clear at this time and will need further investigations (see subsequent chapters).

As mentioned earlier, it seems that the strongest rainfall enhancement are found in warm sectors of depressions, in Europe, or more precisely from zero up to several hundred kilometers ahead of the frontal trough and about the same distance south of the low pressure center. Farther south, orographic rainfall diminishes because the depth of the moist layer decreases and an inversion or very stable layers above appears.

In fact, Browning et al. (1975) observed orographic effects large only in the pre-cold frontal region, and that in the post-frontal region, the enhancement of rainfall - if any - is not spectacular compared to that in the warm sector. At the surface cold front itself, there is even less systematic orographic influence and heavy rain tends to occur regardless of topography fig 2.6.

Despite the small number of case studies presented by Browning, it is thought that it repre sents a typical situation in autumn or winter along coastal mountain of Western Europe. In a case study of the orographic rainfall in the Glamorgan Hills, Hill and Browning (1980) point out that 75 % of total rainfall on hills are associated with low-level winds from the southwest quadrant ahead of fronts and troughs. Surprisingly enough, orographic enhancement ends with the cold frontal passage. The last statement does not agree, however, with Hobbs et al. (1975) who examined the structure of an occluded frontal system modified by orography (for Cascade Range in North West US).By using aircraft measurements, many soundings and a network of automatic rain gauges they were able to show a definite influence of the mountain on the front and strong orographic enhancement at the cold front rather than ahead as in Browning et al. (1975). The apparent discrepancy seems rather hard to explain. Nevertheless ,the concept of fronts as definite lines indicating a sudden changes of both the circulation and air mass characteristics occuring at the same time might be too simplistic to be applicable to actual situations especially in the case of mountainous areas.In other words, locating the exact position of a cold front might be a difficult task in mountains.

As far as the post-frontal area is concerned, an explanation could lie in the magnitude of the vertical velocity involved; in the case of England, lower hills generate a pattern of vertical velocity more easily offset by post frontal subsidence compared to the case of higher and steeper Cascade mountains.

On the other hand, Williams and Pick (1962), in a climatological study of the precipitation in the Wasatch Mountain area of nortwestern Utah, during the winter season, show that the type of storm (cold low versus non cold low storm) is of considerable importance in determining the areal distribution of orographic precipitation. In fact, their data show a noticeable higher orographic enhancement for non-cold low storm.

The explanation lies in the fact that cold lows formation over the western North American plateau are usually the result of strong baroclinic situations with pronounced deepening of upper trough as it moves in. Accordingly, strong large-scale upward vertical motion are created which can be comparable or greater than the orographic vertical motion - which is the order of magnitude of $U \cdot \Delta h$ - reducing the influence of topography on the distribution of precipitation.

Orographic enhancement of rain can occur in many other situations than those described above. For example, monsoon rain in the western Ghats in India is thought to be a case of " pure " orographic rain (Sarker,1966) with convection triggered by topography apparently not playing an important role (see chapter 6).

On the other hand, looking at climatological data of many countries, it seems that orographic enhancement of convective rain is less, in general, than stratiform rain. The reason is likely to be related to the fact that updrafts in deep convective clouds are one or even two order of magnitude more than the vertical motion generated by topography (usually of the order of magnitude 10-50 cm/s) implying a possibility of reduced sensitivity to terrain influences in cases of convective upslope flows.

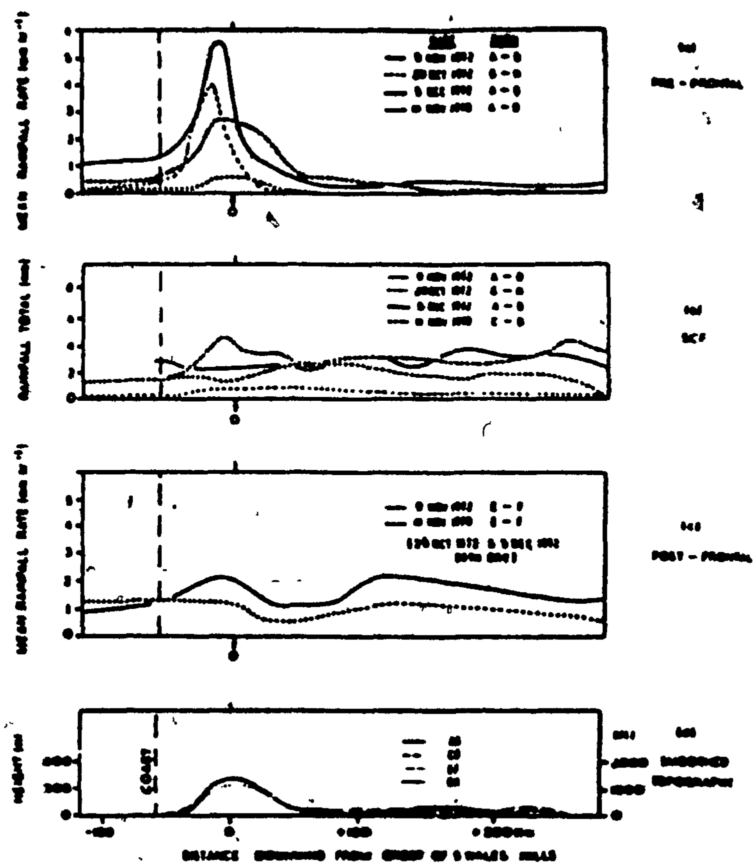

Fig 2.6 Diagrams showing, for 4 case studies, the distribution of rainfall from the Bristol Channel across the South Wales hills to eastern England, along paths 40 km wide whose topography are given in d). The distribution of average rainfall rate ahead of the front (in a), at the surface cold front (b) and behind the cold front (c) are compared (from Browning et al.,1975).

CHAPTER 3: Modeling warm orographic cloud and precipitation rate.

In the first two chapters a general survey of orographic rain was given. In this chapter, we will briefly review some orographic models existing in the literature (section 3.1) and above all to present an alternate way to modelize orographic rain (section 3.2). The objective is to produce a diagnostic model (i.e model with no time dependency) at resolution low enough to predict large rainfall variation over small distances (several kilometers in the horizontal and several hundred meters in the vertical). It is also expected that the model be numerically simple and to contain the essential physics required to explain the vertical and horizontal distribution of orographic rain.

The purpose of such model will be to study the importance and the sensitivity of input parameters on the amount of orographic enhancement for a given topography.These parameters are the large scale variables such as the vertical structure of wind,temperature and humidity profiles and background rainfall rate. A particular attention will be given to the role of the seeder-feeder mechanism in enhancing orographic rainfall rate. Numerical experiments performed on the model ,as we will see, can provide operational forecasters with a better feeling of the physics important in orographic rain. It is also thought that the model is suitable for calculation of efficiency of precipitation of an orographic cloud.

3.1 A review on the modeling of precipitation rate.

We will first introduce the subject of modelization by considering a simple approach which uses the hypothesis that all the condensed material precipitates. To derive an expression for the rainfall rate let us start with the continuity equation for the rainwater substance which can be written;

$$\frac{\partial \rho_R}{\partial t} + \vec{\nabla}_{3D} \cdot (\rho_R \vec{u}) - \frac{\partial}{\partial z}(\rho_R \cdot \vec{V}) = S_R \qquad (3.1)$$

where ρ_R is the rainwater density; $\rho_R = \rho_o Q_R$ with ρ_o the air density and Q_R the rainwater mixing ratio in g of water per g of air. Also $\vec{u}$ and $\vec{V}$ represent the horizontal windspeed vector and the water droplets terminal fall speed respectively. Finally, $\vec{\nabla}_{3D}$ represents the three dimensional gradient operator. On the right hand side of equation 3.1, S_R stands for sources minus sinks for the rainwater substance.

If we consider steady-state and only two dimensions, x and z, (i.e assuming a topographical ridge having an infinite extent in the y direction) then 3.1 becomes

$$\frac{\partial}{\partial x}(\rho_R u) + \frac{\partial}{\partial z}(\rho_R w) - \frac{\partial}{\partial z}(\rho_R \overline{V}) = S_R . \qquad (3.2)$$

Neglecting horizontal variations of the air density ρ_o, and that of the large scale flow, u, combining the second and third term in 3.2 and using $\rho_R = \rho_o Q_R$ gives

$$\rho_o u \frac{\partial Q_R}{\partial x} - \frac{\partial}{\partial z}\left[\rho_o (\overline{V} - w) Q_R\right] = S_R . \qquad (3.3)$$

Finally, using the definition of the rainfall rate,

$$R = \rho_o (\overline{V} - w) Q_R \tag{3.4}$$

and integrating with respect to z and neglecting the first term on the left hand side (which represents the horizontal advection of rainwater mixing ratio) yields the important result:

$$R(x,z) = R(z_\tau) + \int_z^{z_\tau} S_R \, dz \tag{3.5}$$

In eq. 3.5, $R(z_\tau)$ is the rainfall rate at the top of a layer of ~~thickness Δz~~ $= z_\tau - z$. Equation (3.5) can be used to evaluate the horizontal and vertical distribution of the rainfall rate due to the topography.

If we assume stratiform precipitation (or more generally steady-state precipitation), the portion of condensed water vapour converted into rainwater is very high and cloud storage does not need to be considered in quantitative calculations of precipitation rates (according to Wexler and Atlas, 1958 and Kessler, 1969). This means that S_R in eq. 3.5 is simply the rate of condensation of water vapor following the motion which has already been given by equation 2.1;

$$S_R = \text{COND} = - \frac{d}{dt} \left| \rho_o r_s \right| \tag{3.6a}$$

$$= -\rho_o \frac{dr_s}{dt} - r_s \frac{d\rho_o}{dt} \tag{3.6b}$$

Eq. 3.6b represents the variation of water vapor density following the air motion. Equation 3.6b can be further expanded, by using the definition of the saturated water vapor mixing ratio

($r_s = 0.622\, e_s/p$) and by differentiating its natural logarithm. The result is;

$$\frac{dr_s}{r_s} = \frac{de_s}{e_s} - \frac{dp}{p} , \qquad (3.7)$$

Using the Clausius Clapeyron equation

$$\frac{de_s}{e_s} = L \frac{dT}{R_v T^2}$$ into (3.7) yields after dividing by dt

$$\frac{dr_s}{dt} = \left| \frac{L}{R_v T^2}\frac{dT}{dt} - \frac{1}{p}\frac{dp}{dt} \right| r_s . \qquad (3.8)$$

On the other hand, assuming that condensation takes place as a result of saturated adiabatic expansion and that the condensate precipitates, the thermodynamic equation can be written as

$$- L \frac{dr_s}{dt} = C_p \frac{dT}{dt} - \frac{RT}{p}\frac{dp}{dt} . \qquad (3.9)$$

Eliminating dT/dt from equations 3.8 and 3.9 and using $\epsilon = R/R_v$ and $\omega = dp/dt$ gives, after rearranging

$$\frac{dr_s}{dt} = r_s \frac{RT}{p} \left| \frac{\epsilon L - C_p T}{\epsilon L^2 r_s + R C_p T^2} \right| \omega . \qquad (3.10)$$

It should be note that dr_s/dt and $d\rho_*/dt$ can also be expanded as

$$\frac{dr_s}{dt} = \frac{\partial r_s}{\partial t} + u\frac{\partial r_s}{\partial x} + v\frac{\partial r_s}{\partial y} + w\frac{\partial r_s}{\partial z} \Big|_{sat} \qquad (3.11a)$$

and $$\frac{d\rho}{dt} = \frac{\partial \rho}{\partial t} + u\frac{\partial \rho}{\partial x} + v\frac{\partial \rho}{\partial y} + w\frac{\partial \rho}{\partial z}. \qquad (3.11b)$$

Since steady-state is assumed and horizontal variation of all quantities are neglected compared to vertical variations, that is $\partial/\partial t = \partial/\partial x = \partial/\partial y = 0$, then we can write (using $\omega = -\rho_o g w$ and the hydrostatic equation)

$$\frac{dr_s}{dt} = w \left.\frac{\partial r_s}{\partial z}\right|_{sat} = \omega \left.\frac{\partial r_s}{\partial p}\right|_{sat} \tag{3.12 a}$$

Also we have

$$\frac{d\rho_o}{dt} = w \frac{\partial \rho_o}{\partial z} \tag{3.12 b}$$

Comparing 3.12 a with 3.10 gives

$$\left.\frac{\partial r_s}{\partial p}\right|_{sat} = \frac{r_s RT(\epsilon L - C_p T)}{p\,(\epsilon L^2 r_s + RC_p T^2)} \tag{3.13}$$

The ground rainfall rate is obtained by setting $z=0$ in equation 3.5 and using 3.6b, 3.12a and 3.12b. We then have

$$R(x,0) = R(z_t) - \int_0^{z_t} \left[\rho_o \omega \left.\frac{\partial r_s}{\partial p}\right|_{sat} + r_s w \frac{\partial \rho_o}{\partial z} \right] dz \tag{3.14a}$$

$$= R(z_t) - \int_0^{z_t} wG \; dz \tag{3.14b}$$

$$\text{where } G = -\rho_o^2 g \left.\frac{\partial r_s}{\partial p}\right|_{sat} + r_s \frac{\partial \rho_o}{\partial z} \tag{3.14c}$$

is called the generating function (e.g. Kessler, 1969). Note that an expression for $\partial r_s/\partial p)_{sat}$ is given in 3.13 and that $w=w(x,z)$ in equation 3.14b.

Consequently, to obtain the horizontal distribution of the ground rainfall rate we just have to integrate wG in 3.14b from $z=0$ to the top z_t of the orographic cloud. With the formulation of the seeder- feeder mechanism, the quantity $R(z_t)$ hence represents the background rainfall rate that is the rainfall rate falling at the top of the orographic cloud. Equation 3.14 physically means that all the water vapor condensed in the orographic cloud reaches the ground as precipitation.

A model based on equation 3.14 seems to give, in some cases, a good estimation of the rainfall rate due to topography. For instance, Collier (1975), using radiosonde data as inputs for large scale variables, computed rainfall rate over hilly terrain in North Wales and verified his calculations with raingauges readings over an area 100 to 1000 km². He considered the vertical velocity w in equation 3.14a as being the sum of the large scale baroclinic vertical velocity plus the orographic vertical velocity and omitted the second term in the integrand of eq. 3.14a which is the contribution due to the vertical variation of air density. Collier claimed an error as low as 10 per cent in the predicted rainfall for non-convective situations. This seems quite spectacular considering almost total lack of consideration for microphysical processes by using 3.14 and despite a highly parametrized profile for w.

Similarly, Sarker (1966) used an conceptually equivalent version of 3.14 (with no background rainfall rate; i.e $R(z_t)=0$) to compute the orographic rainfall distribution in the Western Ghats (India) during the southwest monsoon. The vertical velocity profile used is based on the mountain wave theory (see chap. 4). Results obtained in Sarker's paper also look quite satisfactory suggesting that the assumption that all the water vapor condensed reaches the ground as rain is not very far from reality at least in those cases.

However, one can ask himself if the above assumption is realistic in general (see discussion in chapter 2). More important, equation 3.14 tells us nothing about the cloud liquid water content of the orographic cloud. Nevertheless, equation 3.14 turns out to give a good answer in occasions of heavy orographic rainfall, the precipitation efficiency being high presumably due in great part to the seeder-feeder mechanism. Supporting this point, Bader and Roach (1977) , in a numerical model for orographic rainfall in warm sectors of depressions, showed that the orographically produced cloud washed out by raindrops falling from a seeder cloud (formed by large scale ascent) can augment the rainfall rate by several mm/h over a hill as small as of a few hundred meters high. They solved the continuity equation for the cloud liquid water content and assumed that all condensation of water vapor is automatically converted into cloud water and that the rainfall enhancement is only due to the washout of orographic cloud droplets by the seeder rain.

On the other hand, Gocho (1978) is of the opinion that the neglect of the precipitation drift (first term on left hand side of equation 3.3) can also cause an overestimation in the increase of precipitation around the hill due to the seeding as well as a too windward location for the distribution of rainfall rate across the hills in Bader and Roach's model.

An interesting model which combined orographic precipitation formed by adiabatic ascent (in the feeder cloud) with precipitation increases due to the seeding mechanism has been proposed by Bell (1978). Conceptually, it utilizes equation 3.5 but replaces the integrand S by two sources that is

$$S = S_1 + S_2$$

$$\text{where} \quad S_1 = k\rho_o\omega\frac{\partial r_s}{\partial p}\bigg|_{sat} \qquad (3.15)$$

and

$$S_2 = \int_0^\infty Q_c N\bar{V}E\pi a^2 \, da \qquad (3.16)$$

with
Q_c = cloud liquid water content
N = Marshall-Palmer drop size density
$\bar{V}$ = terminal drop fallspeed
E = efficiency of collection
a = dropsize radius

and the restriction that the sum $S_1 + S_2$ be less or equal to the maximum precipitation rate $(\rho_o \omega \partial r_s/\partial p)_{sat}$.

The first term S_1 is the same as wG (except for the contribution due to the vertical variation of air density which is neglected in Bell's model). The generating function is multiplied by a constant k which varies between 0 and 1 depending on how much the orographic cloud is efficient in transforming the water vapor condensed into rainwater. The term S_2 simulates the washout (or accretion of cloud drops by falling rainwater) over all drops of radius a. Despite good verification of the model, the parameterization of the cloud liquid water as well as the parameterized value for the constant k in equation 3.15 are rather arbitrary and might even lead to wrong conclusions concerning the role of the seeder-feeder mechanism in increasing the rainfall rate through equation 3.16. Moreover, the vertical velocity profile used (similar to fig 2.1) is highly empirical and is therefore a weak point in Bell's model.

Storebo (1976) also supports the idea of an important role played by the seeder-feeder mechanism proposed by Bergeron. One other significant point also found by Storebo is that increases of precipitation across hills seem insensitive to the properties of condensation nuclei, especially to the number density.

Colton (1976) presents a fine-mesh mesoscale numerical model, finite difference solution for the rainfall distribution over the Sierras and the Smith River Basin in California. Computed results agrees well with observations but Smith (1979,p189) is of the opinion that Colton's assumptions of 100 per cent release of condensate with no delay and a reflective upper boundary condition at 11 km would degrade his results.

Finally, Carruthers and Choularton (1983) reformulated the Bader and Roach model by including a much better treatment of airflow and the effect of wind-drift of precipitation. They used a dynamical model in which the atmosphere is divided into three layers of different but uniform stability, They found that wind-drift moves the position of maximum orographic enhancement downwind over both long (half width a > 10 km) and short (a < 10 km) hills. It also significantly reduces the total and maximum enhancement over short hills. Moreover, they argue that the Bader and Roach model slightly overestimates the enhancement over short hills while it is adequate over long hills. Although Carruthers and Choularton provided a reasonable model, the author of this thesis thinks that curvature of the wind profile (second derivative of windspeed with respect to z) rather than the temperature profile plays a major role in determining the vertical velocity over hills in orographic rain (if there is no release of potential instability). This is strongly supported by Sarker (1966) and Gocho (1978).

On the other hand, it seems rather peculiar that Carruthers and Choularton's model (as well as Bader and Roach's model) do not reproduce the fact that the observed rainfall rate is found to be more dependent on windspeed and less dependent on the pre-existing rainfall rate.

Finally, it appears that no models exists which solve the complete form of continuity equation for both cloud water and rainwater while using an appropriate solution for the dynamical problem of orographic rain. Gocho (1978) presents a model which solve only the rainwater equation and uses Sarker's theory for the dynamical part. His model, however, is too expensive to run and is then not suitable for sensitivity tests. The model presented below is an attempt to improve on the modeling of orographic rain. A complete testing of the model is given in chapters 5 and 6.

3.2 Formulation of a 2 dimensional numerical orographic model

a) Basic equations

The basic equations are the continuity equations for water substance and the differential equation for the vertical perturbation velocity. The continuity equation for cloud water and rainwater are;

$$\frac{\partial \rho_c}{\partial t} + \nabla\cdot(\rho_c u) = S_c \tag{3.17a}$$

$$\frac{\partial \rho_R}{\partial t} + \nabla\cdot(\rho_R u) - \frac{\partial}{\partial z}(\rho_R \overline{V}) = S_R \tag{3.17b}$$

with ρ_c and ρ_R being the cloud and rainwater density defined as before and S_c and S_R denote microphysical processes to be discussed later. These equations imply that cloud droplets share the motion of the wind while raindrops have a finite terminal fall speed relative to the air . The vertical perturbation velocity can be written

$$\frac{\partial^2 W}{\partial z^2} + (l^2 - k^2) W = 0 \quad . \tag{3.18}$$

W in the above equation is the vertical velocity, l^2 the Scorer parameter to be discussed later and k, the wavenumber of the sinusoidal ground profile. The reader is referred to chapter 4 for a complete discussion of equation 3.18.

As seen before (eq. 3.1 through 3.3), assuming that the whole system is in a two-dimensional steady-state, the continuity equation for rainwater, 3.17b, is

$$\rho_o u \frac{\partial Q_R}{\partial x} - \frac{\partial}{\partial z}\left[\rho_o (\bar{V} - w)\, Q_R\right] = S_R$$

which can be further expanded to obtain

$$\rho_o u \frac{\partial Q_R}{\partial x} + \rho_o Q_R \frac{\partial}{\partial z}\left[w - \bar{V} \right] + \rho_o (w - \bar{V}) \frac{\partial Q_R}{\partial z}$$

$$+ \quad Q_R \,(w - \bar{V}) \frac{\partial \rho_o}{\partial z} = S_R .$$

We want to solve for the vertical distribution of the rainwater mixing ration Q_R. So we rewrite the above equation to obtain

$$\frac{\partial Q_R}{\partial z} = \frac{1}{\rho_o (w-\bar{V})} \left[- \rho_o u \frac{\partial Q_R}{\partial x} + Q_R (\bar{V}-w) \frac{\partial \rho_o}{\partial z} + \rho_o Q_R \frac{\partial}{\partial z}(\bar{V}-w) + S_R \right] . \tag{3.19}$$

The same procedure applied to 3.17a leads to

$$\frac{\partial Q_c}{\partial z} = \frac{1}{\rho_o w} \left[-\rho_o u \frac{\partial Q_c}{\partial x} - w Q_c \frac{\partial \rho_o}{\partial z} - Q_c \rho_o \frac{\partial w}{\partial z} + S_c \right] \tag{3.20}$$

Equations 3.19 and 3.20 express the variation of the rain and cloudwater mixing ratios with altitude. We do not have to worry about the possibility of having $w = \bar{V}$ in equation 3.19 since we examine, in this thesis, cases where the terminal fall speed $\bar{V}$ is generally greater than the vertical velocity w (which is usually the case for steady-state precipitation). As a matter of fact, orographic rainfall generally varies from 2-8 mm/hr and according to Kelkar (1959) the most probable drop-diameter corresponding to this rate of precipitation is 1.00-1.25 mm. The terminal velocity corresponding to this drop-diameter is about 4.5 m/sec (Best, 1950 or Gunn and Kinzer's data). On the other hand, the maximum vertical velocity that we are dealing with is of the order of 10-50 cm/s which is effectively less than the above terminal fall speed. This means that the denominator of the first term on the right hand side of 3.19 is generally different from zero.

However, in equation 3.20, $w = 0$ is quite likely to occur especially near the crest of the topography ridge. At this location equation 3.20 is obviously useless. Moreover, small value of w will generate numerical instability if integrated with respect to z. To overcome this problem we can express the continuity equation, 3.20, as a derivative with respect to x instead of z, that is

$$\frac{\partial Q_c}{\partial x} = \frac{1}{\rho_o u}\left[-\rho_o w\frac{\partial Q_c}{\partial z} - wQ_c\frac{\partial \rho_o}{\partial z} - Q_c\rho_o\frac{\partial w}{\partial z} + S_c\right] \quad . \quad (3.21)$$

A low value for u, the windspeed, is not examined here since we are interested in strong wind situations. The first term in the bracket on both equations 3.19 and 3.21 represents, in its general sense, advection of the water substance. More precisely, for the rainwater equation 3.19, it is the precipitation drift and for the cloud water equation, it represents the vertical advection of cloud water. The second term in both equations 3.19 and 3.21 accounts for the effect of compressibility. The third term represents the variation with altitude of raindrops mean fall speed with respect to the ground in the rainwater equation and the air divergence for the cloud water equation. The magnitude of the first term in both equations is often the most important of the three while the third term in the rainwater equation might be neglected.

Equation 3.19 can be integrated with respect to z to give the solution of Q_R and equation 3.21 with respect to x to give the solution of Q_c at every grid points. Since there is interaction through the microphysical processes between the two equations, these are solved simultaneously.

In this model, background quantities such as the wind velocity and direction, air density, temperature and humidity are considered basic quantities and are hence assumed constants. It is also supposed that topography with modest dimensions (half width much less than 50 km and height less than 1 km) will not significantly change the assumed horizontally constant distribution of Q_v (water vapor mixing ratio of the basic flow). In other words, ignoring the horizontal temperature and humidity changes due to condensation or evaporation is a valid approximation for saturated airflow over modest topography and it is unlikely to change rainfall amounts. This is the reason we do not consider here the continuity equation for water vapor and heat.

b)Microphysical processes

The quantities S_R and S_c represent the sources and sinks in equation 3.19 and 3.21 respectively. They include condensation, evaporation, autoconversion and coalescence. Since we consider a non-freezing cloud, we do not try to simulate other processes such as deposition, melting or freezing. On the other hand, breakup is not important in orographic rain because, as mentioned above, the most probable drop-diameter is about 1 mm and rarely exceeds 3 mm which is about the threshold for breakup to be a likely event. The set of equations 3.19 and 3.21 represent a model where clouds store water and where some microphysical processes are reproduced. Moreover, it implies a delay in the formation of precipitation in the orographic cloud and will permit us to investigate, among other things, if the orographic cloud can produce rain without being seeded from above.

We will now look in details at the microphysical processes we intend to simulate.

Condensation

The condensation rate will be expressed in the same form as before, that is (see section 3.1)

$$COND = - wG \tag{3.22}$$

Because G is always negative, we will obtain condensation of water vapor into clouds with w positive and evaporation with w negative (downward motion). For condensation to take place we need a moist atmosphere.

Washout of cloud by rain

Equation 3.16 can be used to evaluate the washout of cloud by rain. However, to save computer time, Kessler's parameterization (1969) has been adopted instead of the above equation, that is;

$$\text{Washout} = 5.22\times10^{-6}\ m\ M^{7/8}\ \exp(kz/2) \qquad (3.23)$$

where $m = \rho_o(Q_c + Q_v - Q_{vs})$. The variable m represents the cloud water density plus water vapor density minus saturated water vapor density. The units are in kg/m³s for the washout when m and M, the latter being the rainwater content, expressed in g/m³ and z in km. Notice that when air is saturated , m simply represents the cloud liquid water content. The washout process is equivalent to the continuous collection process by collision and coalescence. The former terminology is used here to emphasize the fact that the seeder and feeder (orographic). cloud are treated separately and that the background rainfall can enhance the precipitation rate through the process. If such background rainfall is zero then the process simply simulates the growth of droplets by coalescence within the orographic cloud.

Autoconversion

The autoconversion process is represented by the expression;

$$\text{AUTOC} = k_1(\rho_o Q_c - k_2) \qquad (3.24)$$

where Q_c is the cloud water mixing ratio, k_1 the autoconversion rate and k_2, the autoconversion threshold. It is possible to adjust these parameters to simulate different situations. The values given by Kessler (1969) are taken, unless otherwise stated, that is

$k_1 = 10^{-3}$ sec^{-1} and $k_2 = 0.5$ g/m^3.

Evaporation of rain

Following Kessler's parametrization (1969), we have for the evaporation rate (kg/m^{3}s);

$$EVAPR = -5.4443 \times 10^{-7}\ mM^{13/20} \qquad (3.25)$$

The quantity m in eq. 3.25 is slightly different than that in equation 3.23. In the evaporation scheme, we consider m as the following; $m = \rho_o (Q_c + Q_v - Q'_{vs})$ where Q'_{vs} is the perturbated saturated water vapor density which is evaluated by considering the distance ΔD the airflow has moved down at a given point when compared to the position at hill top. Therefore, we write

$$Q' = Q'(T', P')$$

where $T' = T(z) - \Delta D \Gamma_d$ with Γ_d, the dry adiabatic lapse rate and P', the corresponding air pressure, fig. 3.1.

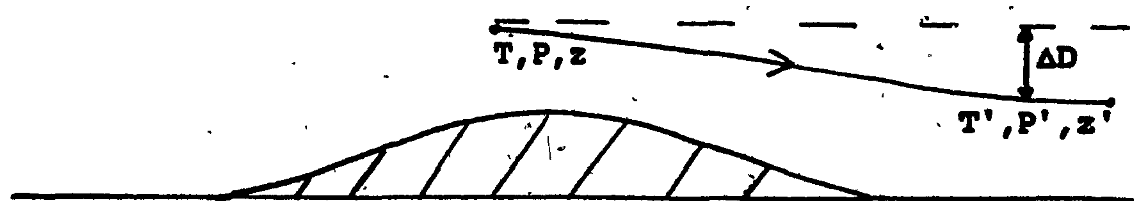

Fig.3.1

Evaporation of rain will take place in unsaturated air (below cloud base, between the seeder and feeder cloud and in the lee of a given topographical obstacle).

With all expressions given above, S_R and S_c in 3.19 and 3.21 are respectively

$$S_R = \text{WASHOUT} + \text{AUTOC} - \text{EVAPR} \qquad (3.26a)$$

$$S_c = \text{COND} - \text{WASHOUT} - \text{AUTOC} - \text{EVAPC} \qquad (3.26b)$$

C) Terminal velocity of raindrops

A raindrop is assumed to fall relative to the air with the mean terminal velocity (averaged over the whole raindrop spectra) given by Kessler (1969)

$$\overline{V} = 5.16 \exp(0.05z)\ M^{1/8} \qquad (3.27)$$

where $\overline{V}$ is given in m/s, z in km and M, the precipitation content in g/m ^{3} ($M=\rho_o Q_R$).

d) Numerical scheme

Both equations 3.19 and 3.21 are of the form

$$Q' = f(Q) \qquad (3.27)$$

where Q' represents the derivative of water substance with respect to x for the cloud water and with respect to z in the rainwater equation. A centre-differenced scheme is unconditionnaly unstable when applied to such equation. Consequently, we will try a forward scheme which seems more appropriate here. But we will integrate equation 3.19 and 3.21 simultaneously in two different spatial variables which are direction of motion (x for the cloud droplets and z for hydrometeors). Although this appears to be non-standard , it physically makes more sense since clouds move horizontally and the precipitation principally vertically. Moreover, other numerical procedures were tried and found rather unstable even with small integration steps.

The scheme of integration used is illustrated in fig. 3.2.

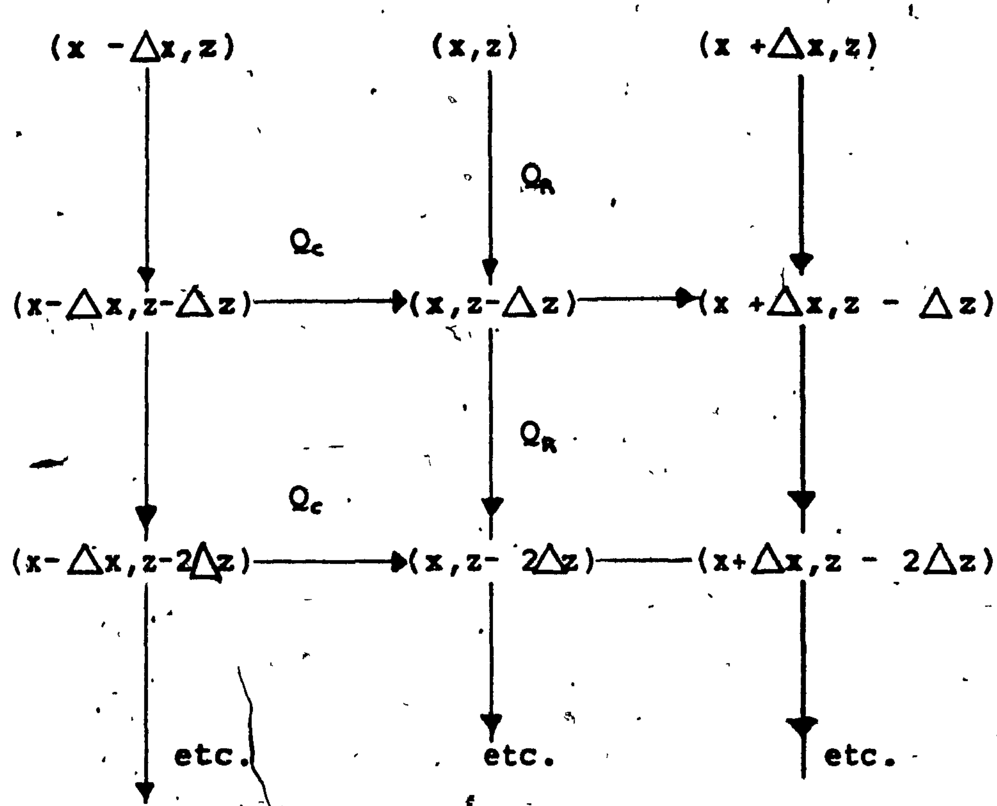

Fig.3.2 Scheme of integration

The new value for the cloud mixing ratio is evaluated at point $(x,z-\Delta z)$ by an horizontal marching from the point $(x-\Delta x,z-\Delta z)$ while the new value for rainwater at the same point is calcaluted by vertical integration from the point (x,z). The overall marching is then from top to bottom in the z direction until the ground is reached. Then the whole procedure is repeated for a new value of x incremented by Δx. Once the value of Q_R is known at a given level it then becomes easy to evaluate the rainfall rate using the following relationship (Kessler,1969);

$$M = \alpha R^{\eta} \tag{3.28}$$

with R in mm/hr and M in g/m^3 ($M=\rho_o Q_R$).

Measurements at various locations have shown that α and η are usually quite uniform, with $0.052 < \alpha < 0.089$ and $0.84 < \eta < 0.94$. In the model developed in this thesis, α will be taken as 0.089 and η as 0.94 which is thought to take into account the fact that cloud liquid water content in orographic warm clouds are higher than that in non-orographic cloud (see Pruppacher and Klett, 1980, p 27).

When the scheme described in fig 3.2 is used, equations 3.19 and 3.21 are written

$$Q_c(x,z-\Delta z) = Q_c(x-\Delta x,z-\Delta z) - \frac{\Delta x}{\rho_o U}\left[\rho_o w\frac{\partial Q_c}{\partial z} + wQ_c\frac{\partial \rho_o}{\partial z} + Q_c\rho_o\frac{\partial w}{\partial z} - S_c\right]_{(x-\Delta x,z-\Delta z)} \tag{3.29}$$

$$Q_R(x,z-\Delta z) = Q_R(x,z) + \frac{\Delta z}{\rho_o(\overline{V}-w)}\left[-\rho_o U\frac{\partial Q_R}{\partial x} + \rho_o Q_R\frac{\partial}{\partial z}(\overline{V}-w) + Q_R(\overline{V}-w)\frac{\partial \rho_o}{\partial z} + S_R\right]_{(x,z)} \tag{3.30}$$

The rainfall rate at the surface is obtained from the value of Q_R at the last grid point in the vertical using the equation 3.28 and $M=\rho_o Q_R$. Note that S_R and S_c are given by 3.26a,b and evaluated at point $(x-\Delta x,z-\Delta z)$ and (x,z) respectively.

e) Environmental and boundary conditions

Environmental conditions such as pressure,density, wind speed and temperature are not assumed to be modified by the topography and are taken as inputs of the basic atmosphere. Changes of water vapor mixing ratio due to topography are not included in the calculation of rainfall and cloud water quantities. This is an important approximation whose justification lies in the fact that,for stratiform clouds, the amount of water lost (condensed) across mountain ridges of small extent (half width less than 50 km) is small and is not likely to significantly change the results of calculation of rainfall rates. Moreover, the model does not include the net heating which occurs due to condensation, deposition loss of liquid water both from the seeder cloud (by precipitation) and the feeder cloud (washed out), nor does the model include the effect of cooling due to evaporation of rain. The former is discussed in Carruthers and Choularton (1983) and it turns out that its effect is insignificant for the range of hill lengths for which the feeder-seeder process is likely to be the dominant mechanism of orographic enhancement (i.e $a << 200$ km).

If the environmental airmass is not saturated,the model can take it into account by the following procedure. At a given level, we first calculate the distance to reach saturation (that is equivalent to calculate the lifting condensation level). If this distance is greater than the orographically induced displacement,ζ,then no condensation can take place at this level. On the other hand,if the upward distance an airmass needs to be lifted is less than ζ and if there is vertical motion then condensation takes place and equation 3.22 is used to evaluate the amount of such condensation. Hence, we can include the effect of having a non-saturated atmosphere on the calculation of the rainfall rate enhancement.

Since we are using finite differences, we need boundary conditions; one lateral and one vertical boundary condition. Generally speaking, boundary conditions will be taken as the value found in the environmental atmosphere at a distance far away from orographic influence. For example, the orographic cloud liquid water content and the rainfall rate at the left edge of the domain are simply taken the same as the background environment.

The same rule is applied for the vertical boundary condition except that the physical location of this upper boundary condition is made variable. That is, we start integrating in the vertical at a slightly different location as we go downwind along the topography.

This is thought to be an improvement - at least in principle - over what is found in other models. In fact, in his conceptual model of the seeder-feeder mechanism, Bergeron (1949) assumed an horizontal boundary condition. This implies that the maximum upward limit of the orographic cloud is unaffected by the irregular terrain which is not correct. Bader and Roach (1977) have improved the treatment of the upper boundary condition by specifying the rainfall from above as a constant along a surface which parallels the irregular terrain (fig. 3.3). In the current model, the location of the upper boundary condition will depend on the orographically induced displacement ζ according to the relationship

$$h' = \zeta(x,z{=}D_c) - Z_g + D_c \qquad (3.31)$$

where h' is the height of the upper boundary condition above the ground, $\zeta(x,z{=}D_c)$, the streamline displacement evaluated at a height D_c specified at the left edge of the domain and finally Z_g represents the elevation of the ground (fig. 3.3). The incoming (background) rainfall rate is assumed fixed at the upper boundary

$$z = z_u(x) = \zeta(x,z{=}D_c) + D_c$$

The upper limit D_c defines not only the extent of the domain of integration in the vertical but also the physical maximum extent of the orographic cloud at the left edge of the domain (where ζ tends to zero).

It should be note that at $z{=}z_u(x)$, equation 3.28 is inverted, in order to convert the background rainfall rate R (mm/h) into precipitation water content M (g/m³), that is;

$$\text{at} \quad z = z_u(x) \quad (x), \; M_o = \alpha R_o^{\eta} \qquad (3.32)$$

f) Vertical motion and upward displacement

We have avoided so far mentioning any reference to the way vertical motion, w, and orographically induced displacement, ζ, are calculated. In fact, we obviously need to evaluate w in equation 3.23 and 3.30. Unfortunately , any attempt to compute w and ζ requires the modeling of airflow over topography which turn out into a complex task unless many assumptions are made.

However, because of its simplicity the use of the two-dimensional mountain wave theory to solve the problem is attractive and will be the subject of the next chapter. It should be noted that the vertical motion hence calculated is only due to topography and the background vertical motion would have to be added on the result. However, in our model the background rainfall rate is assumed to already contain the information about that large scale vertical motion and the latter is therefore omited in this study.

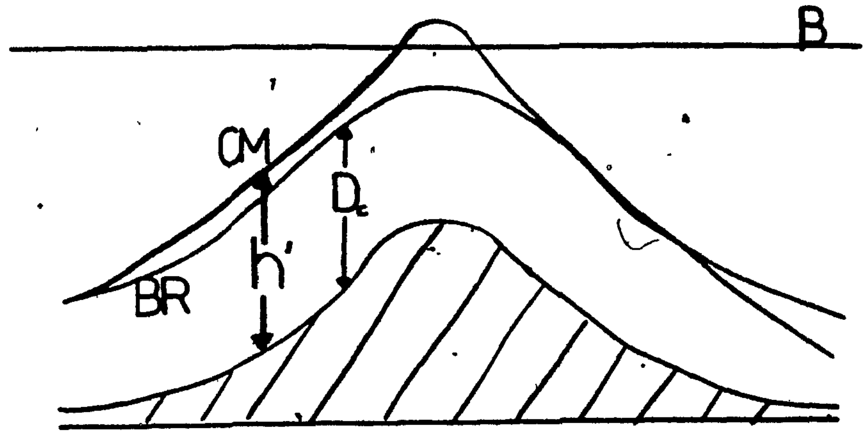

Fig. 3.3. Upper boundary condition (upper limit of integration which is the first point of integration in the vertical in the model). Current model's boundary condition is represented by CM, Bader and Roach's condition by BR and Bergeron's horizontal condition is also indicated (B).

CHAPTER 4: MODELING AIRFLOW OVER TOPOGRAPHY

It has been quite common to assume that the vertical velocities due to a mountain are confined to the region directly over the mountain and that the slope of the streamlines decreases to zero at some midtropoosphere level (like fig 2.1). Dynamically such models might be incorrect as are the attempts to derive them from the governing equations. Moreover, it is possible that the use of such models would introduce appreciable error in the calculation of vertical velocities and condensation rates.

In actual situations, the lifting aloft may begin well upstream of the mountain and values of vertical velocities and upward displacement can be significantly stronger than what obtained by the simple theory mentioned in chapter 2. More important, the strength and general distribution of vertical velocity depend to a great extent on the atmospheric structure and not only on the topography profile. Therefore, in order to correctly evaluate the airflow over topography we need a better theorical framework which is fortunately available through the mountain wave theory approach.

The theorical researches on the problem of the disturbance of an atmospheric current flowing over a mountain range have been undertaken by various authors (e.g. Queney (1948),Scorer (1949) and others). Results have shown that most of the characteristics observed features can be explained , to a very large extent, by the hydrodynamical theory of internal, small adiabatic perturbations in a stratified atmosphere without friction. We will summarize here aspects of the theory relevant to the problem of orographic rain.

(Note: lee waves will not be discussed since it is not relevant to the problem of orographic rain.)

4.1 Vertical motion and streamline displacement over a sinusoidal corrugation of the ground.

The disturbance in an air current whose velocity may vary with height, caused by a wave-like corrugation of the ground of wavenumber k is obtained in this section. In the second section, the result is extended to a single ridge by the method of Fourier integrals. We assume a two-dimensional flow in the vertical plane xz, with the z axis vertical and the x axis in the direction of the undisturbed wind. The ground is assumed to have an infinite extent in the y direction (perpendicular direction). We consider frictionless, steady, laminar and isentropic flow.

The basic equations are the two equations of motion (x,z), equation of state, adiabatic equation and the equation of continuity.

Starting from these equations, Scorer (1949) obtained, after linearization (small amplitude theory), the following wave equation for a sinusoidal ground profile.

$$\left[1 - \frac{f^2}{U^2k^2}\right]\frac{\partial^2 \psi_o}{\partial z^2} + \left[\frac{-g}{c^2} - \beta + \left(\frac{g}{c^2} + 2\beta\right)\frac{f^2}{U^2k^2}\right]\frac{\partial \psi_o}{\partial z} + \left[\frac{g\beta}{U^2} - \frac{1}{U}\frac{\partial^2 U}{\partial z^2} - k^2\right]\psi_o = 0 \tag{4.1}$$

where in the above; f= the Coriolis parameter
U= undisturbed wind speed
k= wavelength of ground corrugation
ψ_0 = stream function
c= speed of sound
β= $1/\theta(\partial\theta/\partial z)$; coeficient of stability

We can ignore the Coriolis effects if

$$\frac{f^2}{U^2k^2} \ll 1 \tag{4.2 a}$$

With $f = 10^{-4}\ s^{-1}$ and U= 15 m/s the condition is satisfied when

$$L \ll 1000 \text{ km} \tag{4.2 b}$$

where L is the wavelength of the ground profile ($=2\pi/k$).

The equation (4.1) then becomes

$$\frac{\partial^2\psi_0}{\partial z^2} - \left[\frac{g}{c^2} + \beta\right]\frac{\partial\psi_0}{\partial z} + \left[\frac{g\beta}{U^2} - \frac{1}{U}\frac{\partial^2 U}{\partial z^2} - k^2\right]\psi_0 = 0 \tag{4.3}$$

Scorer (1949) further showed that $g/c^2 + \beta = (-1/\rho)\partial\rho/\partial z$. By using the integration factor

$$I = \exp\left[-\frac{1}{2}\int\frac{1}{\rho}\frac{\partial\rho}{\partial z}\,dz\right] = \sqrt{\rho_0/\rho} \tag{4.4a}$$

and by setting

$$\psi_0 = I\psi \tag{4.4b}$$

where ρ_0 is the density at height z= 0, we can eliminate the first derivative in equation 4.3 and obtain;

$$\frac{\partial^2\psi}{\partial z^2} + \left[\frac{g\beta}{U^2} - \frac{1}{U}\frac{\partial^2 U}{\partial z^2} - k^2 - \frac{1}{2\rho}\frac{\partial^2\rho}{\partial z^2} + \frac{1}{4\rho^2}\left(\frac{\partial\rho}{\partial z}\right)^2\right]\psi = 0. \tag{4.5}$$

The first two terms within the bracket of (4.5) are of the order of 1 km^{-2} compared with values of the order of $5X10^{-8}$ km^{-2} for the last two. So we can reduce the equation 4.5 to

$$\frac{\partial^2 \psi}{\partial z^2} + (l^2 - k^2) = 0 \tag{4.6}$$

$$\text{where} \quad l^2(z) = \frac{g\beta}{U^2} - \frac{1}{U}\frac{\partial^2 U}{\partial z^2}$$

This parameter l^2 is usually known as the Scorer's parameter and is hence dependent on the stability β and on the second derivative of the wind with respect to altitude. It is therefore clear that vertical velocity and streamlines profiles depend to a large extent on the atmospheric structure.

On the other hand, the latent heat released by condensation should be included in the dynamics. Sarker (1966), shows that by replacing the dry adiabatic lapse rate by the saturated adiabatic lapse rate Γ_s provides a useful approximation in treating the problem. Under this assumption the Scorer parameter hence becomes (in first approximation);

$$l^2(z) = \frac{-g \mid dT/dz - \Gamma_s \mid}{TU^2} - \frac{1}{U}\frac{\partial^2 U}{\partial z^2} \tag{4.7}$$

In many situations, the first term on the rhs dominates over the second. However, concerning the problem of orographic rain, it is often observed that the temperature profile is along the moist adiabatic and that a low level jet is present. This means that the second term is more likely to dominate over the first and that the curvature of the wind profile determines how the airflow behaves over the topography.

To obtain an equation for vertical velocity w and streamline displacement , ζ , we just note that by definition

$$W = \partial\Psi/\partial x \qquad (4.8\ a)$$

$$\text{and} \qquad \zeta = \Psi/U \qquad (4.8\ b)$$

and we can write equation (4.6) as

$$\frac{\partial^2 W}{\partial z^2} + (l^2 - k^2)W = 0 \qquad (4.9)$$

The above equation relates the variation of W with height assuming a sinusoidal topography of wavenumber k. Since Ψ, W and ζ are complex quantities, the complete solution will be of the form (also using equation 4.4a,b);

$$w(x,z) = \text{Real} <(\rho_o/\rho)^{1/2}\, W(z) \exp(ikx) >$$

where W(z) is the solution of 4.9.

The above results have no practical direct application, since an unlimited sinusoidal ground profile is rarely found in nature. But their generalization by Fourier integrals can be utilized in the solution of the case of an arbitrary mountain.

4.2 Solution for a single symmetrical mountain ridge

A very convenient equation for the ground surface is the "bell-shaped" ridge, fig. 4.1

$$Z_g = \frac{a^2 b}{a^2 + x^2} \qquad (4.10)$$

It can be also represented by

$$Z_g = ab \int_0^{\infty} \exp(-ka) \cos kx \, dk$$
$$= \zeta(x,0)$$

which is very useful in obtaining the mathematical solution for w and ζ.

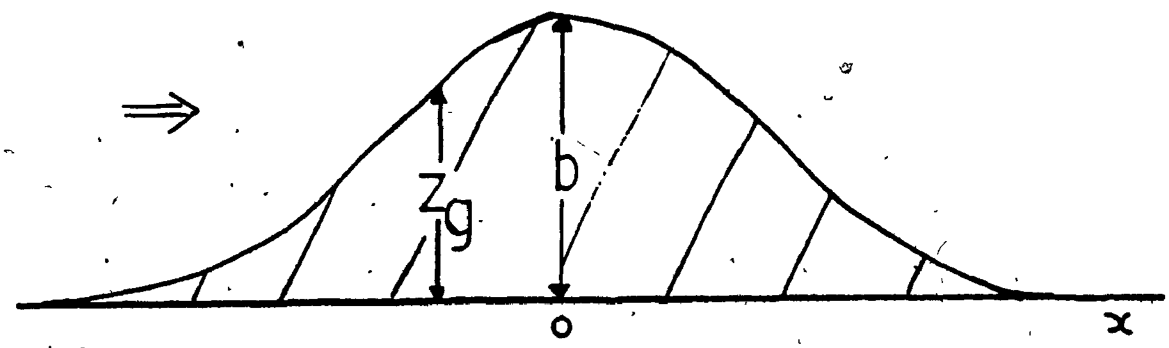

Fig 4.1 ; the bell-shaped ridge; b is the maximum height and a the width of the ridge. Z_g represents the height of terrain above sea level. Negative x values are on the windward side while positive x values on the leeward side.

An airstream having neutral static stability ($dT/dz = \Gamma_d$ or Γ_s in the moist case) and no curvature of its wind profile ($1/U \times \partial^2 U/\partial z^2$) would have $l^2 = 0$ (in eq. 4.7) and the vertical displacement of a streamline ζ would be given by

$$\zeta(x,z) = \frac{ab(a + z)}{(a + z)^2 + x^2} \qquad (4.11)$$

where the amplitude of the vertical displacement of fluid particles slowly falls off with height. Note here that the coordinate z is the elevation above the ground surface such that $\zeta(x,0) = Z_g$.

Such an airstream refers to the potential-flow regime (ideal solution) and is valid when the inverse of l(z) is much bigger than the mountain half width "a" (see Gill(1982), p 275).

The vertical velocity is, using 4.8a and 4.8b;

$$w(x,z) = U(z)\cdot \partial\zeta/\partial x \tag{4.12}$$

Combining 4.12 and 4.11, it is easy to show (by setting $\partial w/\partial x = 0$ in 4.12) that the maximum vertical velocity occurs at a distance $x = \pm\ a/\sqrt{3}$ (near the ground) for the bell-shaped mountain.

For a non-zero but constant value of l^2, the solution for the bell-shaped mountain can be derived by solving eq. 4.6 and using 4.8b (see Queney ,1948 for the derivation). The result is;

$$\zeta(x,z) = \frac{U_o}{U_z}\left[\frac{\rho_o}{\rho_z}\right]^{1/2} ab\ \frac{\{\ a\cos lz\ -\ x\sin lz\ \}}{a^2 + x^2} \tag{4.13}$$

The important difference between (4.11) and (4.13) is that in the latter the streamline displacement has a sinusoidal variation and does not falls off with height. Using equation 4.12, it is possible to argue that vertical velocities will be stronger in the latter case. Moreover, the point of maximum vertical velocity will not correspond to the point of maximum slope of the ground surface in 4.13 (whereas it does in equation

4.11).

It should be noted that equation (4.13) can be derived from eq. 4.6. In fact using the hydrostatic approximation (which is equivalent to assuming k << 1 Gill,1982), equation 4.6 becomes

$$\frac{\partial^2 \Psi}{\partial z^2} + l^2 \Psi = 0$$

The solution of such equation is

$$\Psi(x,z) = \text{Real} < \Psi_s(x) \exp(ilz) > \qquad (4.14a)$$

or by using 4.8b

$$U \zeta(x,z) = \text{Real} < U_o \zeta_s(x) \exp(ilz) > \qquad (4.14b)$$

where $\zeta_s(x)$ is a complex function whose real part defines the surface topography. For the bell-shaped mountain, it can be shown that

$$\zeta_s(x) = \frac{ab}{a^2 + x^2}(a + ix) \qquad (4.15)$$

which yields to (using 4.15 in 4.14b);

$$\zeta(x,z) = \frac{U_o}{U_z}\left(\frac{\rho_o}{\rho_z}\right)^{1/2} ab \frac{\{ a\cos lz - x\sin lz \}}{a^2 + x^2} \qquad (4.16)$$

which is identical to equation to 4.13 (after multiplicating by the integration factor 4.4 and taking the real part).

So far, we have looked at solutions for $l^2 > 0$ in equation 4.7. However, if l^2 is negative and constant with z (e.g. neutral static stability and $(1/U)X\partial^2U/\partial z^2$ being positive constants) the solution for ζ will be

$$\zeta(x,z) = \text{Real} <\zeta_s(x) \exp(-L'z) > \left|\frac{\rho_o}{\rho_z}\right|^{1/2} \frac{U_o}{U_z}$$

$$= \frac{a^2 b}{a^2 + x^2} \exp(-L'z) \left|\frac{\rho_0}{\rho_3}\right|^{1/2} \frac{U_0}{U_3} \qquad (4.17)$$

where L' is the modulus of the complex value of l. Comparing equation 4.17 and 4.13 and 4.11 we can conclude that taking into account the vertical structure of the atmosphere through quantities such as the static stability and the wind profile drastically affects the vertical structure of streamline displacements. More precisely, vertical velocities are expected to be significantly greater with an atmosphere having $l^2 > 0$ (solution 4.13) than one having $l^2 < 0$ (solution 4.17). We will take an example to illustrate the point from a practical point of view; if the temperature profile is along the saturated adiabatic lapse rate and if there is a low level jet stream present ($1/U \times \partial^2 U/\partial z^2 < 0$) it follows from the above (see also equation 4.7) that vertical velocity due to the mountain will be significantly higher when $l^2 > 0$. In terms of vertical propagation of energy it means that if $l^2 > 0$, energy is propagated upward without absorption while when $l^2 < 0$, the solution of ζ is exponentially decreasing and hence there is absorption (see equation 4.17). This provides an explanation why large orographic rainfalls tend to occur when $l^2 > 0$ (condition already given p 25). Further investigation on the importance of the parameter l on orographic enhancement will be undertaken in chapter 5.

4.3 Solution for an asymmetrical ridge

In many occasions, the ground profile has a shape depicted in fig. 4.2 which corresponds to the equation

$$Z_g = \zeta(x,-h_o) = \frac{a^2 b}{a^2 + x^2} + a' \tan^{-1}(x/a) \qquad (4.18)$$

where the ground level is taken here as $z=-h_o$ in order to avoid upstream negative values of Z_g. The solution ζ is similarly obtained by combining 4.14b with $\zeta_s(x)$ given by (Sarker,1966);

$$\zeta(x,z) = \left[\frac{\rho_o}{\rho_s}\right]^{1/2} \frac{U(-h_o)}{U(z)} \text{Real} \left[\zeta_s(x) \exp(ilz) \right] \qquad (4.19)$$

$$\zeta_s(x) = \frac{ab(a+ix)}{a^2 + x^2} + a' \left[\tan^{-1}(x/a) + \frac{i}{2} \ln \frac{(a^2+x^2)}{a^2}\right]$$

The vertical velocity is simply

$$w(x,z) = U_s \, \partial\zeta/\partial x$$

$$= U(-h_o)(\rho_o/\rho_s)^{1/2} \text{Real} \left| \exp(ilz)\, \partial\zeta_s(x)/\partial x \right| \qquad (4.20)$$

Note: the subscript $-h_o$ corresponds to the ground level which is used for mathematical convenience.

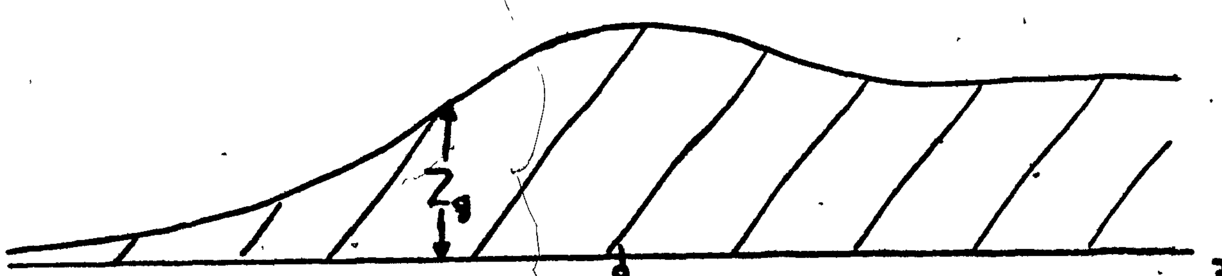

Fig 4.2. Ground profile described by equation 4.18.

4.4 Vertical variation of the Scorer parameter

So far, we have consider l being constant with z. However, in actual situations it is rarely the case and we need to consider l=l(z) which complicates the solution of equation 4.6.

One simple way to bypass the mathematical problem is to divide the atmosphere into two or more layers where l is piecewise constant. Such approach was taken by Sarker (1966) who divided the atmosphere into 3 layers in which l^2 is assumed constant and positive in the lower and upper layer and negative in the middle layer. He used equation 4.18 to approximate the topography of the Western Ghats (India) and calculated l from the wind profile during the southwest monsoon event (assuming $dT/dz = \Gamma_s$ in equation 4.7)

Computed results of orographic rainfall based on equation 4.6 for the vertical velocity seem to agree quite well with observations despite the extreme simple assumption that the rate of precipitation is equal to the rate of condensation.

Consequently, the dynamical part of the solution given by Sarker (1966) and slightly modified by Gocho (1978) has been adopted in this thesis since it is somewhat general and can reduce to a 2 layers model or a one layer model if needed. Expressions for streamline displacements and vertical velocities are thus given in appendix B for a 3 layers and for a 2 layers model.

Finally, it is worth noting that equation 4.18 is quite general since a great amount of topography profiles can be approximated by simply adjusting parameters a,b and a' to a particular situation.

4.5 Validity of the results

In this chapter it has been shown that vertical velocity and streamline displacements may depend to a great deal on the atmospheric vertical structure. This is an important result already well known in the mountain wave theory. We have given expressions for the vertical motion and streamline displacements for the windward side as well as the leeward side of both symmetrical and asymmetrical mountain ridge. Solutions for other types of topography can be easily derived from the approach given by Sarker (1966) provided it has a simple Fourier transform.

However, the theory of small adiabatic perturbations , used above, requires as an essential condition that the perturbation may be considered as an infinitesimal disturbance. In the case of a typical mountain range, the condition is fulfilled if the height b is small compared to both the width a and to L (where L $= l^{-1}$). The last statement is equivalent to say that vertical velocity must be small compared to the wind speed U.

Nevertheless, it seems probable according to Queney (1948) that the results are still qualitatively valid when the ratio b/a or b/L are as large as 1/4 or even 1/2 in some cases. For instance, if U= 10 m/s, the theory of small perturbation is practically applicable to any typical mountain top as high as 1 or 2 km if its total width is not smaller than 10 km.

For the above results to be valid it is also necessary that the half width " a " be much less than 100 km otherwise Coriolis effects would affect the results. Other assumptions made here are given in the beginning of this chapter and are; the motion is nonviscous, laminar and steady. Finally, airflow over the topography obtained in such a way is assumed not to be changed by means of the drag force of the falling water.

The main shortcoming of this theory is that the parameter l must be evaluated from the wind profile obtained from a sounding not too far away from the mountain. Therefore, arises the possibility of that the sounding be modified by the mountain itself. Similarly, another problem with the use of linear theory is that in almost saturated atmosphere, even slight lifting will bring the air to saturation and thus change the static stability. Nevertheless, it is thought that the linear theory provides the best simple estimation of vertical motion and streamline displacements due to topography and will then be used as an input to the microphysical model developped in this thesis (see chap.3 and chap.5).

CHAPTER 5: THE BEHAVIOUR OF A 2-D NUMERICAL OROGRAPHIC MODEL

The behaviour of a two-dimensional numerical orographic model based on equations 3.29 and 3.30 is presented in this chapter.

The solution for the vertical motion and streamline displacement are calculated according to the linear theory of orographically induced adiabatic perturbation given in chapter 4 (see also appendix B). The reader is reminded that adopting such a solution and coupling it with the thermodynamical-microphysical model given by equations developped in chapter 3 means that we are assuming no direct feedback between the dynamical part and the microphysical processes of the model. Such a procedure is however a good approximation as discussed in chapter 3.

Note: the above approach would not be appropriate if we studied the orographic -convective precipitation. In fact, the local generation of an orographically induced cumulonimbus in a conditionally unstable airmass implies a strong feedback between dynamics and microphysics.

The shape of the topography profile is taken as the bell shaped ridge, equation 4.10. The half length "a" which characterizes the hill or mountain width will be taken in the range 5 to 30 km. This range is small enough for Coriolis effects to be insignificant and sufficiently large to be above the limit where non-hydrostatic effects play an important role. Heights chosen will be up to 1 km; over higher hills,associated upward displacement of the airflow may alter the structure of the seeder cloud and also influence any mid-level precipitation. Another problem we would have to face in case of hill tops higher than 1 km is that the feeder cloud would have an upward extent which would require in many cases the modeling of subfreezing precipitation processes. The slope (which can be represented by the aspect ratio b/a) also has its restrictions; it should not be superior to 0.3, otherwise three-dimensional effects would be important (see Carruthers and Choularton, 1982).

The temperature profile often follows the moist adiabatic lapse rate in cases of heavy orographic rainfall. Such a profile is adopted here and only specification of the surface temperature is hence needed. Temperature at any level is given by;

$$T(z+\Delta z) = T(z) + \Gamma_s \Delta z \qquad (5.1)$$

where

$$\Gamma_s = \frac{1 + 5.42 \times 10^3 \, r_s / \epsilon T}{1 + 8.39 \times 10^6 \, r_s / \epsilon T^2} \Gamma_d \qquad (5.2)$$

(see Iribarne and Godson, 1973, p 159).

Unless otherwise stated, the domain of integration will generally consists of 50 grid points in the horizontal and about the same number in the vertical. Integrations and computations are performed from top to bottom with a step of integration Δz and from left to right with a step of integration Δx (fig. 5.1).

At the upper boundary of the domain of integration (which is not necessarily horizontal), the rainfall rate is assumed to be constant and taken as the background rainfall rate. The rainwater mixing ratio at that point is then easily obtained from the rainfall rate by inverting equation 3.28 . At the upper boundary, the cloud liquid water content is specified either as zero or as a constant which can be taken as the mean value of the cloud liquid water content of the seeder cloud (background environment). At the left edge of the domain, the cloud liquid water content is specified as zero.

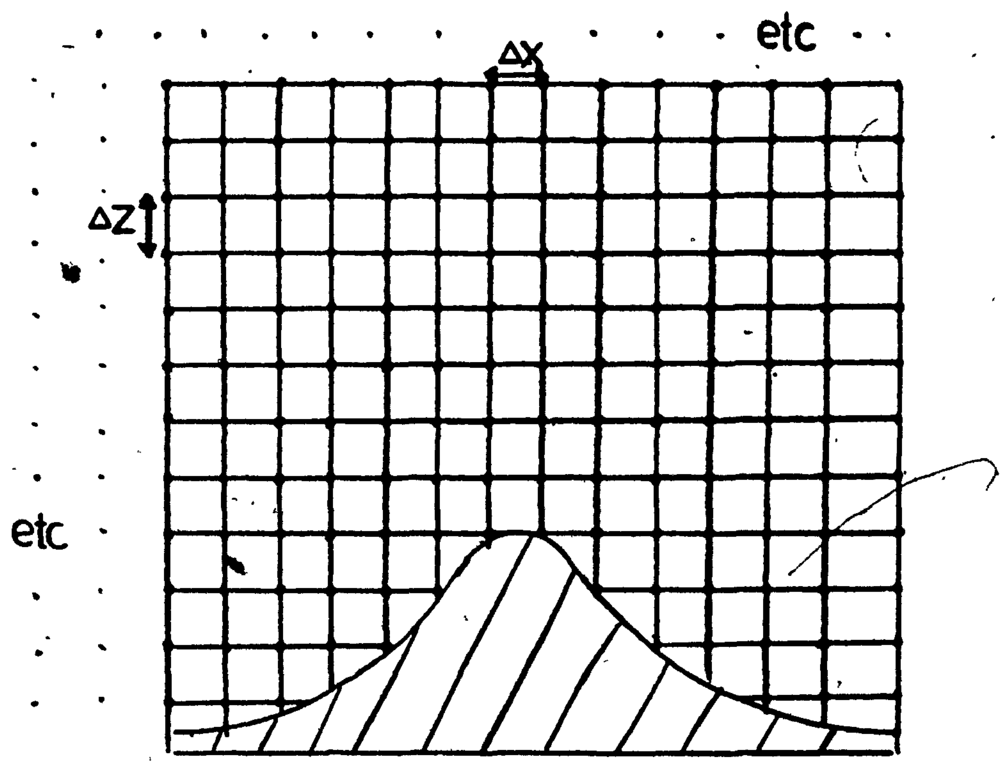

Figure 5.1: Domain of integration

The top of the domain (which does not necessarily correspond to the upper boundary condition of the orographic cloud) is generally taken as z= 4 km. On the other hand, the domain of integration varies along x and is bounded by $z = z_u(x)$. It is believed that a higher top for the domain of integration would not significantly change calculations of ground rainfall rate since most of orographic enhancement takes place at low levels.

Although temperature below 0°C are possible within the domain of integration and considering that there is no provisions for ice micophysics processes, we will consider the model to be valid only for those cases having a freezing level relatively high (say at least 2.5 km high).

Smoothing operators are used to remove undesirable small scale variations in some of the computed quantities such as the horizontal profile of the ground rainfall rate and the orographic cloud water content (the smoothing operator used in the model is described in appendix D). Finally, the rainfall rate at the ground is obtained by a simple linear extrapolation of the calculated value at the last two grid points in the vertical.

A computer program accompanies this thesis and was written in Fortran IV language.

5.1 Results of sensitivity experiments

The behaviour of the relatively simple model will be assessed below. A simple way to achieve this goal is to run sensitivity tests. Such tests are important because they not only provide information about the effects of the various assumptions but also indicate the relative importance of different factors in the amount of maximum orographic enhancement ΔP_{m} (difference between the maximum surface rainfall rate, P_{gm}, and the background rainfall rate, P_o).

Table 5.1 summarizes sensitivity tests done with the model.

The first set (tests # 1-4) deals with the increase of the maximum rain enhancement ΔP_m as a function of a specific meteorological parameter. The second set (tests #5-6) investigates the effect of varying hill length and height and the wind structure (through l_1, l_2, H) on the maximum orographic enhancement, ΔP_m.

Experiment	To test effect of varying	Special changes
1	windspeed maximum 5- 30 m/s	
2	relative humidity 0.7 - 1.0	b= 250m Δx = 5 km for U_m= 20 and 30 m/s and Δx=2.5 km for U_m = 10 m/s.
3	background rainfall rate 0 - 8 mm/h.	D_c = 2.0 km
4	Θ_w: potential wet bulb temperature 8 - 25°C	
5	a: hill mean width 5 - 30 km	b = 250 m
6	wind structure; l_1, l_2, H	Δx= 5 km a) varying l_2 b) varying H c) using 2-D potential flow model ideal sol.)
7	Kessler's parametrization constants: α, η, k_2 and QC_o .	α=0.1,0.089,0.071,0.052 η=1.0,0.94,0.89,0.84 k_2=0.3,0.5 and 1 g/m³ QC_o = 0,0.1 and 0.3 g/m³
8	space steps Δx and Δz	Δx=1,2.5 and 5 km Δz=50,100 and 200 m

Table 5.1 Summary of sensitivity experiments

Finally, the last set (test # 7-8) examines the sensitivity of changing boundary conditions , parametrization constants and space steps on the maximum rain enhancement ΔP_m.

The sensitivity test presented in this study corresponds to a low-level jet situation. The windspeed profile will be represented by a trigonometrical function that satisfies the equation below;

$$-\frac{1}{U}\frac{\partial^2 U}{\partial z^2} = \text{constant} = l^2 \qquad (5.3)$$

In every case, the atmosphere is divided into two layers separated by the level of maximum speed, with the Scorer parameter l^2, different but constant in each layer. The height of the maximum speed (U) is H and the value l_1 and l_2 designate the Scorer parameter in the lower and upper layer respectively. With this notation, the wind profile is;

$$U(z) = \begin{cases} U_m \cos l_1 (H-z) & z \le H \\ U_m \cos l_2 (H-z) & z > H \end{cases} \qquad (5.4)$$

In all sensitivity experiments, only one parameter is changed while all others are kept constants for a specific test. Unless otherwise specified input conditions are

$Po = 2.0$ mm/h	$a = 20$ km
$U = 20$ m/s	$b = 500$ m
$\Theta_w = 15°C$	R.H. = 100 %
$l_1 = 1.0$ km^{-1}	$D_e = 2.5$ km
$l_2 = 0.13$ km^{-1}	$QC_o = 0.1$ g/m^3
$H = \pi/3$ km	
$\Delta x = 2.5$ km	
$\Delta z = 100$ m	

which represents our basic set of conditions.

In the first sensitivity test, the windspeed maximum is varied from 5 to 30 m/s. Figure 5.2 shows that orographic enhancement ΔP_m increases relatively rapidly with the maximum windspeed U_m. For higher value for D_c, the orographic cloud depth at the left edge of the domain of integration, ΔP_m is greater. Figure 5.3 shows the maximum condensation rate and cloud liquid water content in the orographic cloud as a function of the windspeed corresponding to case B of figure 5.2. The condensation rate and the cloud liquid water content also increase in a linear fashion with windspeed. It should be noted that for a given topography and temperature and wind profile, the only way to change the condensation rate in the present model is to change the windspeed component perpendicular to the hill. Another result (not shown here) is that the position of maximum enhancement moves slightly towards the hill crest as the windspeed is increased (max. displacement of one grid point, e.g about 5 km).

Diminishing the relative humidity of the basic flow causes a dramatic decrease of orographic enhancement as depicted in figure 5.4. For a strong windspeed (case A), the influence rapidly starts for relative humidity (r.h.) below 0.95 while for relatively weak windspeed (case C), the threshold seems lower (0.88). In any cases, no orographic enhancement takes place for r.h. lower than about 0.82. With a non-saturated flow, condensation will take place only if the orographically-induced upward displacement is greater than the LCL (lifting condensation level). With low r.h., this LCL level is so high that no condensation can occur and consequently no orographic enhancement

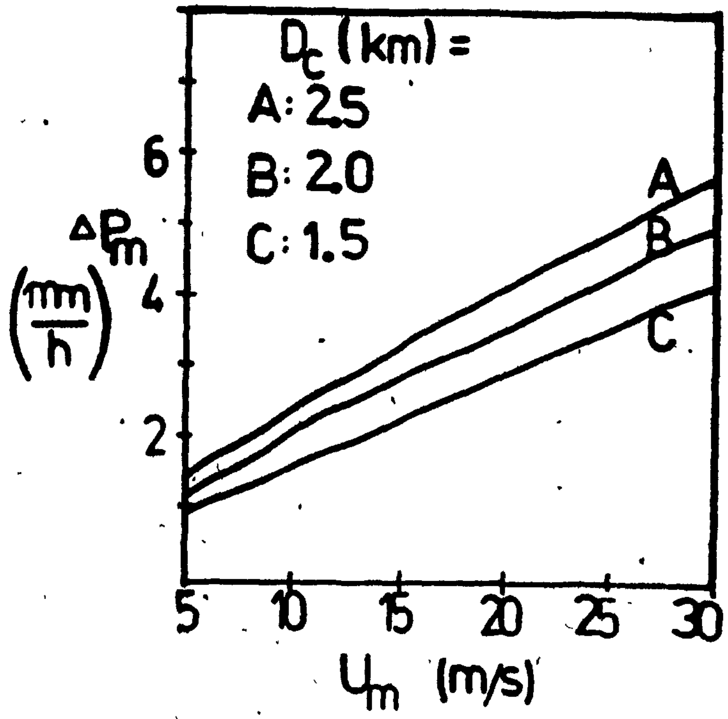

Figure 5.2. Variation of the maximum rainfall rate enhancement ΔP_m with U_m and D_c..

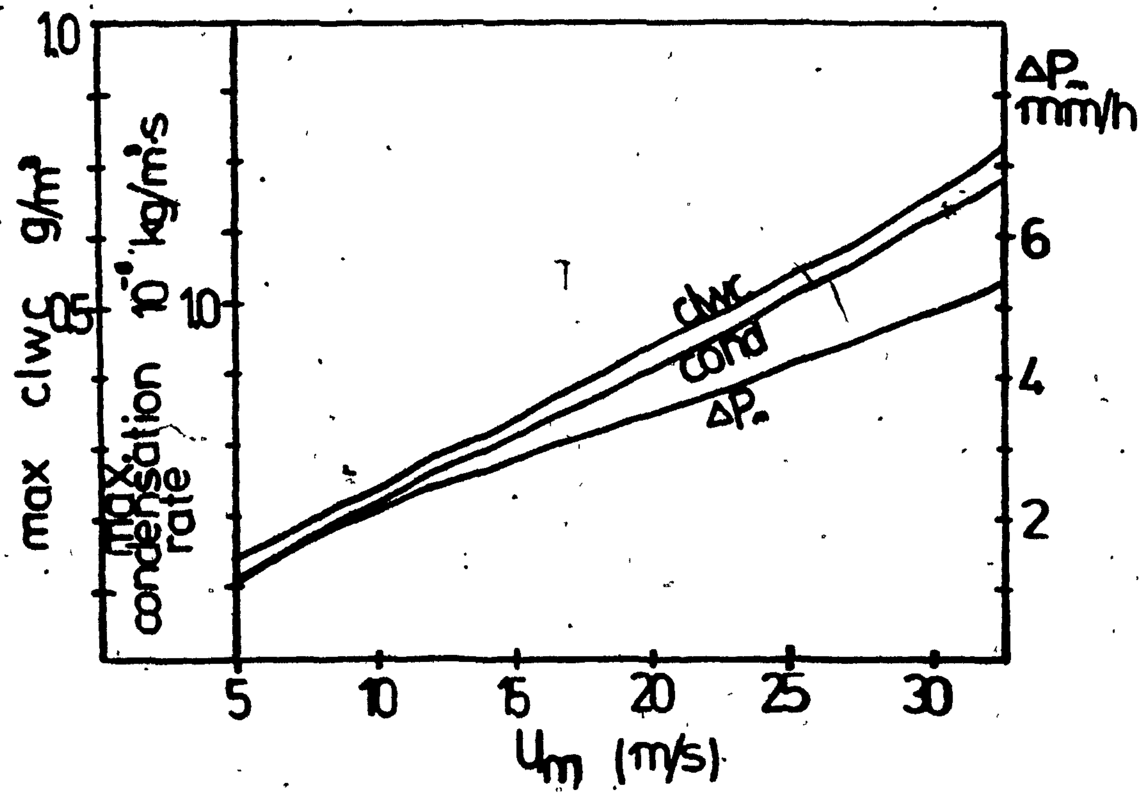

Figure 5.3. Computed maximum cloud water content, condensation rate and orographic enhancement as a function of maximum speed.

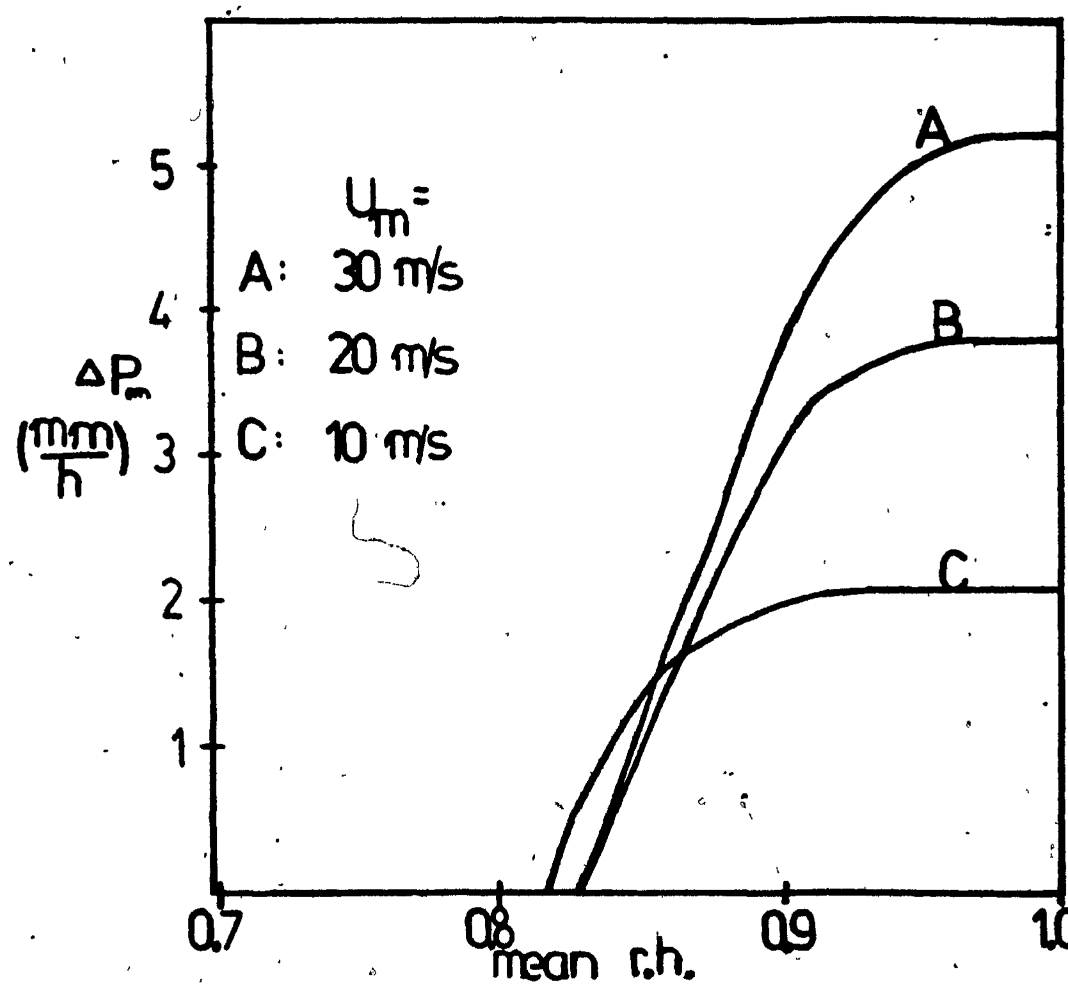

Figure 5.4. Computed maximum rainfall rate enhancement as a function of mean relative humidity (r.h.) of the up-wind flow for different maximum wind speeds.

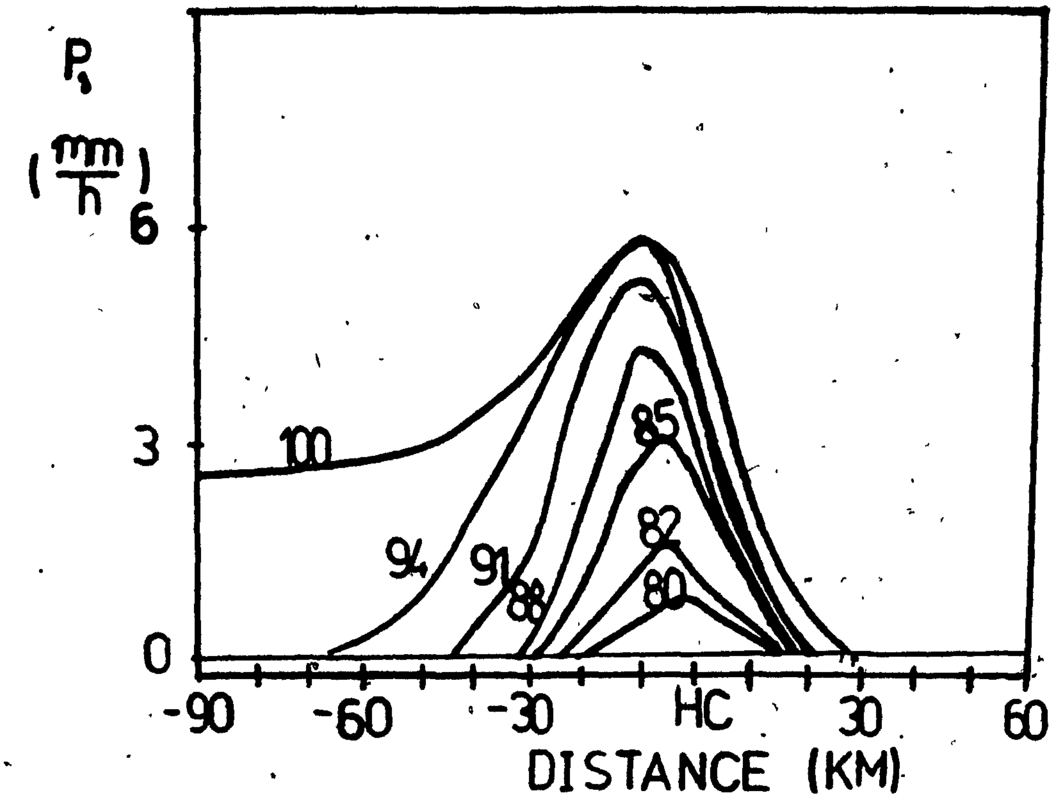

Figure 5.5. Rainfall rate distribution along the topography as a function of relative humidity (%) of the upwind flow.

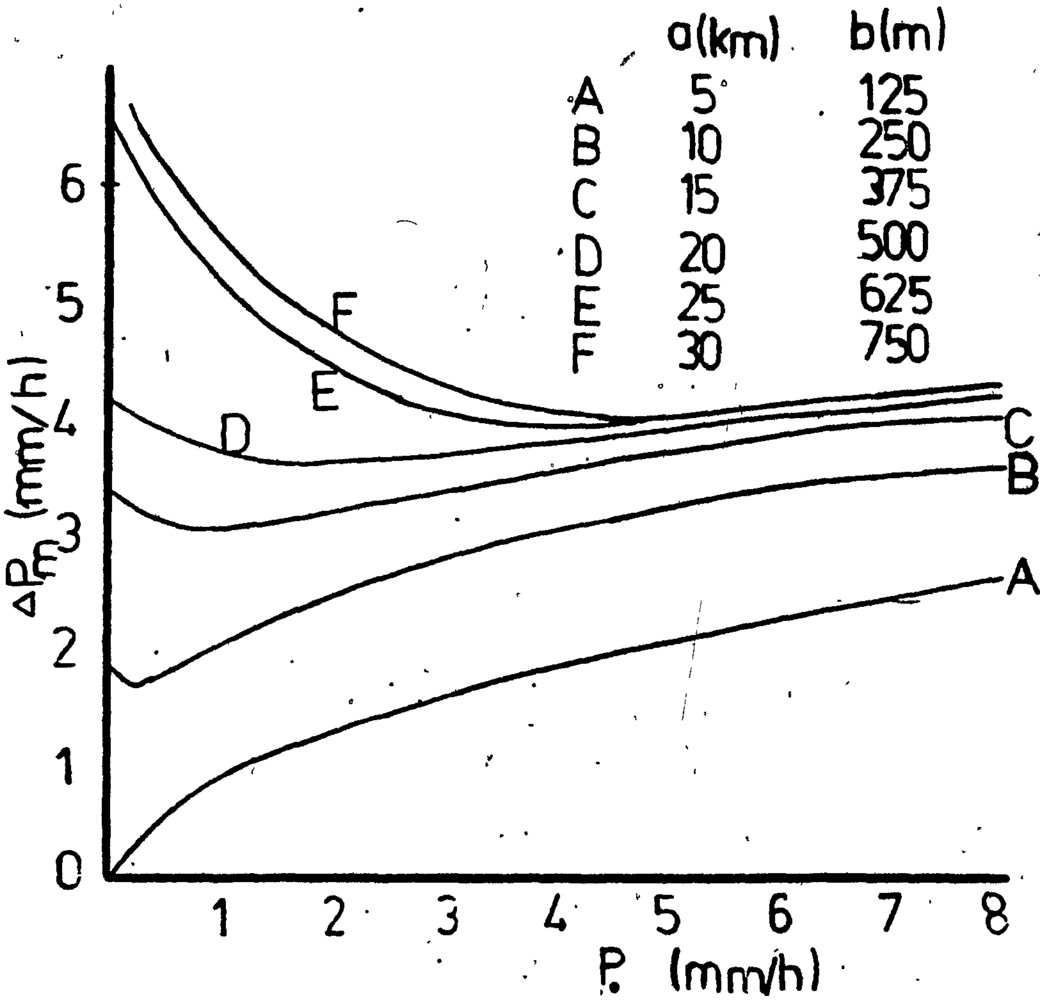

Fig. 5.6 Computed maximum precipitation enhancement ΔP_m as a function of the background rainfall rate P_o.

results. This model feature also produces the following result; with reduced r.h., orographic precipitation is not only reduced but also restricted to near the hill crest,HC,(figure 5.5). Very similar results concerning this sensitivity test was obtained by Bader and Roach (1977).

When the background rainfall rate is increased, the exact sensitivity with respect to ΔP_m depends on the hill size, figure 5.6. For small hills (curve A), ΔP_m depends to a large extent on the background rainfall rate P_o (especially for P_o smaller than 1.0 mm/h) while for large hills (curve E,F), the behaviour of ΔP_m with respect to P_o is entirely different. In fact, the orographic enhancement ΔP_m slightly diminishes for low P_o and slightly increases for high P_o. That means that the maximum rainfall rate P_m ,($P_m = \Delta P_m + P_o$), is about constant or slightly increases with P_o for large hills.

Because P_m is less dependent on P_o , we can say that for large hills (a > 20 km), the seeder-feeder mechanism does not play a major role in orographic rain. However, for small hills (a < 10 km), curve 5.6 shows a stronger dependence of ΔP_m on P_o and consequently the seeding rain is quite important in orographic enhancement in that case. For intermediate hills (10 km $\leq$ a $\leq$ 20 km) a transition of "regime" appears on figure 5.6. Notice that in this experiment the aspect ratio (b/a) is kept constant for all cases A through F. This ensures that the maximum vertical velocity is about the same in each of the cases.

The effect of increasing θ_w is illustrated in figure 5.7 for relatively large hills (a = 20 km). Again, we have a linear dependence with the sensitivity of θ_w on ΔP_m comparable to that

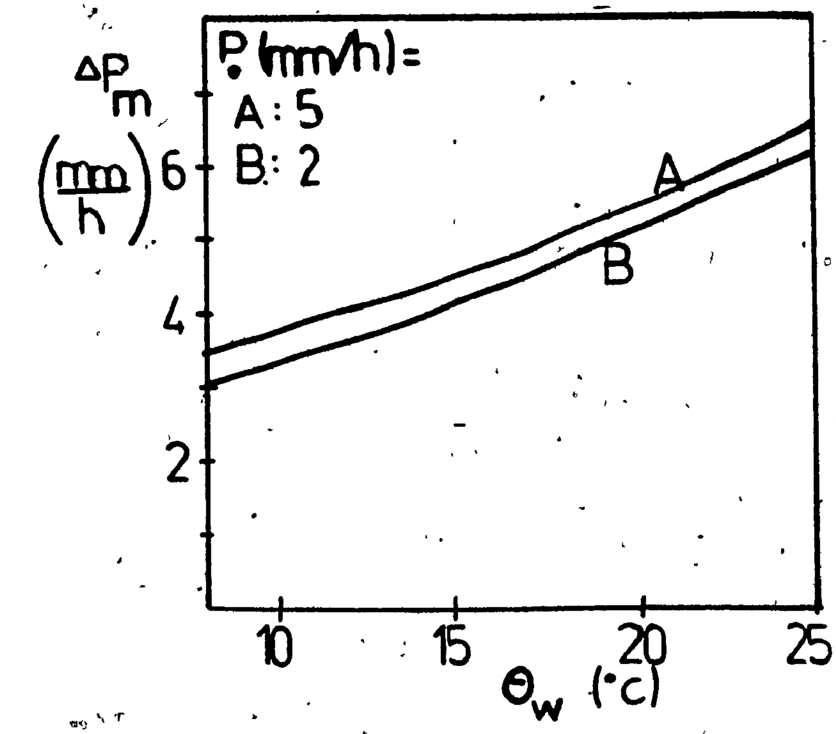

Figure 5.7. Computed maximum orographic enhancement as a function of the wet bulb potential temperature θ_w.

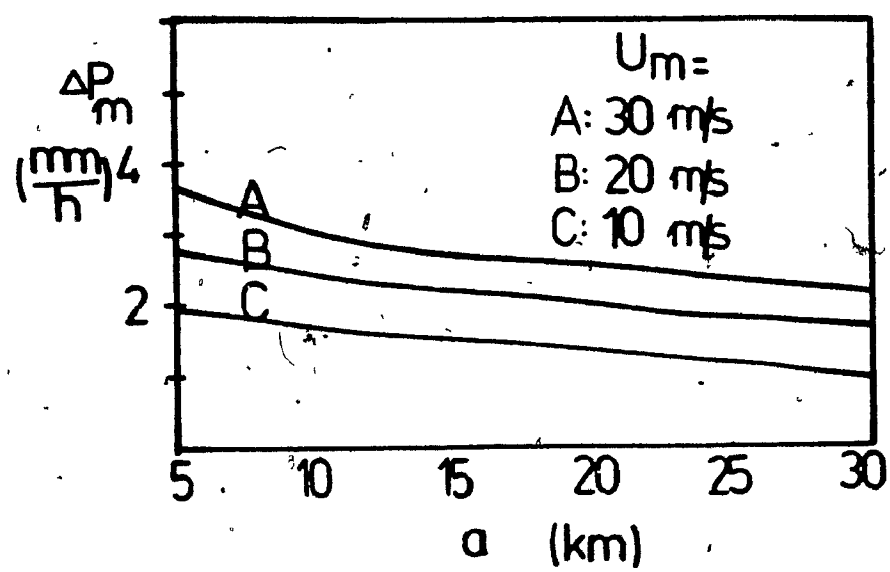

Figure 5.8. Computed maximum rainfall rate enhancement as a function of hill half width "a" for different maximum wind speeds.

of U_m over ΔP_m found in fig. 5.3. Notice that a low θ_w (e.g 8-10° C) is associated with maritime polar airmass in mid-latitudes (fall or winter months) whereas high θ_w (about 25° C) characterizes tropical airmass.

Varying the hill mean width brings about a moderate change in the orographic enhancement ΔP. Reducing "a", the hill half width means a stronger mean slope and obviously stronger vertical velocity which results in a greater ΔP_m. As a matter of fact, the scale for vertical motion is $w = U \cdot \nabla H$ where ∇H is the gradient of topography along x. For a bell-shaped ridge (equation 4.18) at $x=-a$, the vertical velocity is the order of $w = U \cdot 2b/a$, which is inversely proportional to a. For a small height ($b = 250$ m), the dependence of "a" on ΔP_m is shown in fig.5.8 for 3 different wind speeds.

Testing the influence of varying l_1, l_2 and H on the orographic enhancement is slightly complicated by the fact that these parameters are related to the basic flow, U(z), through equation 5.4. For example, in order to isolate the effect of changing H alone without changing the surface windspeed, it is necessary to select l_1 in such a way that the surface windspeed U_0 remains constant. Table 5.2 depicts results obtained with the present model (model P) over a wide range of H (cases A,B,C,D) after taking into account the above restriction for l_1 and H. Both the maximum vertical velocity aloft (W_m) and near the ground (W_{gm}) and the maximum ground rainfall rate (P_{gm}) are compared with results obtained by using the potential flow theory (model PF, given by equation 4.11) for the treatment of the airflow over the topography. In each of the cases, the wind profile is obtained by equation 5.4 and given in figure 5.9.

The comparison shows that the potential flow solution leads to an underestimation of the orographically-induced vertical velocity and orographic enhancement (cases A,B,C). Moreover, one can see that a low level windspeed maximum (at level $H=\pi/6$ or $\pi/3$) with strong rate of decrease of the wind below it (high l_1) and low curvature above (low l_2) will give, with the present model,the highest value for vertical velocity and maximum rainfall rate (case A,E). Any of the above features which is missing will give less ascent. For example, both high level jet case (case D,fig. 5.9) or a situation characterized by a strong curvature above the jet (case F) will give lower vertical velocities and hence lower rainfall rate enhancement. Notice that in all cases A through F, the maximum wind speed and surface windspeed are the same (fig. 5.9).

Figure 5.10 compares for case A, the vertical velocity profile both computed by model P and model PF. Notice that the potential flow solution gives lower vertical velocities and is symmetrical with respect to the hill crest. Figure 5.11 reproduces the ground rainfall rate profile P_0 as a function of distance for each of the cases A,B,C,D obtained with model P and case A again but with model PF. It clearly shows that the wind structure is quite important in determining the rainfall rate enhancement.

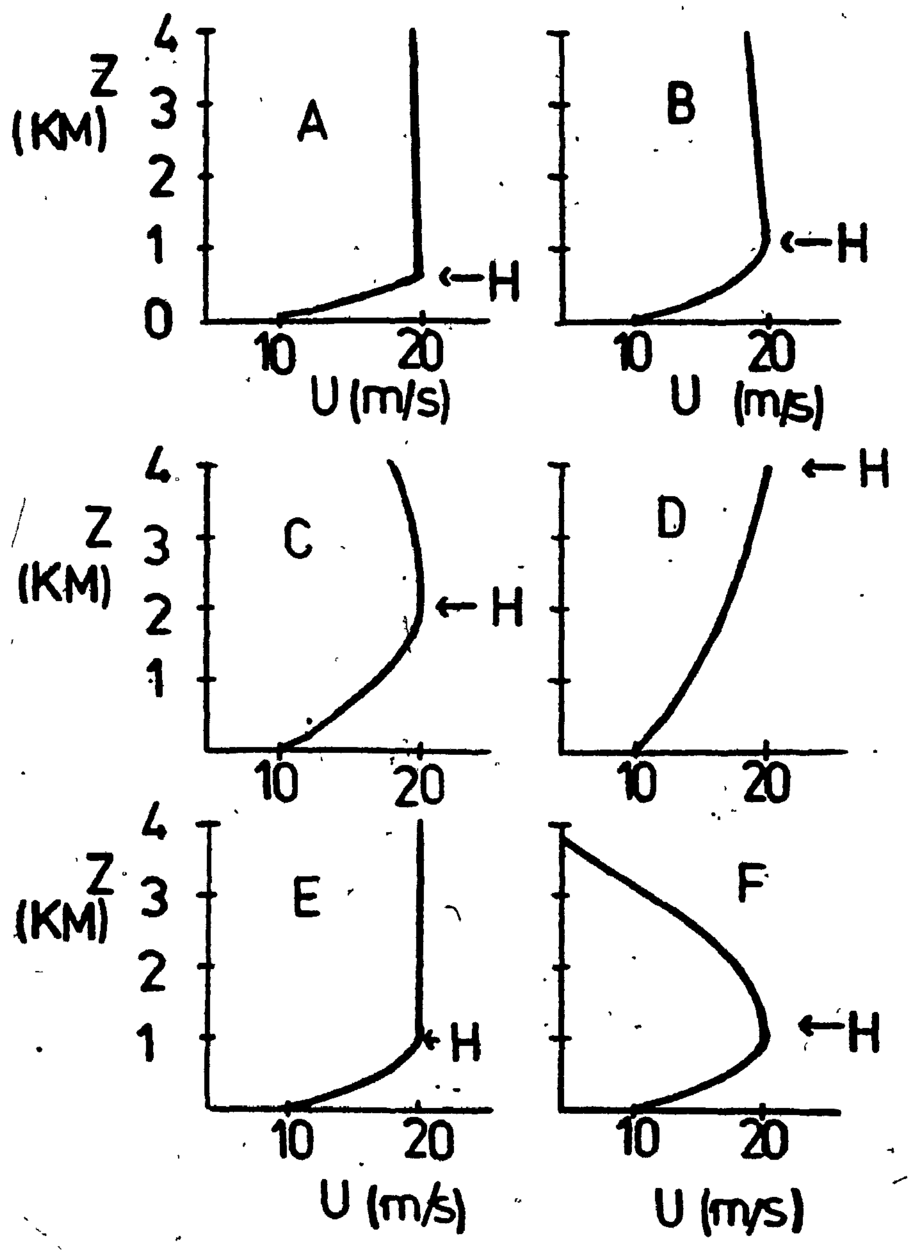

Figure 5.9. Wind profiles utilized for cases A,B,C,D,E, and F.

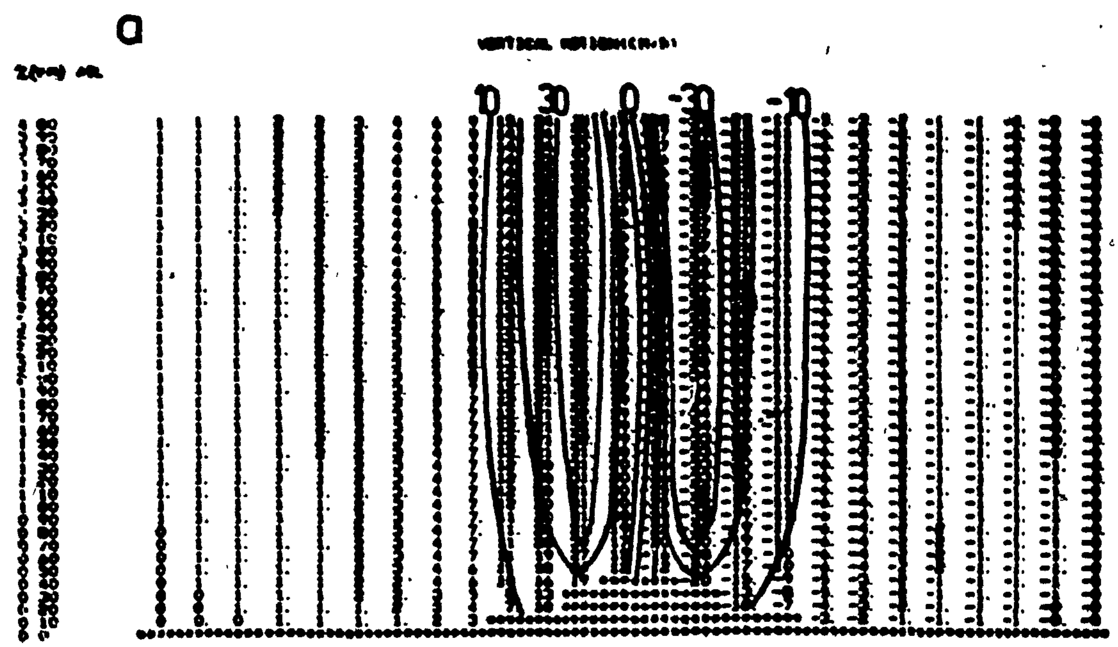

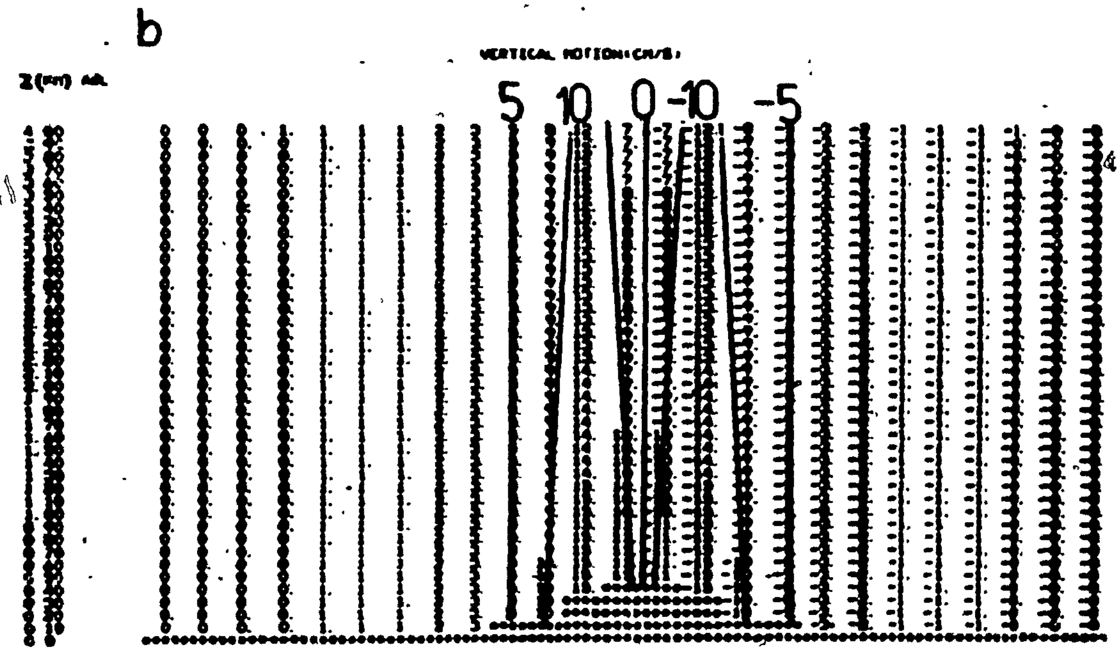

Figure 5.10. Vertical velocity distribution computed by a) the present model, b) the potential flow model.

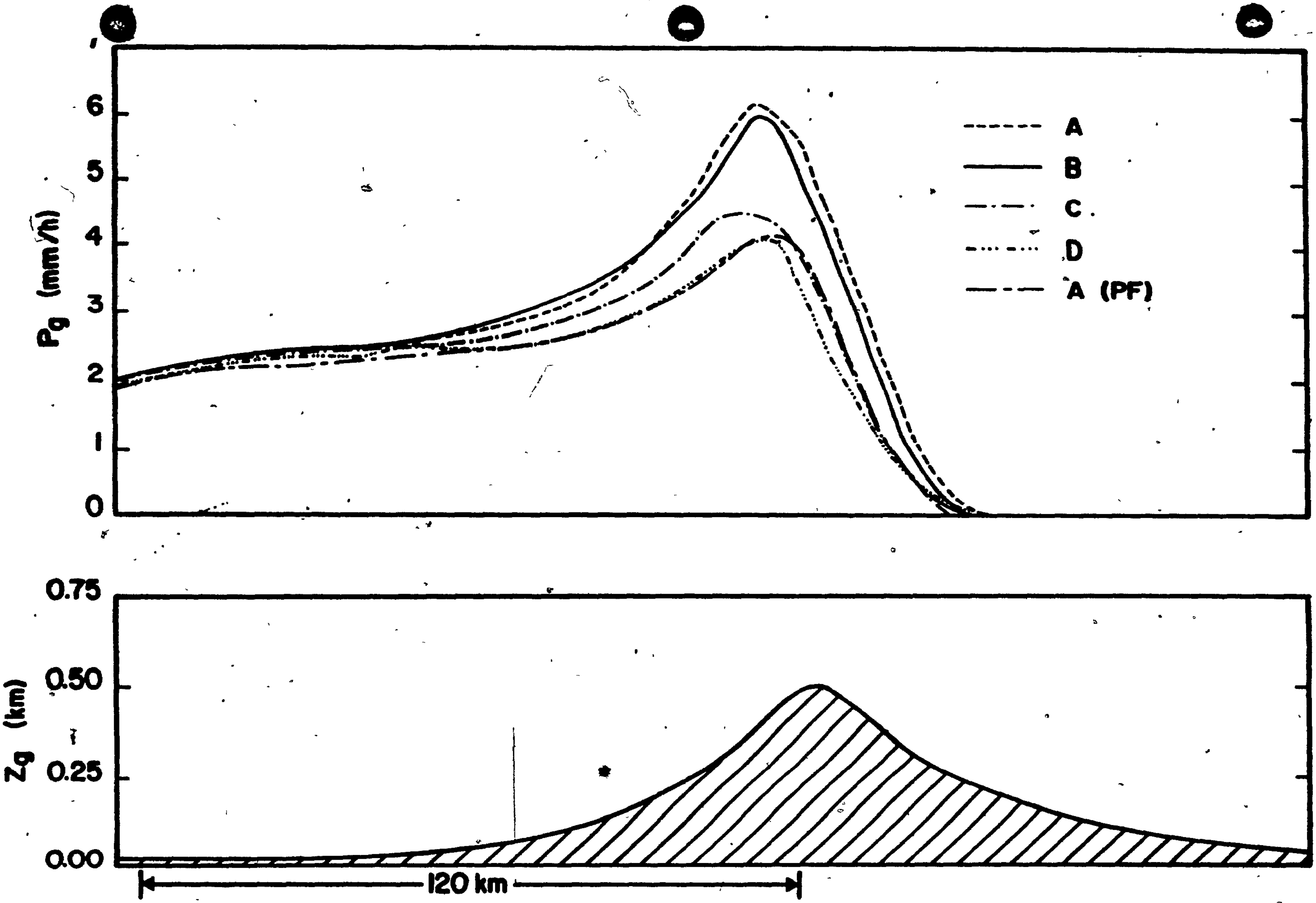

Figure 5.11. Computed surface rainfall rate distribution as a function of distance along the topography for cases A,B,C,D and for case A ,using the potential flow model.

case	model	l_1 km^{-1}	l_2 km^{-1}	H km	W_{max} cm/s	W_{1km} cm/s	P_{1km} mm/h
A	P	2	1/16	$\pi/6$	33	19	6.3
	PF				15	15	4.0
B	P	1	1/8	$\pi/3$	29	17	5.9
	PF				15	15	3.9
C	P	1/2	1/4	$2\pi/3$	17	16	4.5
	PF				15	15	4.0
D	P	1/4	1/2	$4\pi/3$	15	15	3.9
	PF				15	15	4.1
E	P	1	1/100	$\pi/3$	37	17	6.3
	PF				15	15	3.9
F	P	1	1/2	$\pi/3$	17	16	4.2
	PF				15	15	4.0

Table 5.2: Results of sensitivity experiments on l and H obtained by the present model (P) and the potential flow solution (PF).

The set of cases B,E,F tests the effect of varying only l_2 (curvature above the level H). The results show that only for strong curvature above a low level jet (case F), orographic enhancement is low and comparable to potential flow solution.

The results of testing l_1,l_2 and H seem to agree with observations. As a matter of fact, as discussed in chapter 2, low level jet situation are often found in connection with heavy orographic rainfall and it is thought that the treatment of the dynamics adopted in the present model help understanding the influence of the wind profile on the vertical velocity. The potential flow solution ignores the influence of the vertical variation of the wind on the strength of vertical motion and its therefore not recommended in situations of low-level jets.

In a model which contains constants of parametrization and/or boundary conditions which are more or less arbitrarly defined, the effect of changing those on the model response need to be examined. We have seen in equation 3.28 that two constants α and η relate the rainfall rate to the rainwater content. Sensitivity test are done in the range of values for α and η given in chapter 3. Results of table 5.3 indicate an important sensitivity of the orographic enhancement ΔP_m, as those constants are changed, only for low values of α and η (case 4). However, for orographic rain, α and η are found relatively high and probably closer to values given in case 2 of table 5.3 where the sensitivity is reduced.

Table 5.3: Effect of varying α and η.

	α	η	ΔP_m (mm/h)
1.	0.100	1.00	3.0
2.	0.089	0.94	4.1
3.	0.071	0.89	5.9
4.	0.052	0.84	9.9

Sensitivity test was performed on autoconversion threshold (constant K_2 in equation 3.23). Results show that for basic input conditions of the present model, the effect of varying k_2 on the orographic enhancement is very small (see table 5.4).

Table 5.4: Effect of varying the autoconversion threshold

	k_1 (g/m³)	ΔP_m (mm/h)
1.	0.3	4.2
2.	0.5	4.1
3.	1.0	4.1

Simarly, changing the boundary condition for the cloud liquid water content does not significantly affect much of the orographic enhancement (table 5.5). However, for QC_0 higher than 0.3 g/m³, the computed rainfall distribution near that boundary might be perturbated. However, disturbances introduced by changing QC_0 at the lateral boundary does not seriously contaminate the central area of the grid.

Table 5.5: Effect of varying QC_0

	QC_0 (g/m³)	ΔP_m (mm/h)
1.	0.0	4.2
2.	0.1	4.1
3.	0.3	4.5

Finally, the last sensitivity test performed on the present model is depicted in table 5.6. It consists of changing the space steps utilized in numerical computations and examine the effect on ΔP_m. It is found that very special set of values Δx and Δz make the solution numerically stable (case 2). Ounce this set is obtained the model can be run with other values of Δx and Δz provided the ratio $\Delta x/\Delta z$ remains the same. For two experiments with different space steps, but having the same ratio $\Delta x/\Delta z$, (case 2 and 4), the orographic enhancement does not vary in a significant way.

5.2 Typical behaviour of the present model

The general behaviour of the model is illustrated by a typical simulation. Parameters are those of the basic input conditions already given earlier. The basic state atmosphere values for temperature, pressure, density and wind profile are given in figure 5.12. Other quantities represent the water vapor mixing ratio Q_v , Q_{vs} the saturated value of Q_v , the background cloud water mixing ratio QC_0 and rainwater mixing ratio QR_0.

Table 5.6: Effect of varying space steps

	Δx (km)	Δz (m)	ΔP_m (mm/h)	comments
1.	1.0	100	-	unstable
2.	2.5	100	4.2	stable
3.	5.0	100	5.4	stable but not realistic on the lee side
4.	5.0	200	3.7	stable

A typical distribution for the vertical motion computed by the present model is given in figure 5.13. The maximum vertical velocity is located a short distance upwind near the maximum slope and ~~at~~ level z= 1.4 km which slightly lies above the jet level (at $z=\pi/3$ km). One can notice that over the hill crest the vertical velocity is relatively weak and changes its sign above 1.8 km. Also, on the upwind side, within the domain of integration, the vertical velocity slowly increases with height except close to hill crest where the maximum value is found at lower altitudes. Figure 5.13 also reveals asymmetrical pattern.

with respect to the hill crest although the topography profile is perfectly symmetrical (bell-shaped ridge).

Figure 5.14 presents the upward vertical displacement which is found to increase with z on the upwind side and decrease on the lee side. It represents at a given level the airflow vertical displacement due to the topography.

The orographically-induced condensation rate computed by the present model appears on figure 5.15. The pattern follows closely that of the vertical velocity since condensation rate are closely linked to w (see equation 3.22). Since the model does not calculate condensation rates in the seeder cloud (mainly above 3 km in this example), the value zero is output whereas the true condensation rate due to the topography is not necessarily zero. This is an approximation which is, however, consistent with the fact that most of water vapor is found in the low levels and that drier air above the orographic cloud leads to very little condensation at higher levels. This is supported by Bergeron (1965) who concludes that the main modeling of the rainfall distribution must occur within the lowest air-layer of 0.5 to 1 km depth. Therefore, an orographic cloud of 2.5 km depth used in this model is thought to be sufficient and neglecting orographically-induced condensation higher above will not affect main results too drastically.

The maximum cloud water content in this experiment is about 0.38 g/m³ and this maximum is located at x=-5 km and near the orographic cloud top (fig. 5.16). The constant value of 0.1 g/m³ represents the physical delimitation of the seeder cloud which is located above the feeder cloud. Cloud evaporation takes place on the lee side to reduce the cloud water content (CLWC) down to zero.

The corresponding vertical distribution of orographic rainfall rate is depicted in figure 5.17. Above the top of the domain of integration, the background rainfall rate is constant (P_o =2 mm/h) and again delineates the physical extent of the seeder cloud (located mainly above 2.7 km). The increase of rainfall rate appears quite nicely here on the upwind side between x=0 and x=-a (a= 20 km). Evaporation of rain on the lee side rapidly reduces the rainfall rate down to zero. One can notice that on the lowest 1.5 km above the hill, about 75 percent of the orographic enhancement takes place which is an agreement with radar and raingauge observations by Hill et al (1981) and with the conceptual model of seeder-feeder mechanism advanced by Bergeron (1965).

An interesting quantity to evaluate is the efficiency of precipitation (or efficiency of washout) of the orographic cloud. With the present formulation of the seeder-feeder mechanism, this efficiency (EFP) is written

$$EFP = \frac{P_\tau}{C_\tau} \qquad (5.5)$$

where

$$C = \int_{-\infty}^{0}\int_{0}^{z_\tau} COND\, dz\, dx \qquad (5.6)$$

represents the rate of condensation per unit width perpendicular to the airflow in the orographic cloud (in kg/m s) and

$$P_t = \int_{-\infty}^{0} (P_s - P_o)\, dx \tag{5.7}$$

is the total orographic component of rainfall rate per unit width at the ground. With P_s and P_o expressed in units of $kg/m^2 \cdot s$, P_t given in units of $kg/m \cdot s$, EFP is then given as a percentage. Notice that z_t in the above equations is the top of the feeder cloud evaluated at each position x. Integration limits in the horizontal direction are from $-\infty$ up to the hill crest ($x=0$). However, the actual left edge of the domain is finite and taken as $-x_o$.

Calculations based on equations 5.5 through 5.7 show that for low hills (curve A in figure 5.18), EFP increases very rapidly with the background rainfall rate whereas for longer hills (curve E,F) the sensitivity of EFP with respect to P_o is significantly less. Curves B,C and D depict intermediate cases (moderate hill dimensions). An important implication of figure 5.18 is that the seeder-feeder formulation seems more crucial for small hills than for large hills because of the high sensitivity of EFP with respect to P_o. In other words, specifying the background rainfall rate is not as important for large hills (say $a > 20$ km) as it is for small and moderate hills ($a < 20$ km). This behaviour appears in agreement with various cloud experiments and observations reported in Smith (1979). This is also in line with results of figure 5.6.

The efficiency of precipitation as the maximum windspeed U_m is increased is displayed in figure 5.19. It shows a decrease of EFP as U_m increases which is due to a faster increase of the

BASIC STATE ATMOSPHERE

Z(M)	T(DEG K)	WIND(M/S)	RO(KG/M**3)	P(MB)	QV(G/G)	QVS(G/G)	QC(G/G)	QR(G/G)
4000	264.4	18.7	0.8	601	0.003530	0.003530	0.0001272	0.0002174
3900	267.1	18.7	0.8	604	0.003765	0.003765	[illegible]	[illegible]
3800	267.7	18.8	0.8	617	0.004103	0.004103	[illegible]	[illegible]
3700	268.3	18.8	0.8	[illegible]	[illegible]	[illegible]	[illegible]	[illegible]
3600	[illegible]	19.0	0.8	634	[illegible]	[illegible]	[illegible]	[illegible]
3500	268.9	[illegible]	0.8	643	0.004354	0.004354	[illegible]	[illegible]
3400	269.5	[illegible]	0.8	651	0.004678	0.004678	[illegible]	[illegible]
3300	270.1	[illegible]	0.8	660	0.004823	0.004823	[illegible]	[illegible]
3200	270.7	19.3	0.8	669	0.004973	0.004973	[illegible]	[illegible]
3100	[illegible]	19.3	0.9	678	0.005124	0.005124	[illegible]	[illegible]
3000	[illegible]	19.3	0.9	687	0.005278	0.005278	[illegible]	[illegible]
2900	[illegible]	[illegible]	0.9	695	0.005433	0.005433	[illegible]	[illegible]
2800	273.4	19.5	0.9	703	0.005540	0.005540	0.0001114	[illegible]
2700	273.7	19.5	0.9	715	0.005749	0.005749	0.0001101	[illegible]
2600	274.5	19.6	0.9	724	0.005910	0.005910	[illegible]	[illegible]
2500	274.3	19.6	0.9	734	0.006072	0.006072	0.0001070	[illegible]
2400	275.4	19.7	0.9	743	0.006236	0.006236	[illegible]	[illegible]
2300	275.9	19.7	1.0	753	0.006403	0.006403	[illegible]	[illegible]
2200	276.5	19.8	1.0	762	0.006569	0.006569	[illegible]	[illegible]
2100	277.0	19.8	1.0	772	0.006737	0.006737	[illegible]	[illegible]
2000	277.6	19.9	1.0	783	0.006907	0.006907	0.0001031	[illegible]
1900	278.1	19.9	1.0	792	0.007079	0.007079	0.0001010	[illegible]
1800	278.6	19.9	1.0	802	0.007252	0.007252	[illegible]	[illegible]
1700	279.2	19.9	1.0	812	0.007427	0.007427	[illegible]	[illegible]
1600	279.7	19.9	1.0	823	0.007603	0.007603	[illegible]	[illegible]
1500	280.3	20.0	1.0	833	0.007780	0.007780	[illegible]	[illegible]
1400	[illegible]	20.0	1.1	844	0.007959	0.007959	[illegible]	[illegible]
1300	[illegible]	20.0	1.1	854	0.008139	0.008139	[illegible]	0.0001617
1200	[illegible]	20.0	1.1	[illegible]	0.008321	0.008321	[illegible]	[illegible]
1100	[illegible]	20.0	1.1	873	0.008504	0.008504	[illegible]	[illegible]
1000	[illegible]	20.0	1.1	[illegible]	[illegible]	[illegible]	[illegible]	[illegible]
900	[illegible]	20.0	1.1	897	0.008873	0.008873	[illegible]	[illegible]
800	[illegible]	[illegible]	1.1	[illegible]	[illegible]	[illegible]	[illegible]	[illegible]
700	[illegible]	[illegible]	1.1	[illegible]	[illegible]	[illegible]	[illegible]	[illegible]
600	[illegible]	[illegible]	1.1	931	0.009437	0.009437	[illegible]	[illegible]
500	285.[illegible]	[illegible]	1.1	942	[illegible]	[illegible]	[illegible]	[illegible]
400	[illegible]	[illegible]	1.1	953	0.009817	0.009817	[illegible]	[illegible]
300	[illegible]	[illegible]	1.1	965	0.010011	0.010011	[illegible]	[illegible]
200	287.[illegible]	13.[illegible]	1.2	976	0.010205	0.010205	[illegible]	[illegible]
100	[illegible]	11.6	1.2	988	0.010400	0.010400	0.0000834	0.0001427
[illegible]	[illegible].1	10.0	1.2	1000	0.0105[illegible]	0.010546	0.0000827	0.0001412

Figure 5.12. Typical basic state atmosphere.

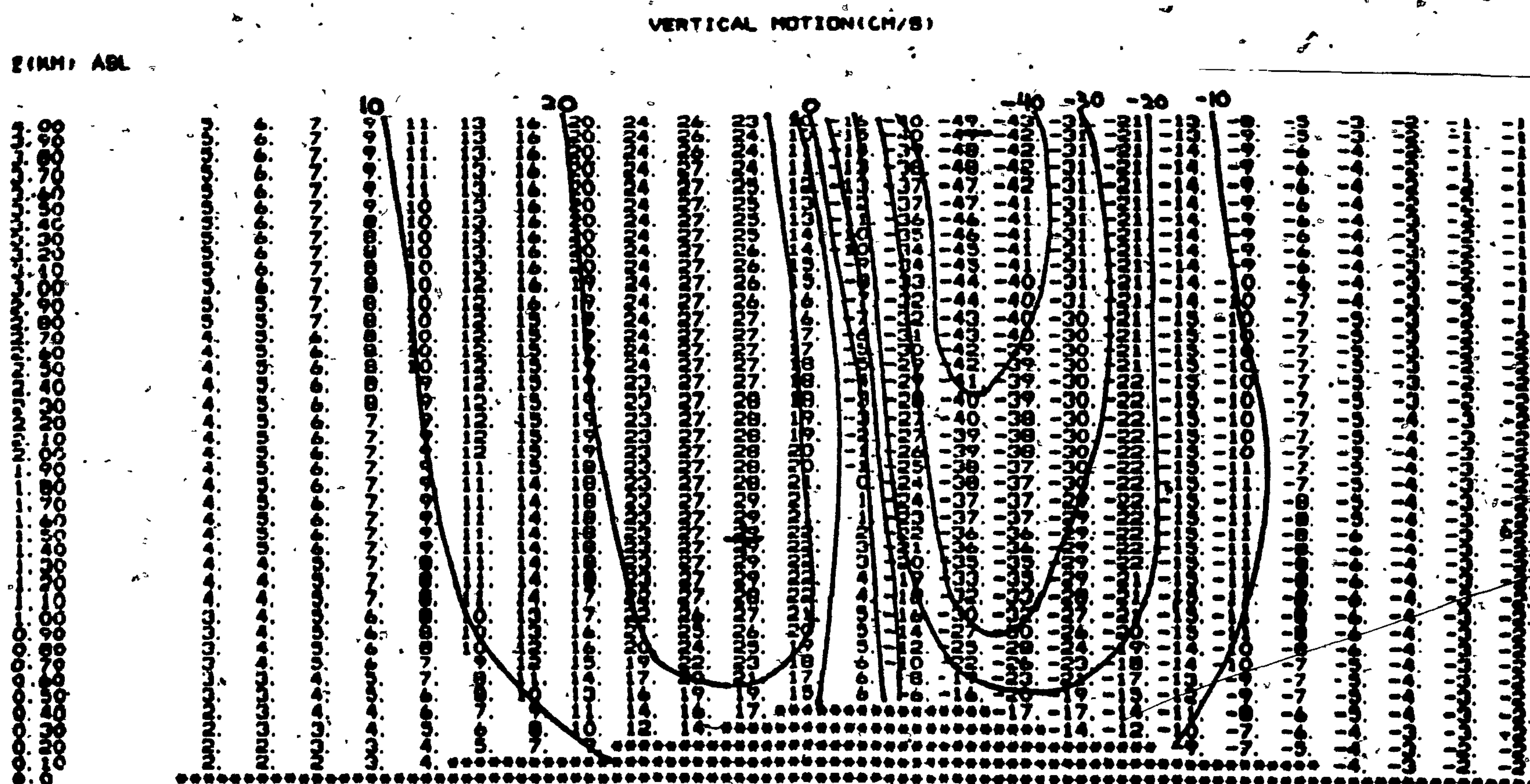

Figure 5.13. Computed vertical velocity distribution. ($\bar{U}_{\infty}$= 20 m/s)

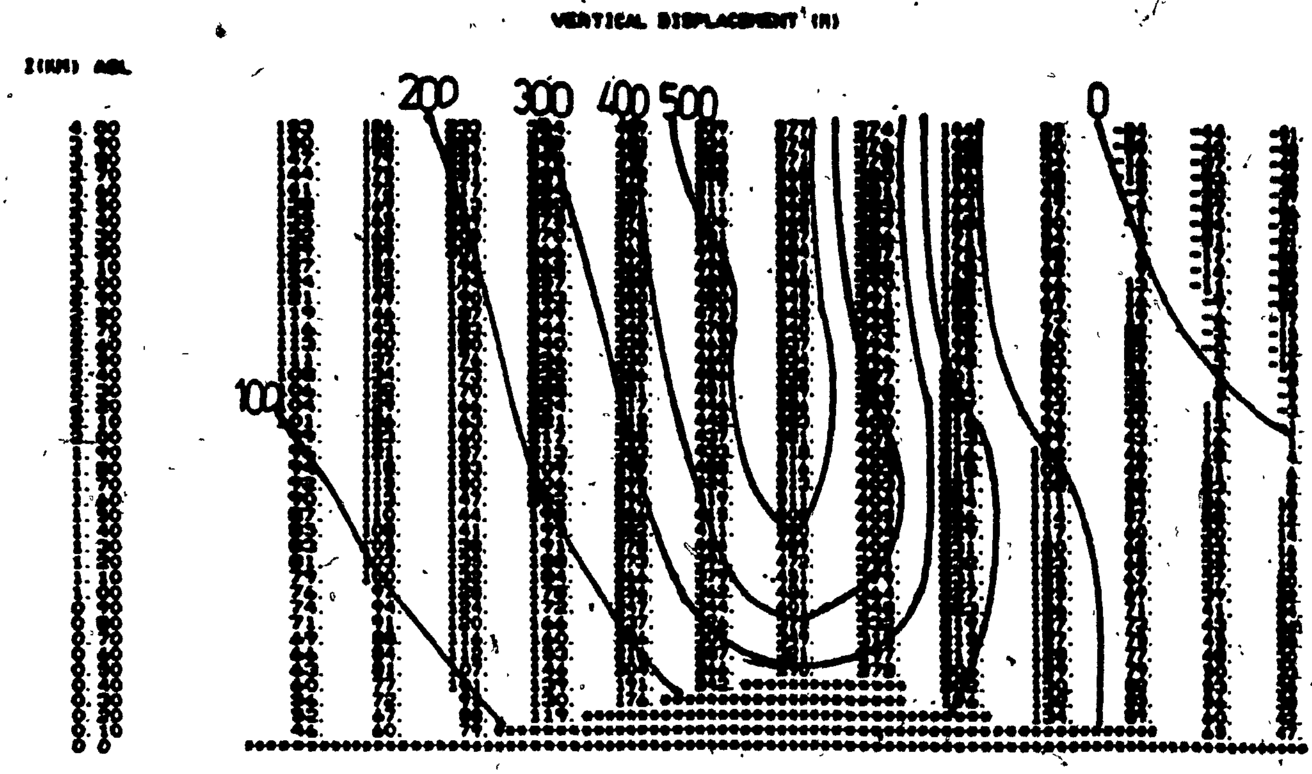

Figure 5.14. Computed vertical displacement distribution.

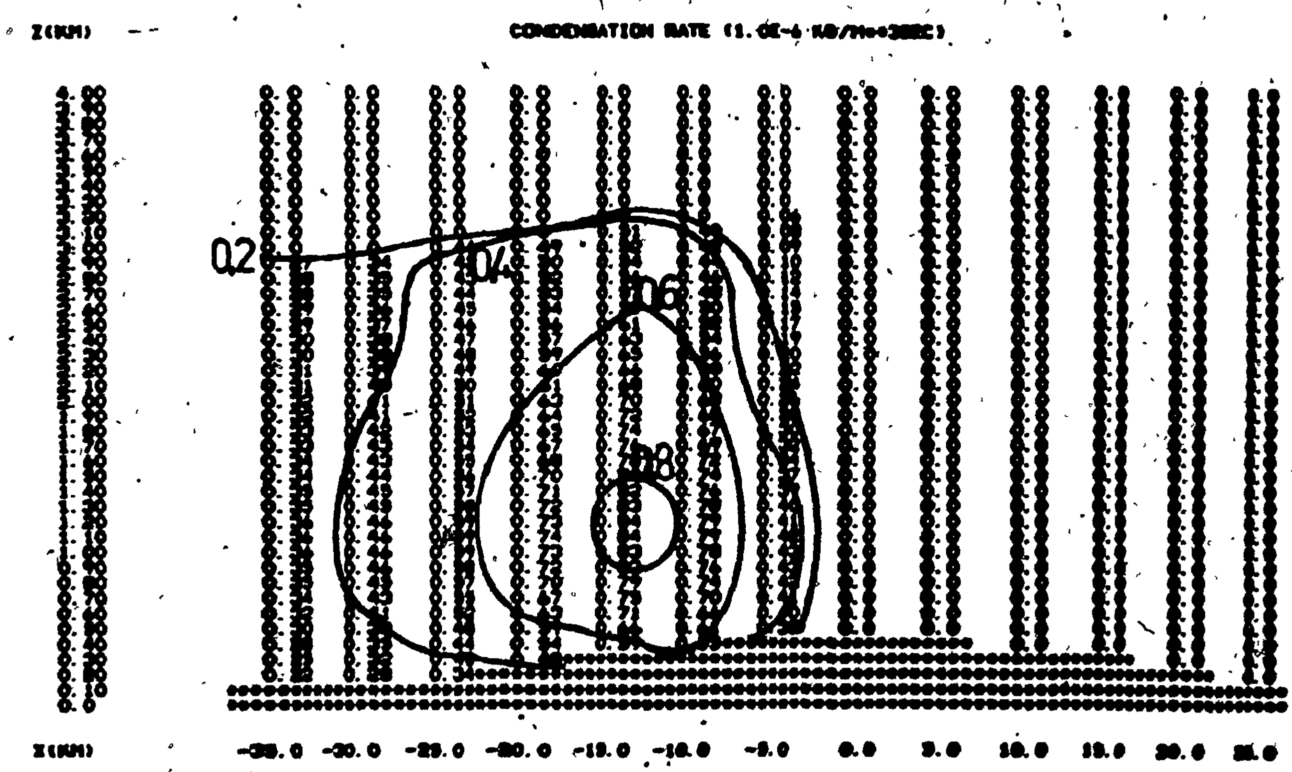

Figure 5.15. Computed orographically-induced condensation rate.

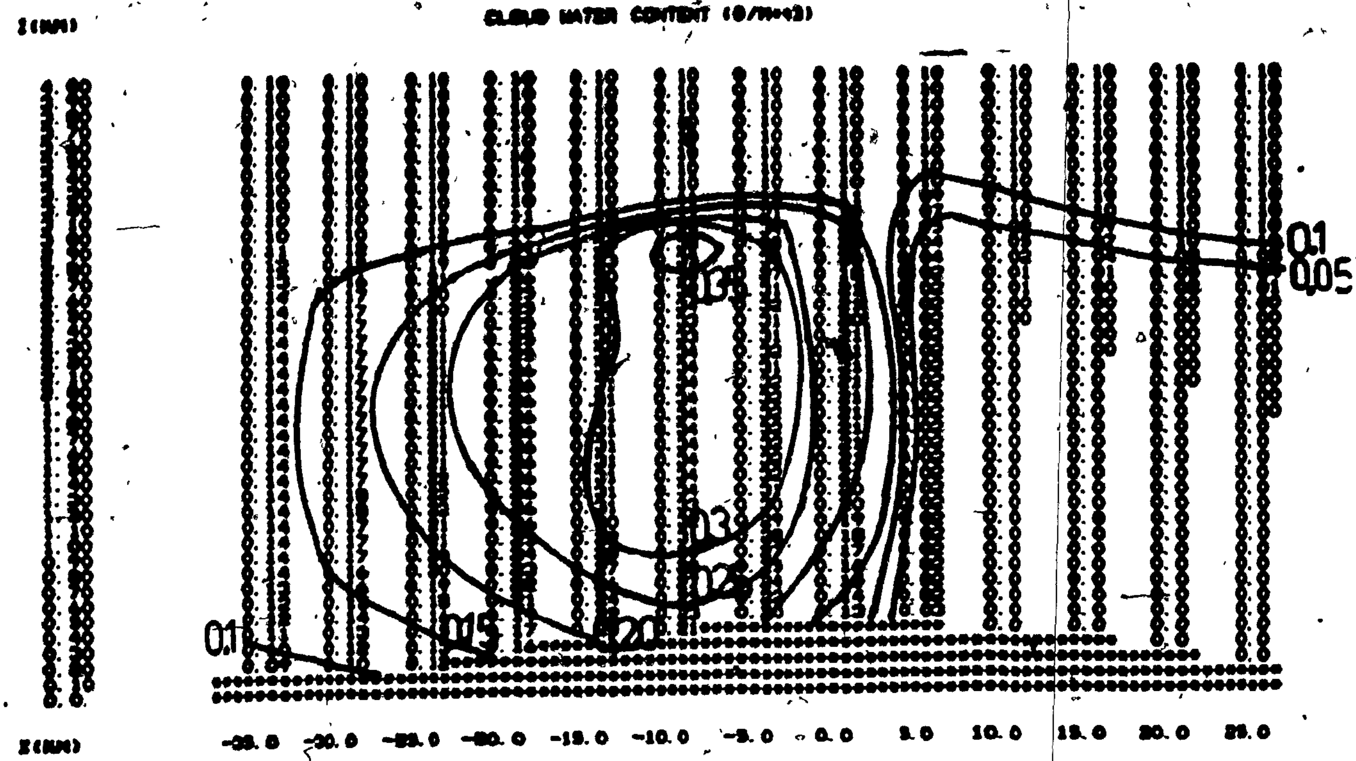

Figure 5.16. Computed distribution of cloud water content.

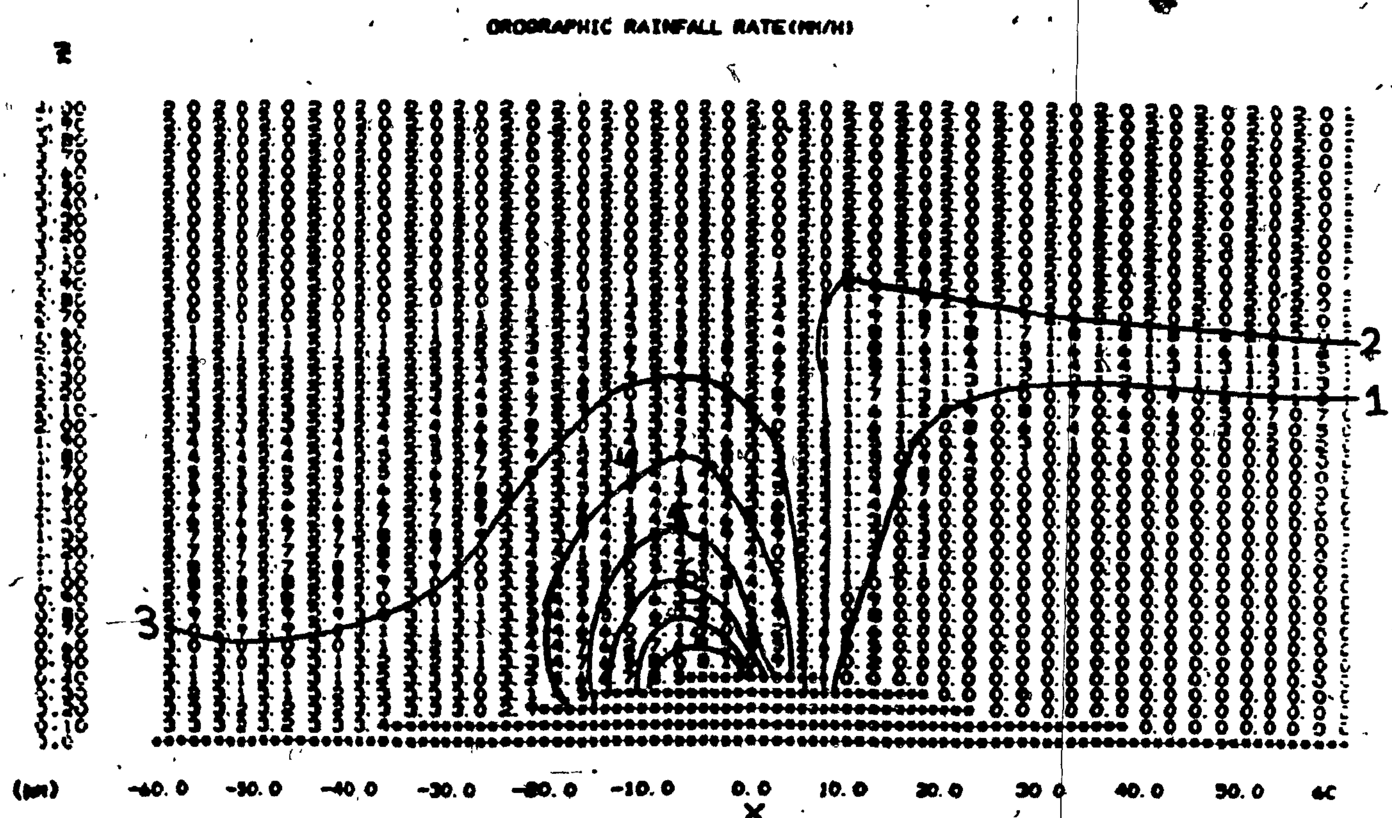

Figure 5.17. Computed distribution of orographic rainfall.

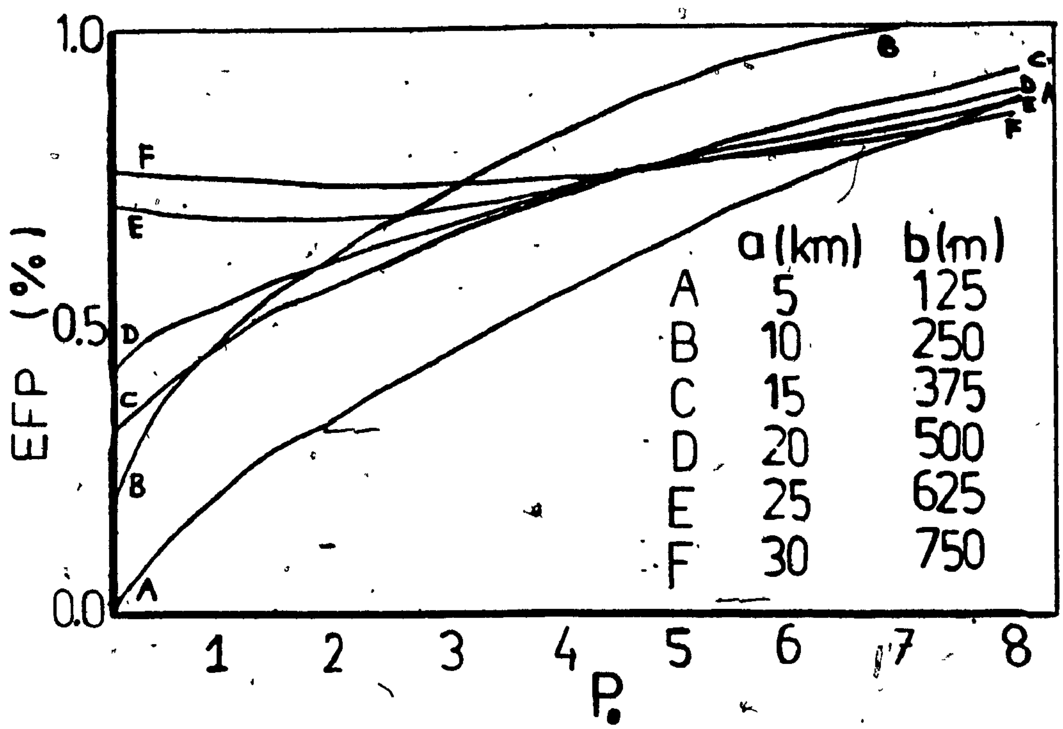

Fig. 5.18 Efficiency of precipitation (EFP) as a function of the background rainfall rate, P_o, for different hill dimensions.

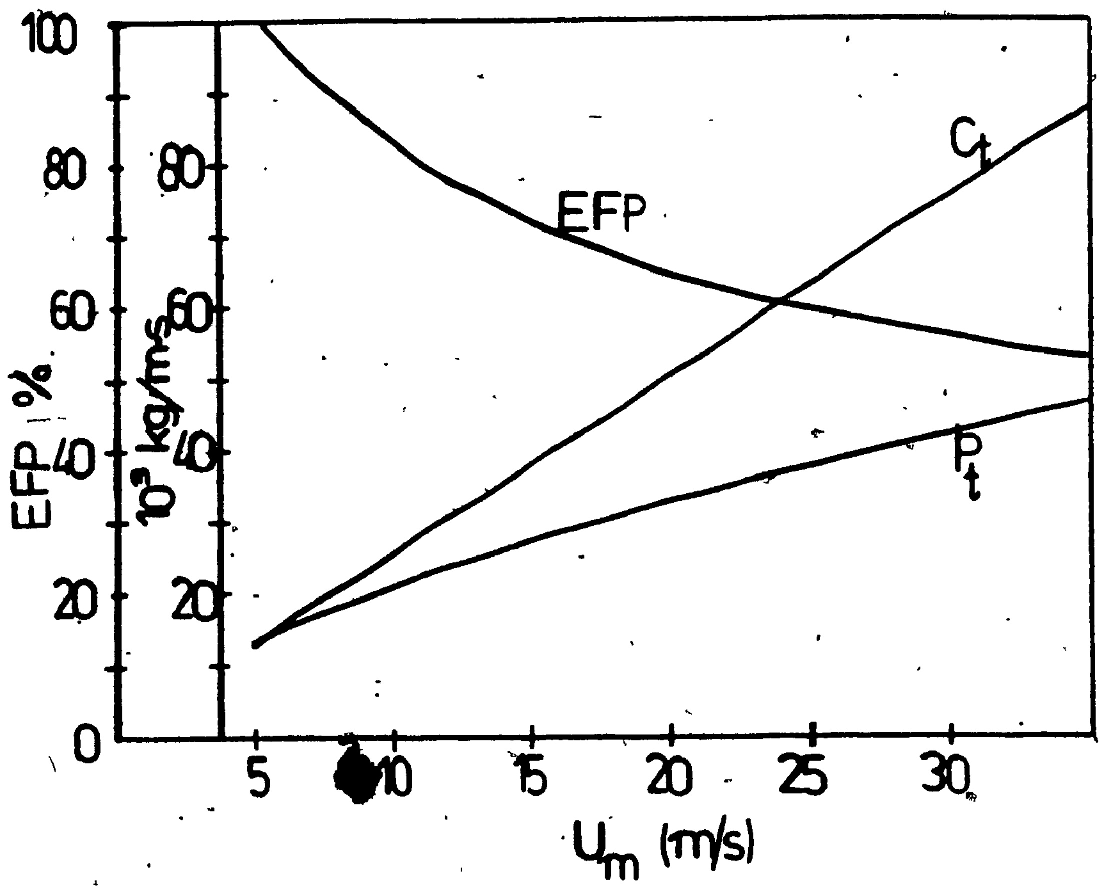

Fig. 5.19 Efficiency of precipitation (EFP) as a function of the maximum wind speed. P_t is the integrated component of the rainfall rate and C_t, the integrated component of the condensation rate.

condensation rate per unit width, C_t, than that for P_t, the total orographic component of rainfall rate per unit width at the ground.

The hill dimension is expected to significantly affect the position (x_m) where the maximum rainfall rate occurs at the ground as depicted in table 5.7.

case	hill dimensions	P = 0.5 mm/h x_m (km)	x_m/a	P = 5.0 mm/h x_m (km)	x_m/a
A	a = 5 km b = 125 m	0.0	0.0	-1.0	-0.2
C	a= 15 km b= 375 m	-2.5	-0.17	-5.0	-0.33
F	a= 30 km b= 750 m	-7.5	-0.25	-11.0	-0.37

Table 5.7
Position of maximum precipitation rate as a function of hill dimensions for 2 different P_o.

For small hills (case A), the position of the maximum orographic enhancement is located near the crest of the hills (at a distance x_m= 0 for P_o =0.5 mm/h and x_m=-1.0 km for P_o = 5.0 mm/h). For moderate hill (case C), it occurs at a location slightly more on the upwind side. Finally, for larger hills, (case F), the maximum rainfall rate occurs on the upwind side at a distance greater than those of the two above cases. The present model hence simulates the fact that for bigger hills and higher background rainfall rate, the location of the maximum enhancement is moved upwind.

Note that the maximum vertical velocity and its location are similar in each of the experiments A through F because of the same aspect ratio (b/a) of the hill. Therefore, the location of x_m probably does not depend on dynamical considerations. In fact, the position x_m of the peak in the rainfall rate predominantly depends whether or not drift effects are important. Carruthers and Choularton (1983) explain that if the half length a is such that

$$a < C_b \bar{U} / \bar{V}$$

where C_b is a scale length for orographic cloud depth, $\bar{U}$, the windspeed and $\bar{V}$, the mean terminal fallspeed of hydrometeors, then the wind drift effects are important. Typical values can be taken as C_b = 2.5 km, $\bar{U}$ = 15 m/s and $\bar{V}$ = 4 m/s leading to a < 10 km. This limit can explain large differences between observed patterns of precipitation over hills having different half width. In Norway, for example, over relatively large hills (a ~ 20 km), the maximum precipitation rate is found well upwind of the crest while for smaller hills (a ~ 2 km), wind drift effect is important and the maximum precipitation rate occurs at the summit or on the lee side. This is fairly consistent with computed results in table 5.7 and with the values just derived above for a.

In the final experiment, the relative importance of each of the terms A,B,C of the rainwater equation are examined. The rainwater equation is repeated here for convenience

$$Q_R(z-\Delta z,x) = Q_R(z,x) + \frac{\Delta z}{\rho_a(\bar{V}-w)}\left[A + B + C + AUTOC + W + EVAPR \right]$$

where

$$A = -\rho_a U(z) \frac{\partial Q_R}{\partial x}$$

represents the horizontal advection of rainwater mixing ratio (precipitation drift effect). The second term in the bracket is

$$B = (\bar{V}-w)Q_R \frac{\partial \rho_0}{\partial z}$$

which accounts for the fact that the atmosphere is compressible and finally;

$$C = \rho_0 Q_R \frac{\partial}{\partial z} (\bar{V}-w)$$

which accounts for the variation with altitude of the fallspeed of precipitation elements with respect to the ground.

Table 5.8 below compares the effect of excluding each of the above terms on the maximum rainfall rate enhancement ΔP_m. It shows that the effect of excluding term A (precipitation drift) or term B (compressibility effect) significantly increases the orographic enhancement and should therefore not be neglected in the conservation equation of the rainwater substance while term C can be ignored without any consequence.

run with	ΔP_m (mm/h)
all terms included	3.9
term A excluded	4.5
term B excluded	5.1
term C excluded	3.8

Table 5.8

Compressibility effect also appears in the condensation rate equation (see eq.3.14c). In some models described in chapter 3, variation of air density effect is not included in the condensation rate. Table 5.9 shows that not taking this term into account causes a significant decrease of the condensation rate, maximum CLWC and precipitation enhancement as calculated by the present model.

compressibility effect	computed maximum condensation rate (X 10^{6} kg/m^3s)	computed max CLWC (g/m^3)	ΔP_{-} (mm/h)
included	0.79	0.45	3.9
excluded	0.53	0.33	2.7

Table 5.9

5.3 Comparison with other models

Most of experiments performed with the present model generally agree with models of Bader and Roach (1977), Carruthers and Choularton (1983) and Gocho (1978).

The main difference between the first two models and the present model is in the treatment of the microphysics of the feeder cloud. As a fact, the first two models almost ignore the modeling of the microphysics and consequently neglect the possibility of rain production in the feeder cloud. As a consequence, it is expected that the behaviour of the current model significantly differs from the first two as the background rainfall rate goes to zero. This is especially true for large hills since the associated feeder cloud can then reach higher cloud liquid water content and then produce precipitation without any background rainfall rate. In the first two models mentioned above, it seems that the rainfall enhancement goes to zero as P_0 approaches zero while it is also the case for the present model (see curve A,B in figure 5.6). However, for larger hills (see curve C through F in fig. 5.6 and 5.19), the behaviour is different.

The model of Carruthers and Choularton (subsequently referred to as CC) represents a considerable improvement over the Bader and Roach's model (subsequently referred to as BR) in the treatment of the airflow. However,CC's paper concludes that , when large enhancements occur, with high windspeeds (U > 15 m/s) the potential flow treatment (an improved version of model PF described here) is sufficiently accurate to be used for hills of all lengths; neglect of stratification leading only to a slight overestimate in the enhancement over long hills.

Although this conclusion seems reasonable in many cases, it is clear from table 5.2 (cases A,B,E) of this thesis that in situation of a low level jet, the PF solution and CC's solution would both underestimate the strength of the vertical velocity and accordingly underestimate the orographic enhancement. The neglect of the second term of equation 4.7 (which represents the curvature of the wind profile) in CC's model leads to an underestimation of the vertical velocity for many LLJ situations.

The point above is thought to be the main reason why in CC's model, the observed sensitivities (e.g Hill et al,1981) of the enhancement on the windspeed are not reproduced.

Figure 5.20 compares results, partly taken from CC's paper, for ΔP_m as a function of windspeed obtained from different models. Curve A reproduces the sensitivity obtained from the present model, curve B with Bader and Roach and curve C with CC's model. It seems, then, that the model developed in this thesis

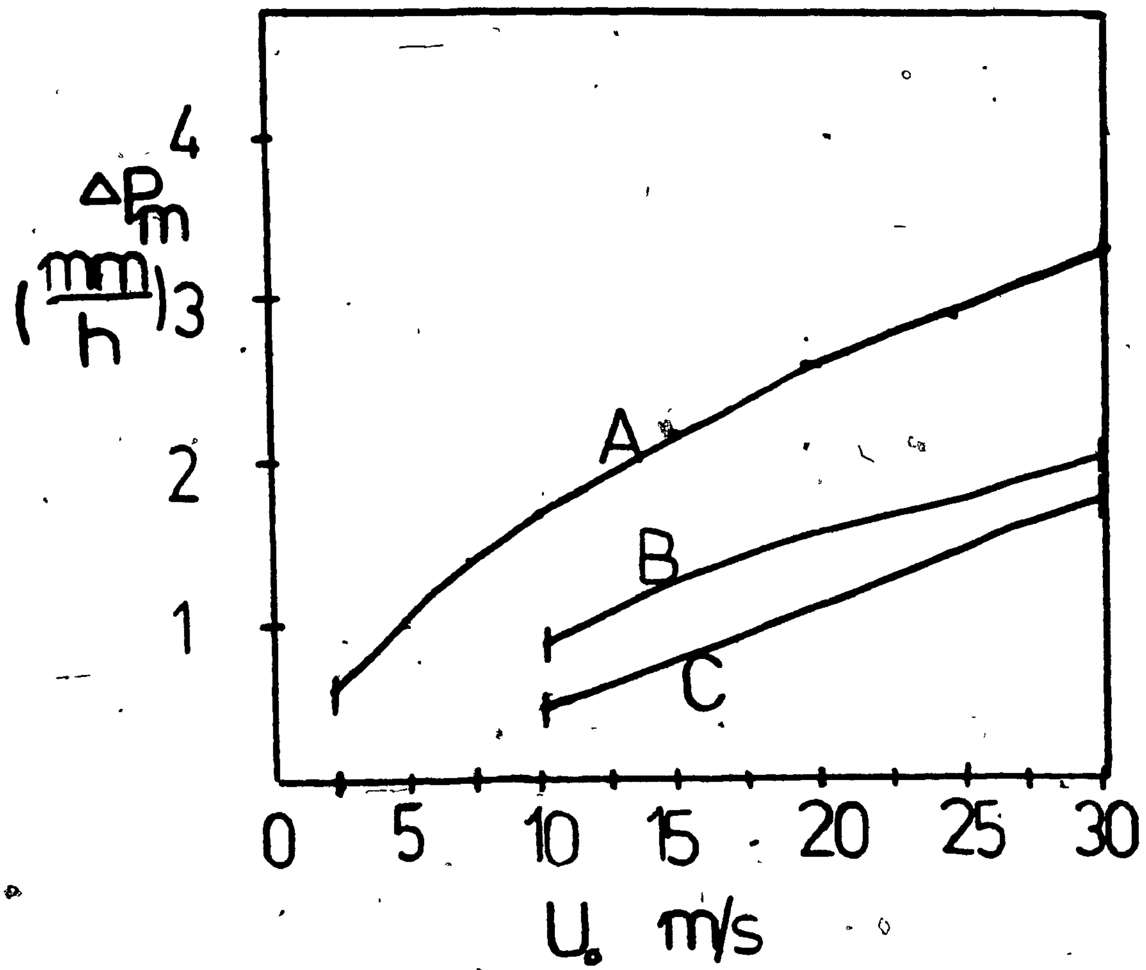

Figure 5.20. Variation of the maximum precipitation enhancement as a function of the surface wind speed, U_0, as computed by different models; A, present model; B, Bader and Roach's model and C, Carruthers and Choularton's model.

has a higher sensitivity of ΔP_m as a function of windspeed than both CC's or BR's model.

5.4 Limitations of the present model

While noting that the model suggested in this thesis appears satisfactory, it is worth discussing its shortcomings.

Although the present model has eliminated some of the limitations of BR's model, it presents some numerical problems. The scheme of integration is conditionally stable; that is instability developed unless integration steps are carefully selected. However, with this "non-standard" scheme used (see eq. 3.29 and 3.30), it is rather hard to find a mathematical expression for the stability criteria. Finding a stable solution must be done trough trial and error. However, a stable solution is usually found with space steps $\Delta x = 2.5$ km and Δz=100 m. The numerical solution is limited by the fact that the response of the model tends to deteriorate as the windspeed tends to zero (EFP becomes over 100 percent, P_s does not exactly tend to zero etc.).

However, the main limitation of the model is thought to come from the fact that the initial depth (D_c) of the orographic cloud is not specified in rigorous way. Figure 5.2 has already shown the dependence of ΔP_m on D_c which is not negligeable. This important limitation is a consequence of the seeder-feeder formulation and also appears in the models of BR and CC mentioned above. On the other hand, a strong gradient in the CLWC and condensation rate near the top of the orographic cloud appears as a result of defining a finite thickness D_c of the orographic cloud (see fig. 5.15 and 5.16).

Shortcomings concerning airflow calculations are already discussed in chapter 4. However, it may be worth adding that the solution for vertical velocity and air displacement is not valid above 5 km (according to Sarker, 1966). But since the present model does not extend above this level, it is not of great concern in this case.

Finally, rainfall enhancement may not be entirely due to orography. It might occur by local frictional convergence processes at low levels, instability or large scale divergence. The vertical velocity arising from these causes are not taken into account in the present model.

CHAPTER 6: CASE STUDIES

In order to assess the relevance of the model described in this thesis to actual situations, the model parameters were matched as far as possible to some cases of heavy orographic rainfall occuring in some regions of the world.

6.1 Western Ghats (India)

Heavy rainfall over Western Ghats (India) during the southwest monsoon is believed to be strongly orographic (Sarker,1966). The Ghats extends for about 1500 km, in the north-south direction. The average west-east vertical cross section of this portion of the Ghats is shown schematically in figure 6.1. An area located in the Bombay region was originally selected (see Sarker).

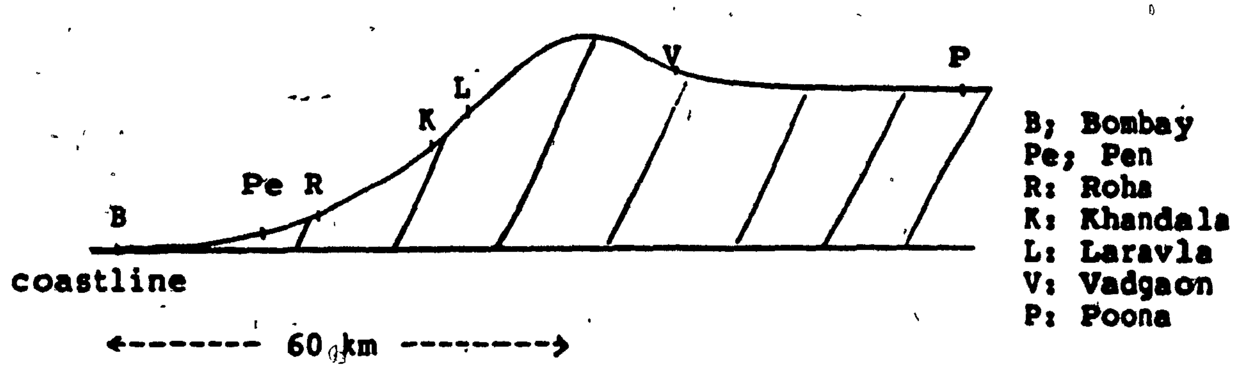

Fig. 6.1 Smoothed profile of Western Ghats (India). (from Sarker,1966).

We will make use of the microphysical-dynamical model developed in this thesis and compared results with both observed and computed results from Sarker's paper. As discussed in chapter 3, the former model is a more complete model than the latter. In fact, Sarker considered that all the condensed material precipitates without any regard to microphysical processes while in the model presented here, a better formulation of the microphysics permit us to evaluate the cloud liquid water content of the orographic cloud and to study some aspects of the physics of such a cloud.

In the 7 cases presented below, the model was run with the data from Sarker's paper (1966) but with the formulation of the seeder-feeder mechanism. This former approach necessitates the specification of the background rainfall rate. However, because of lack of radar data, it might be difficult to define a value for P_0. We are left with the alternative of specifying the background rainfall rate as being that of costal station rainfall rate at Bombay. This is a good approximation if evaporation loss of rainfall on the upwind side is minimized. In fact, the true background rainfall rate should be taken as the rainfall rate at the top of the orographic cloud.

The temperature profile is again defined in each case by θ_w and calculated with equation 5.1 and 5.2. In all runs it is assumed that the air is saturated. The source of the background rainfall rate is, in this case, assumed to be the middle level potential instability. This is, in fact, a reformulation of the problem presented by Sarker. The reader is referred to the above reference for other details concerning the input data.

To reproduce the mountain profile of figure 6.1, equation 4.18 is used with the following values a=18 km, b=520 m, a'=222.8 m and h =256.9 m. The same integration steps were taken for all runs and are Δz = 100 m and Δx = 2.5 km. In all cases, the top of

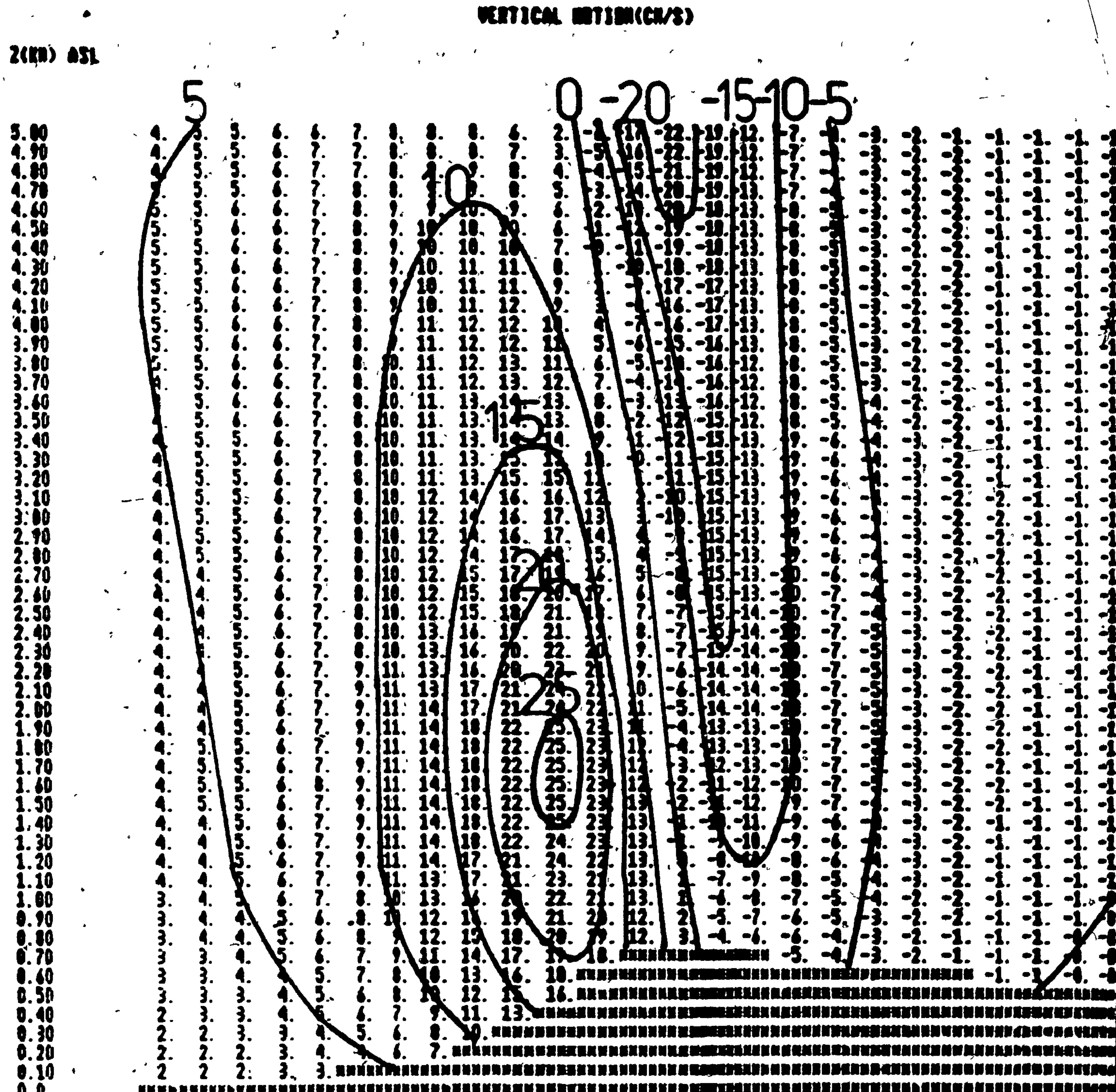

Figure 6.2. Vertical velocity distribution for monsoon case III.

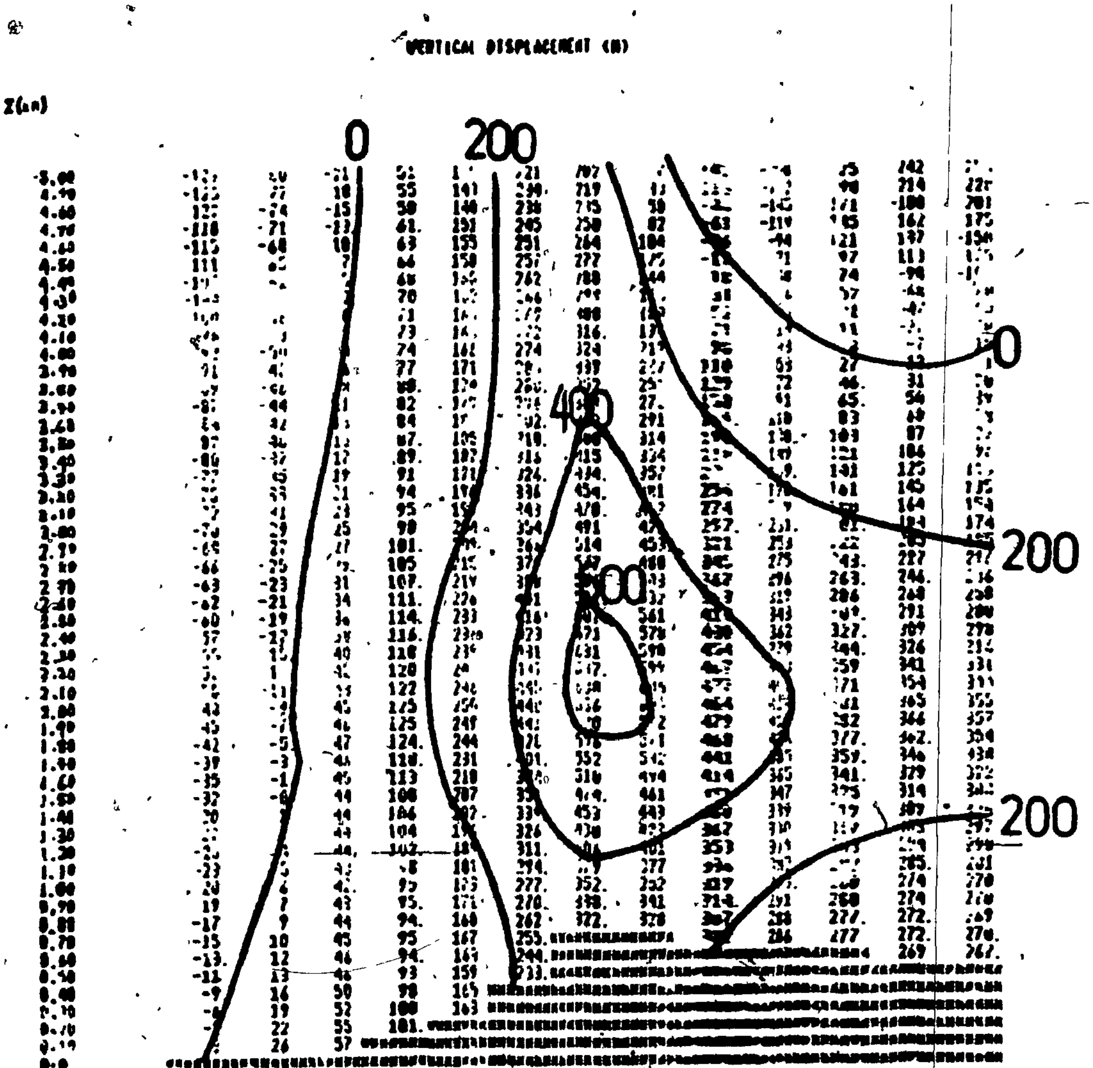

Figure 6.3. Vertical displacement distribution for monsoon case III.

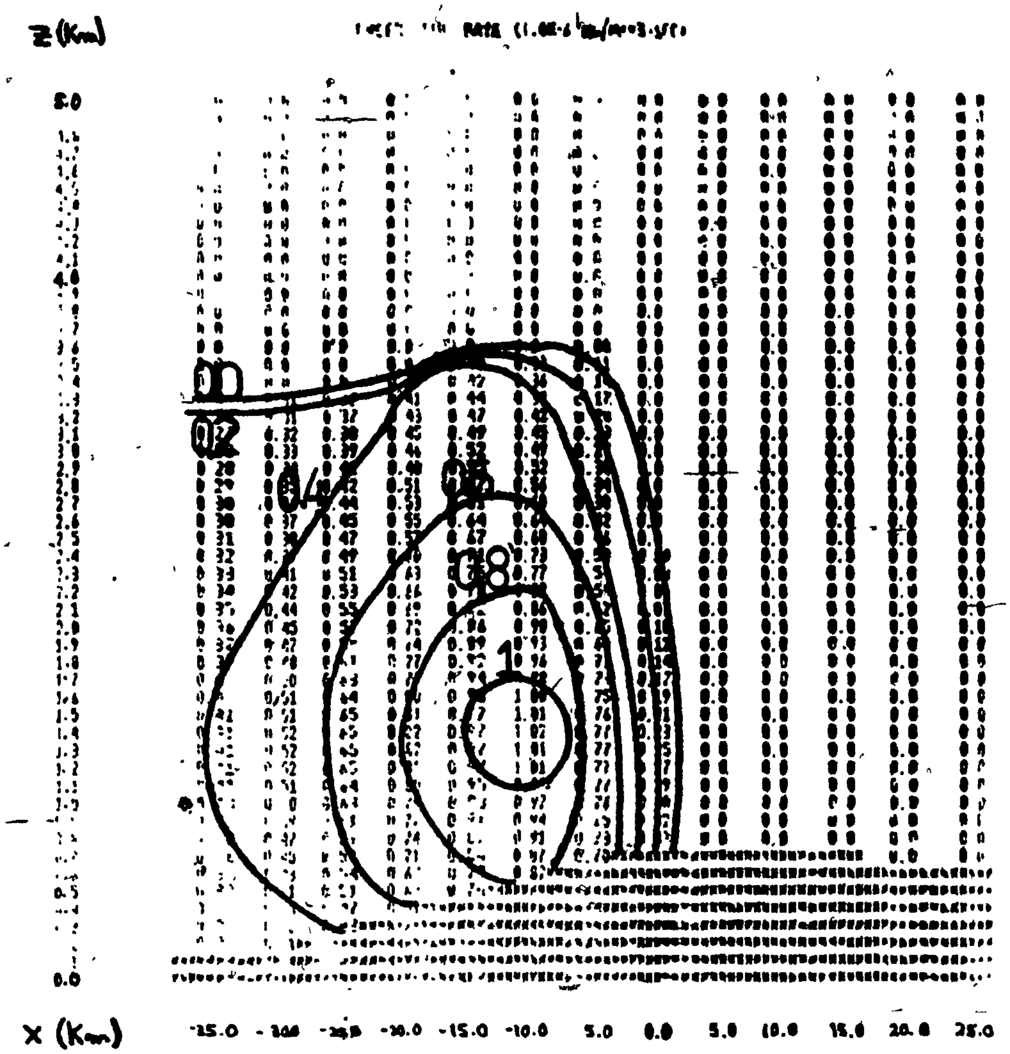

Figure 6.4. Condensation rate distribution for monsoon case III.

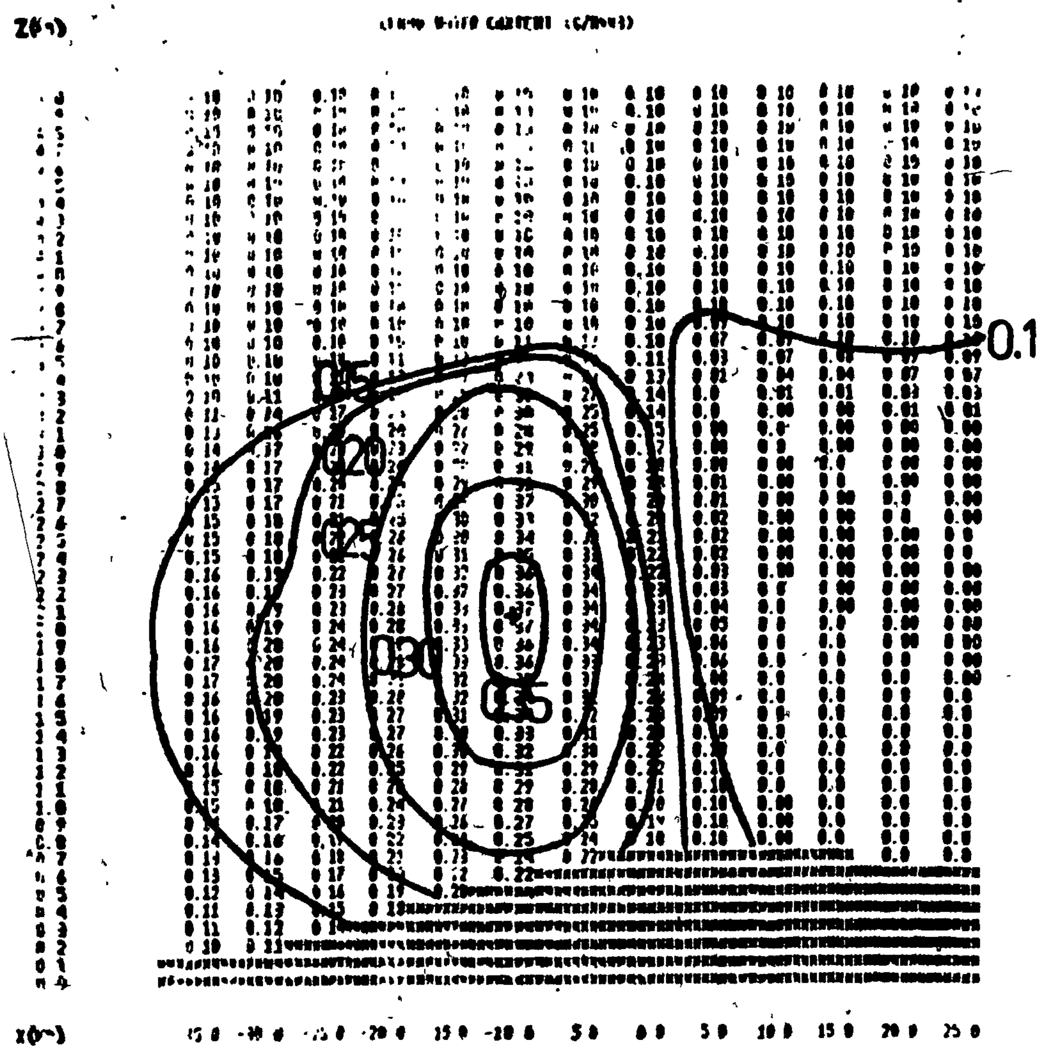

Figure 6.5. Distribution of cloud water content for monsoon case III (g/m³).

the model is fixed at 5 km and the depth of the domain of integration D_c specified at the left edge is taken as 3.0 km, the cloud water content at the upper boundary is assumed to be 0.1 g/m³. A three layers model is used and the reader is referred to appendix B for vertical motion and vertical displacements solutions.

Table 6.1 shows most of the relevant input data while table 6.2 presents results obtained from the model. For the sake of briefness only one case (case 3) will be examined in detail here.

case	I	II	III	IV	V	VI	VII
Date	7/5 1961	6/25 1961	7/6-9 1963	7/11-12 1958	7/21 1959	7/2-4 1960	7/4-6 1958
top of 1 layer $z_o + h_o$ (km)	2.5	3.25	1.75	2.5	2.5	2.0	2.25
top of middle layer $H + h_o$ (km)	5.0	5.25	3.25	4.0	4.0	4.0	2.25
l_1 (km^{-1})	0.6	0.5	0.77	0.6	0.55	0.67	0.7
l_2 (km^{-1})	0.5	0.39	0.39	0.32	0.4	0.27	0.7
l_3 (km^{-1})	0.4	0.5	0.4	0.4	0.36	0.27	0.4
θ_w (°C)	25.0	25.9	24.9	25.9	24.9	25.9	25.9
P_o (mm/h)	6.2	2.0	2.4	2.2	1.8	2.7	2.0
SFC wind speed (m/s)	8.0	6.5	6.0	8.0	9.0	7.0	6.3

Table 6.1 Input data

case	I	II	III	IV	V	VI	VII
Date	7/5 1961	6/25 1961	7/6-9 1963	7/11-12 1958	7/21 1959	7/2-4 1960	7/4-6 1958
W max min (cm/s)	34 -14	29 -15	25 -22	34 -30	34 -22	33 -25	17 -45
QC_0 max (g/m^3)	0.26	0.55	0.37	0.70	0.83	0.61	0.34
EFP (%)	0.78	0.6	0.72	0.69	0.73	0.74	0.78
R (mm/h) computed max.	14.3	8.0	8.0	10.5	11.0	11.5	5.9
R (mm/h) observed max.	12.2	8.6	7.8	9.8	8.5	9.5	3.8
R(mm/h) Sarker max.	8.4	7.7	5.9	8.8	9.0	9.5	2.4

Table 6.2 Results of 7 monsoon cases (India).

Figure 6.2 shows the vertical velocity profile for this occasion; the maximum positive value is 25 cm/sec and is located above the maximum slope of the mountain and at a level 1.7 km above sea level. The maximum negative value is -22 cm/sec near the crest and located at 5 km above sea level. A tilt toward the upwind side in the contours of vertical motion is again revealed in figure 6.2. The maximum vertical displacement is over 600 m and is located about 2.2 km above sea level (figure 6.3). The maximum condensation rate (fig. 6.4) roughly coincides with the maximum vertical velocity in figure 6.2. It should be noted that above a certain level,the condensation rate is zero which

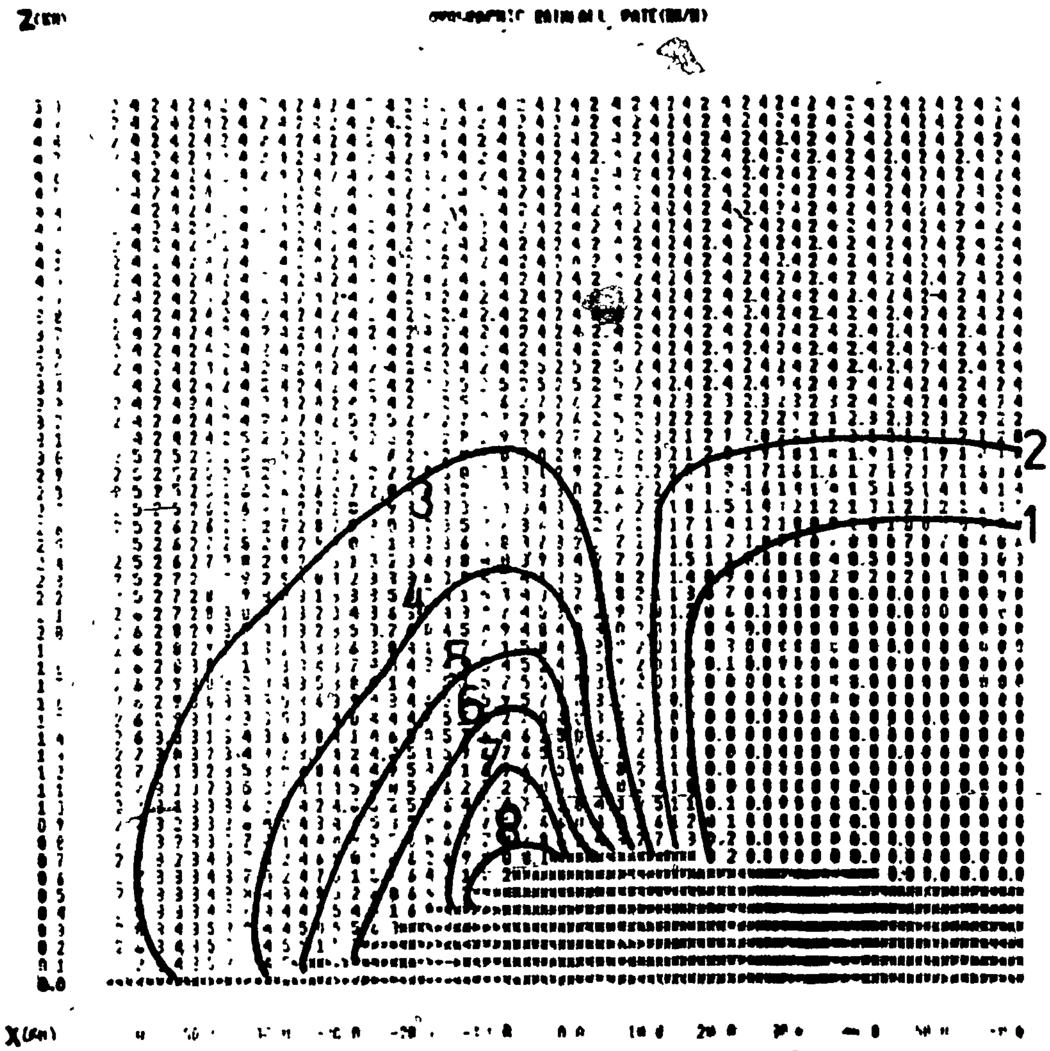

Figure 6.6. Distribution of rainfall rate across the WRN Ghats as a function of distance for case III.

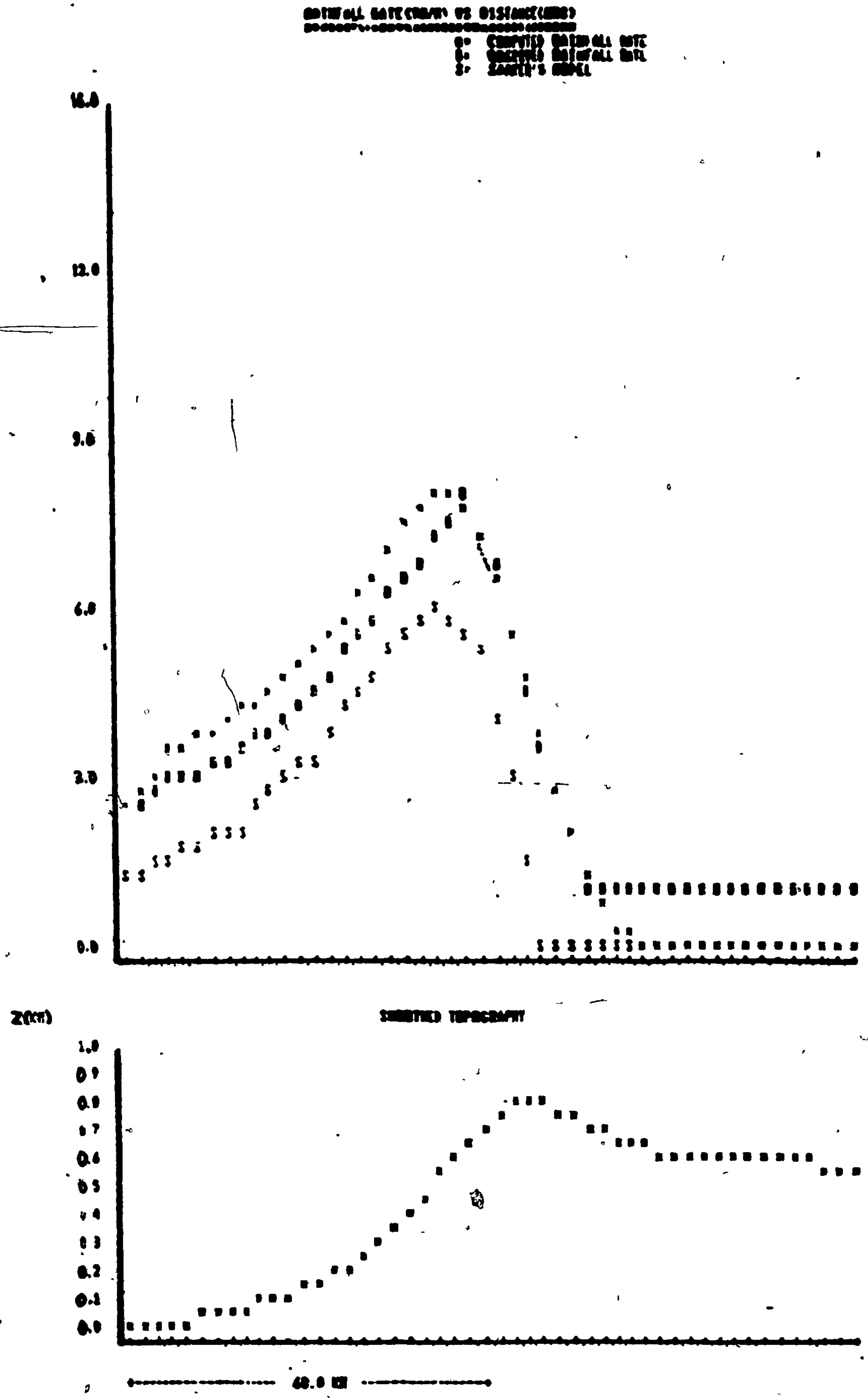

Figure 6.7. Distribution of surface rainfall rate (mm/h) as a function of distance for case III.

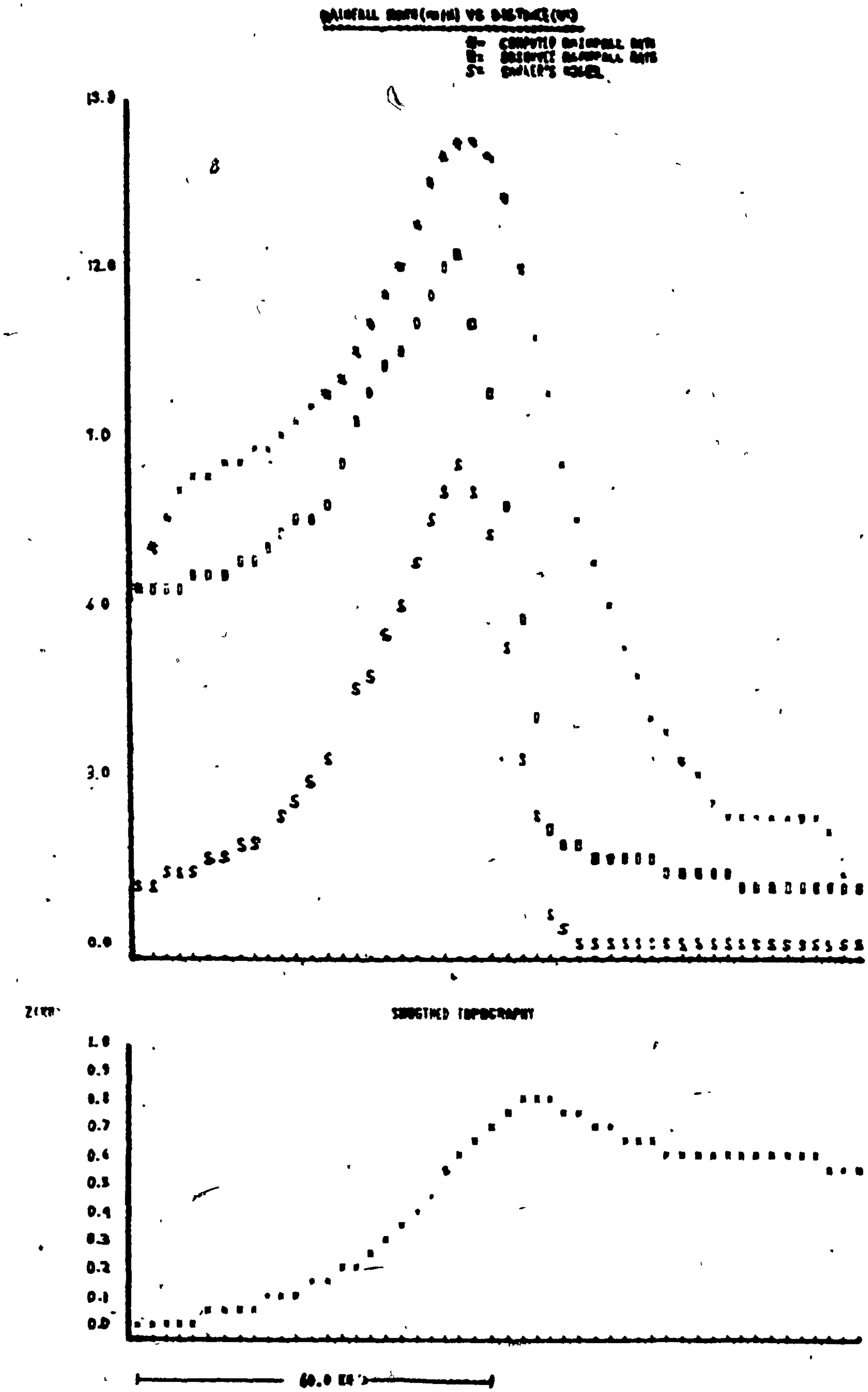

Figure 6.8. Same as figure 6.7, for case I.

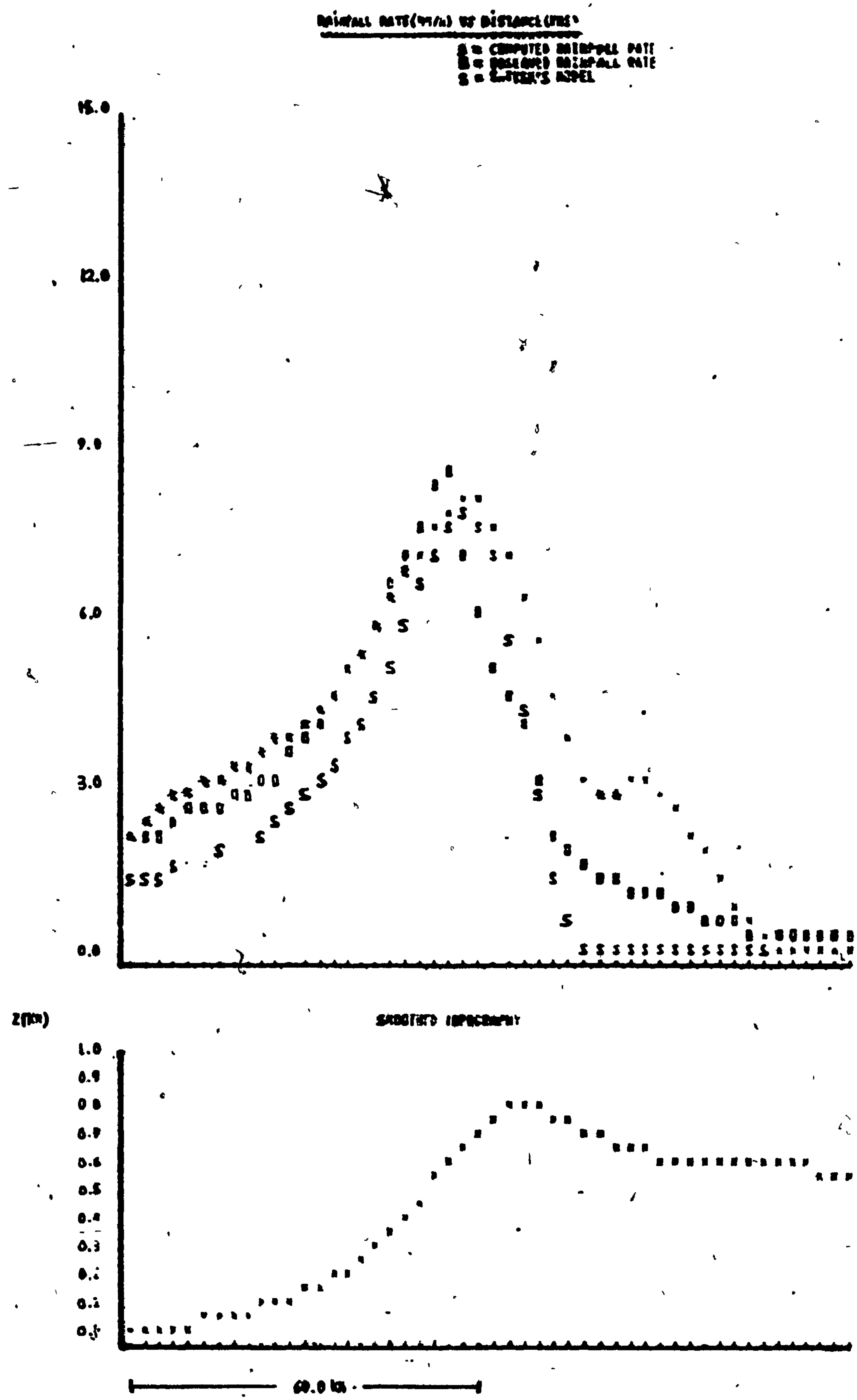

Figure 6.9. Same as figure 6.7, for case II.

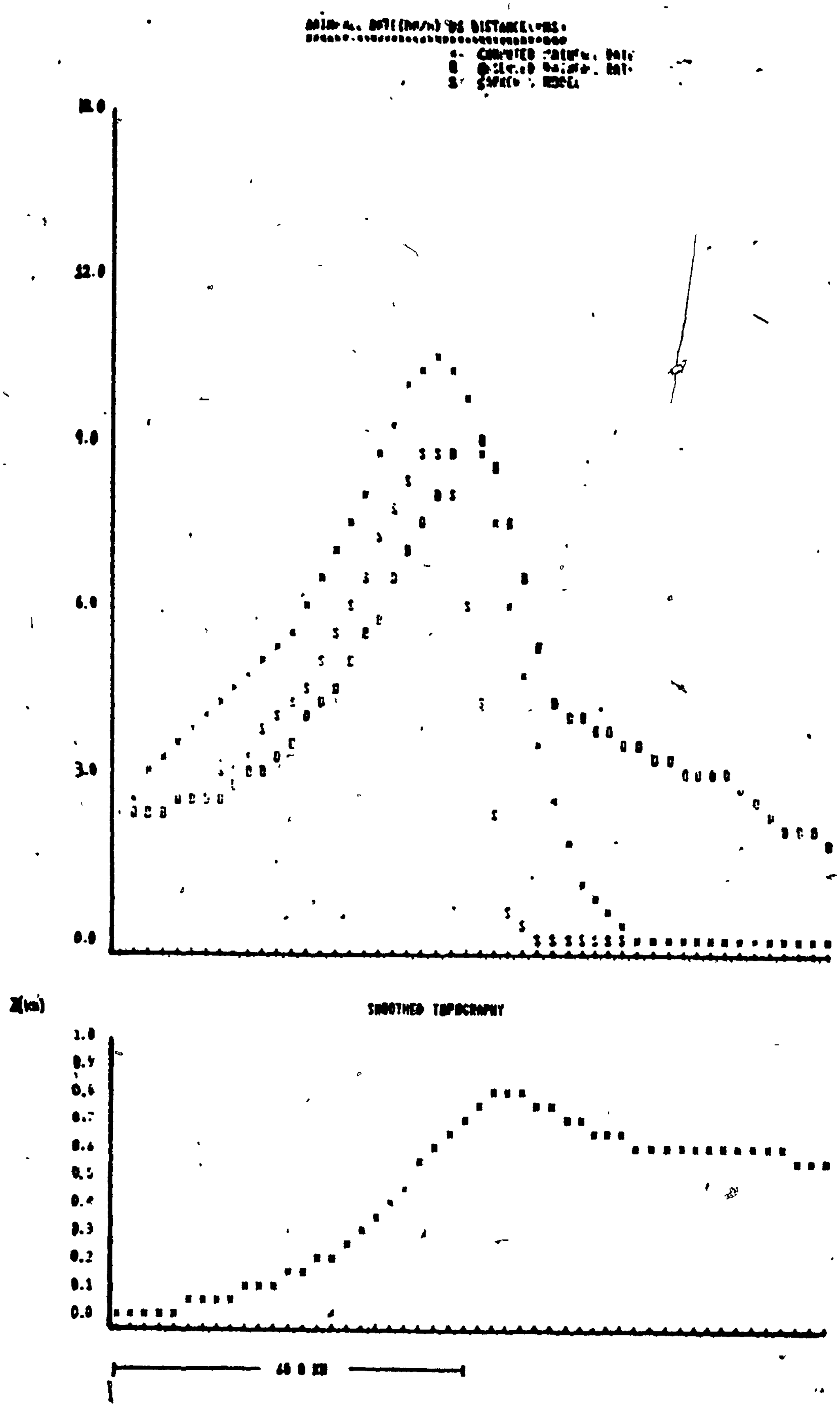

Figure 6.10. Same as figure 6.7, for case IV.

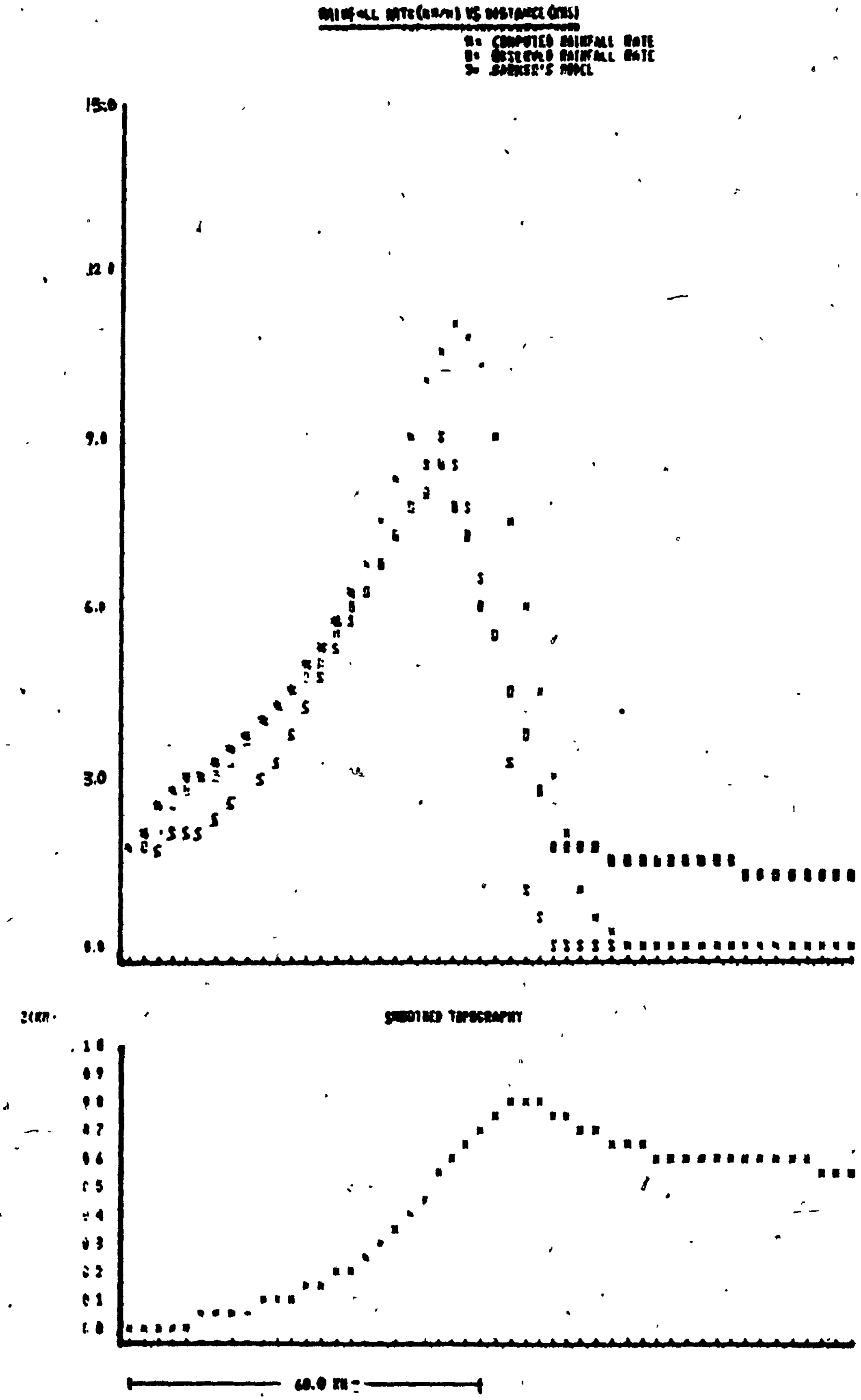

Figure 6.11. Same as figure 6.7, for case V.

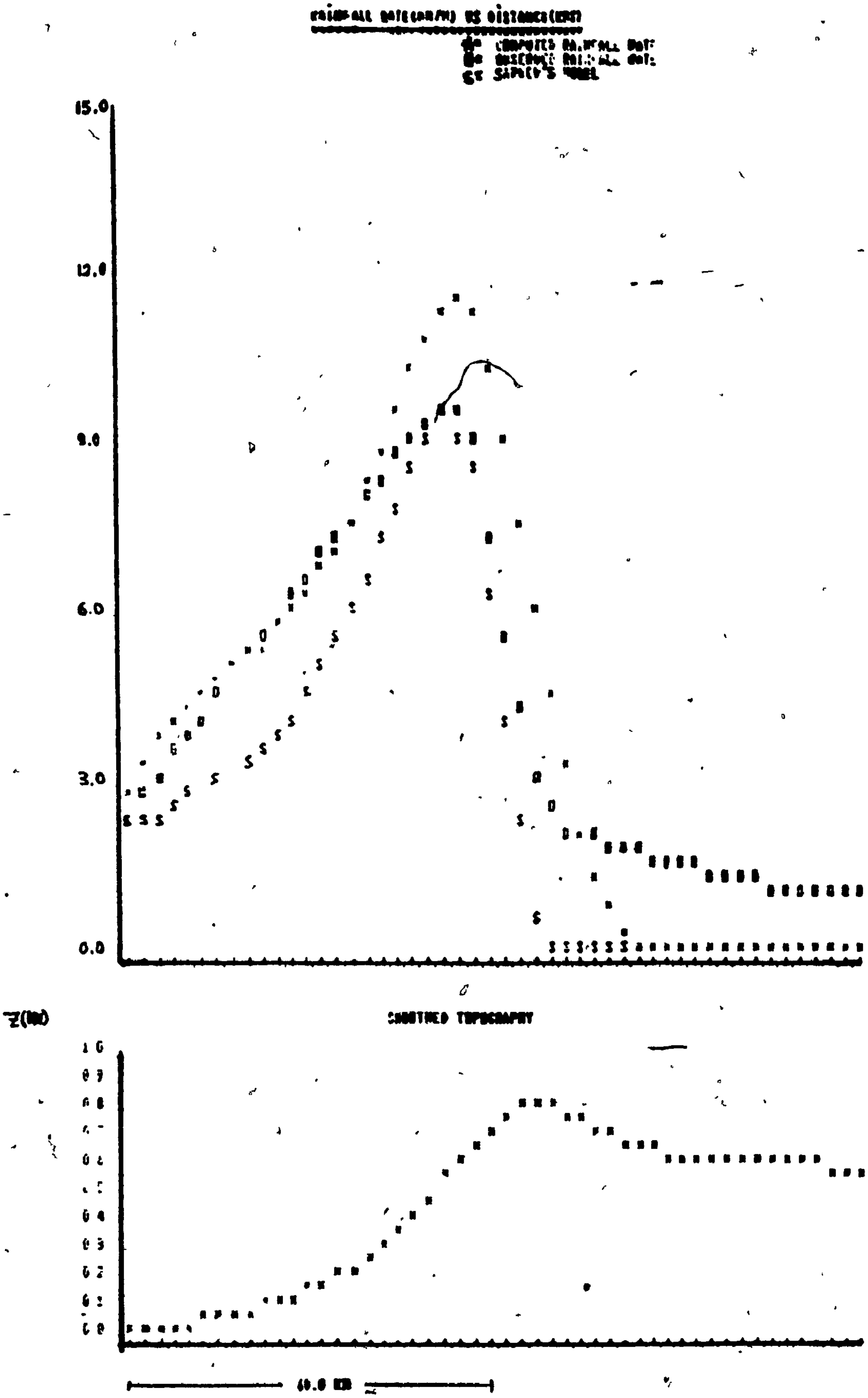

Figure 6.12. Same as figure 6.7, for case VI.

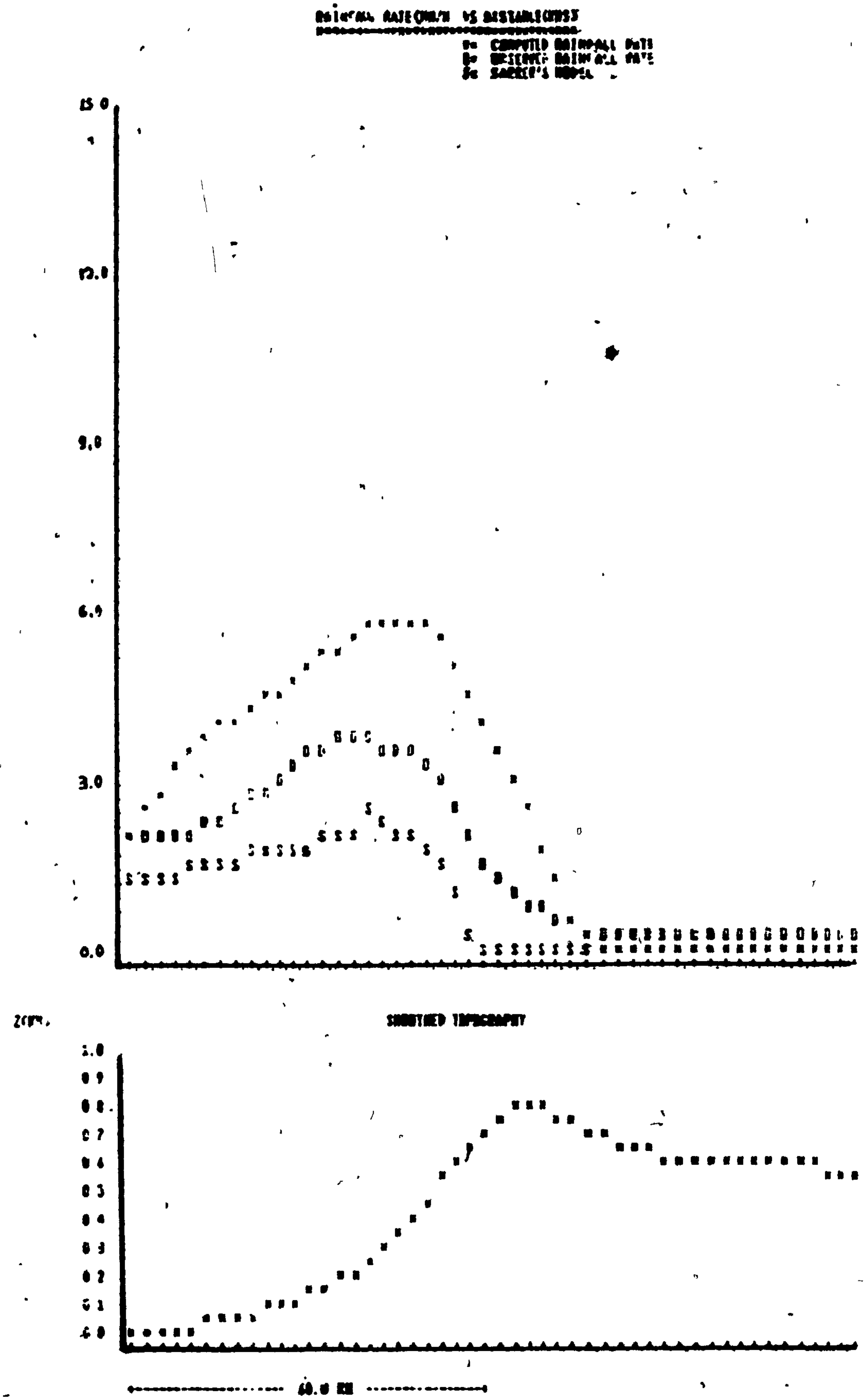

Figure 6.13. Same as figure 6.7, for case VII.

corresponds to the physical limit of the orographic cloud in the model. The actual condensation above this level is obviously not necessarily zero but since the model does not calculate the condensation rate in the seeder cloud a value zero is simply printed there which does not affect any calculations concerning the orographic cloud.

The computed value for cloud water content is illustrated in figure 6.5. The maximum cloud liquid water content is 0.37 g/m^3 and located 2 km above the position x=-10 km. The constant value 0.1 g/m^3 physically delineates the extent of the seeder cloud. Notice that the lowest maximum cloud water content occurs in situation of high P_o (table 6.2). This is thought to be consistent with the seeder-feeder mechanism. In fact, higher P_o will produce a higher washout rate of the feeder cloud and at steady-state less water content will remain in the feeder cloud.

Evaporation of the cloud is clearly visible on the lee side in figure 6.5. The spatial distribution of the rainfall rate at the ground is shown in figure 6.6. The background rainfall rate, which fills the upper part of the domain, is 2.4 mm/h in this case and is considered to be constant in the seeder cloud. Finally, the distribution of rainfall rate at the ground is given in figure 6.7 and is compared both with observations and computed results from Sarker's model. One can see a very good agreement between computed values and observed ones. Moreover, the present model simulates better the distribution that does Sarker's model in that case.

Other cases are summarized in table 6.2. Again, due to space restriction only the ground rainfall rate distribution is shown for these 6 remaining cases (see figures 6.8 to 6.13.). Note that the present model tends to overestimate the magnitude of surface rainfall rate while the opposite behaviour seems to characterize Sarker's model.

The mean error in estimating the maximum rainfall is 20 % for the present model and 17 % for the latter. For many cases the general distribution of the rainfall seems more realistic than that produced by the latter model. For example, the current model can produce rain on the lee side whereas the latter is totally uncapable.

6.2 Northwest Spain (Galicia)

As a second case study, three situations of orographic rainfall from a warm sector are presented using data provided by the " Instituto Nacional de Meteorología " of Spain. The area of study is given in figure 6.14 and is one of the most rainiest region of Spain with mean annual rainfall in the hills between 1500 and 2000 mm with isolated spots over 2000 mm (Atlas climatico de España, 1983).

Three detailed case studies are presented to clarify the structure and mechanism of orographically enhanced "warm sector" rain over hills of Galicia (NW Spain , figure 6.14). The characteristic of such rainfalls is thought to be similar in nature of that observed in England under similar synoptic situation and already described in this thesis.

Some of the largest orographic rainfalls in Galicia are associated with a maritime wintertime occluded low pressure system. In fact, in Western Europe warm sectors of such systems are usually cloudy with uniform precipitation and possibly accompanied by bands of showers which are aligned parallel to the winds at about 700 mb (these rainbands are described by Browning and Harrold,1969). The lifting of moist low level air over the topography is responsible of the orographic enhancement by creating higher condensation in the low levels over the topography. The feeder cloud hence formed is depleted by the washout mechanism which has the effect of increasing the ground rainfall rate as we go along the hill. The seeder-feeder mechanism is especially useful in midlatitude because the background rainfall rate may contain a great deal of information about the important large scale which is ,as an input, incorporated into the present model.In this study, the background rainfall rate is taken as a 24 hour rainfall average rainfall of the following coastal stations: Pontevedra,Vigo (a), Vigo,Salcedo and Laurizan.

At Santiago de Compostela (station # 428, figure 6.14), rainfall is often found to be two or three times that of coastal stations such as Pontevedra (#484), Vigo(#496), Rianxo (#444) etc. In order to simulate the rainfall distribution across hills of Galicia, the present model was fed with a smoothed topography given by the equation;

$$z_g = \frac{a^2 b}{a^2+x^2} + a' \tan^{-1}(x/a) + h_o \qquad (6.1)$$

with
a = 40 km
b = 500 m
a' = - 80 m
h_o = - 140 m

This smoothed topography approximates relatively well the actual terrain height when the latter is averaged over a circle of radius of 10 km centered on a particular point on the axis AB on figure 6.14 (this not true near point A and B,however). Point O represents the averaged highest point on line AB (which is near the location x=0 in equation 6.1). Raingauges used for each of the three cases are listed in table 6.3, whose number corresponds to those marked in figure 6.14.

raingauge	
La Coruna	387
Santiago de Compostela	428
La Estrada	468
Puentecesures	474
Eva-10	437
Rianxo	444
Pontevedra	484
Salcedo	485
Laurizan	486
Vigo(a)	496
Vigo	496e

Table 6.3 Raingauges used in the case study.

Of the many similar situations three have been selected for detailed study. Each case is characterized by an approaching low pressure system in the northwest (figure 6.15a,6.16a and 6.17a). The region under study is hence located in the "warm sector" of the systems such that in each of the cases, the 700 mb is from the southwest quadrant (fig. 6.15b,6.16b and 6.17b). It should be noted that large orographic enhancement at Santiago de Compostela occurs much less frequently with other wind directions because the region is then sheltered by higher hills around.

Tephigrams for each of the cases are plotted in figure 6.18.

The temperatures profiles are approximated by a constant θ_w curve in each of the cases. Although actual profiles are not quite neutral, this approximation is used here for simplicity and does not modify the vertical velocity. In fact, the parameter $l^2(z)$ is dominated by the "wind curvature " effect (see eq. 4.7) in the lower layer (below 3 km here) rather than the temperature profile. In the upper layer, however, since the " wind curvature" becomes very weak, the temperature profile dominates. Fortunately, in the cases studied here, the temperature profile is nearly neutral in the upper layer and is well approximated by specifying a constant θ_w (above 3 km). The wind profile is taken as a trigonometrical function similar to equation 5.4 below the level 700 mb level. Values for l_1,l_2 and H which best fit the actual wind profile are also given in table 6.4.Above 700 mb, the wind data is fit by a straight line and the value l_2 is then taken as zero (since the second derivative of the wind speed with height is zero). Smoothed wind profile is compared with actual data in figure 6.17. One can see a change of curvature at about 3 km (700 mb) which corresponds to a change of the parameter l in the present model. This is also shown on the temperature profile, figure 6.18 which indicates a discontinuity in the stability at about that level which would translate in any case into a change of l through the first term of equation 4.7. However, only the second term of equation 4.7 is assumed non-zero, since we consider the temperature profile along a moist adiabat in 4.7.

Radiosonde data (wind and temperature) were obtained from La Coruña station. Unfortunately, this station is the only one which

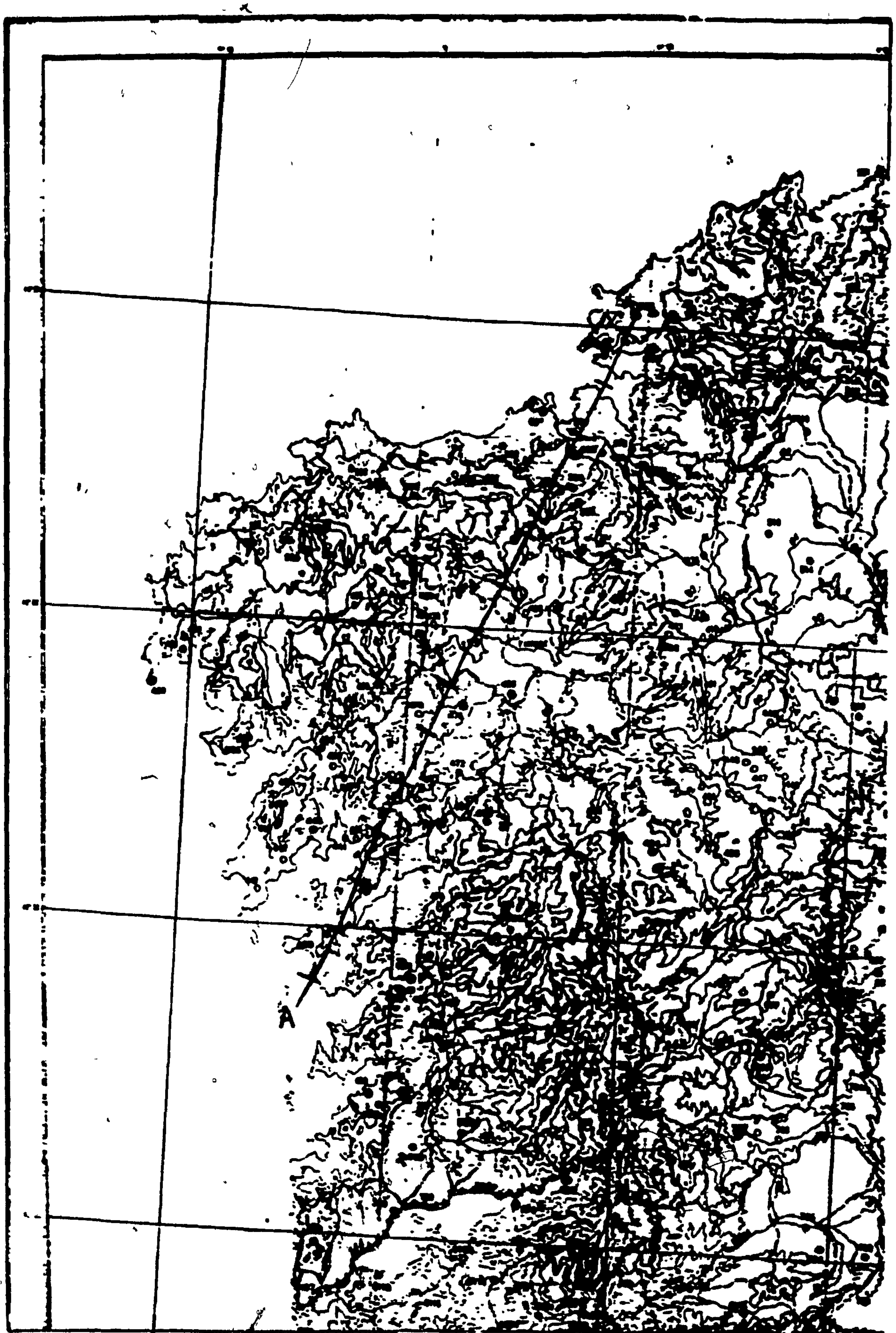

Figure 6.14. Enlarged map of the area of study (Galicia, NW Spain).

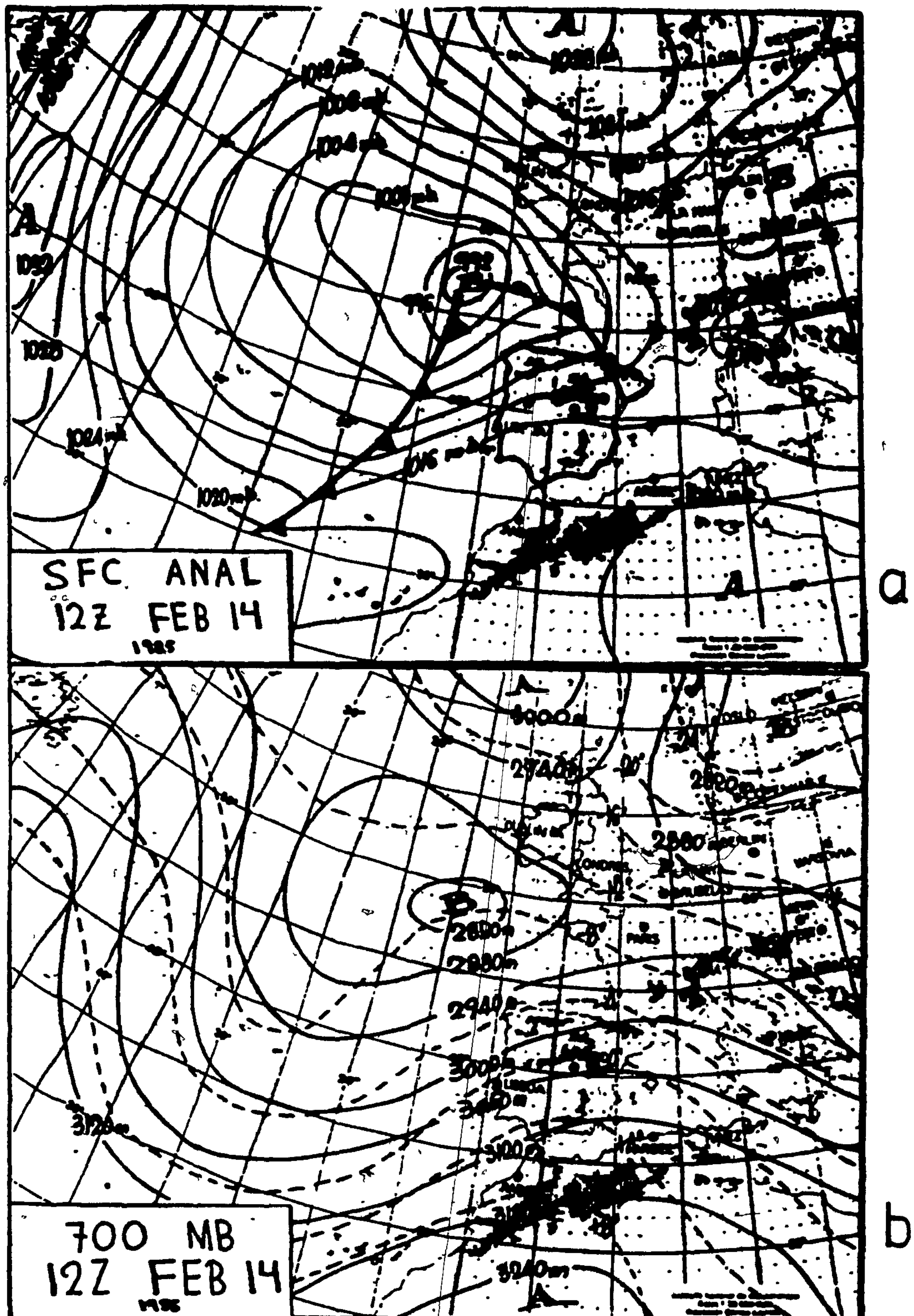

**Figure 6.15. a) Surface analysis for case I
b) 700 mb chart for case I.**

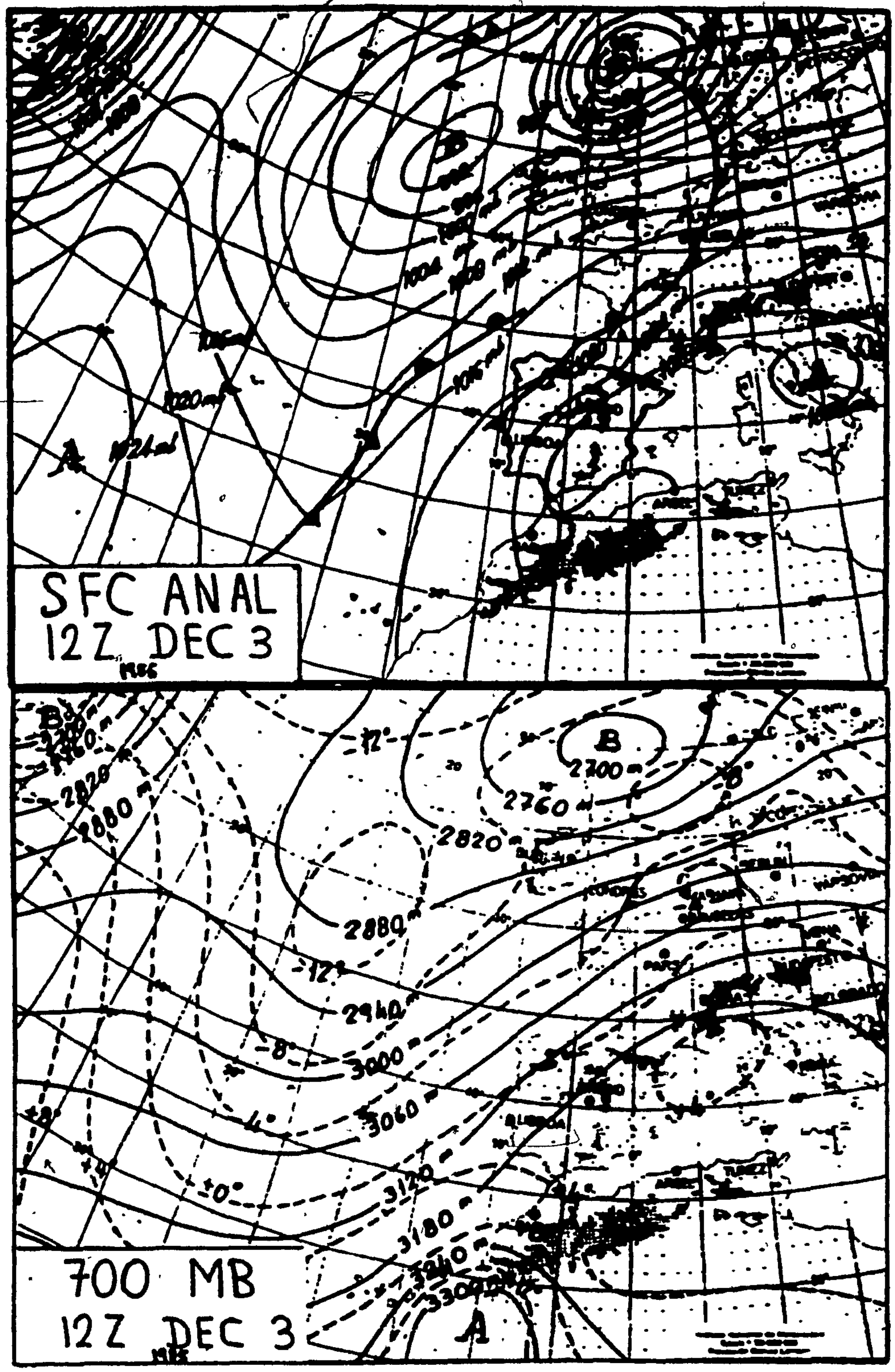

a

b

Figure 6.16. a) Surface analysis for case II
b) 700 mb chart for case II.

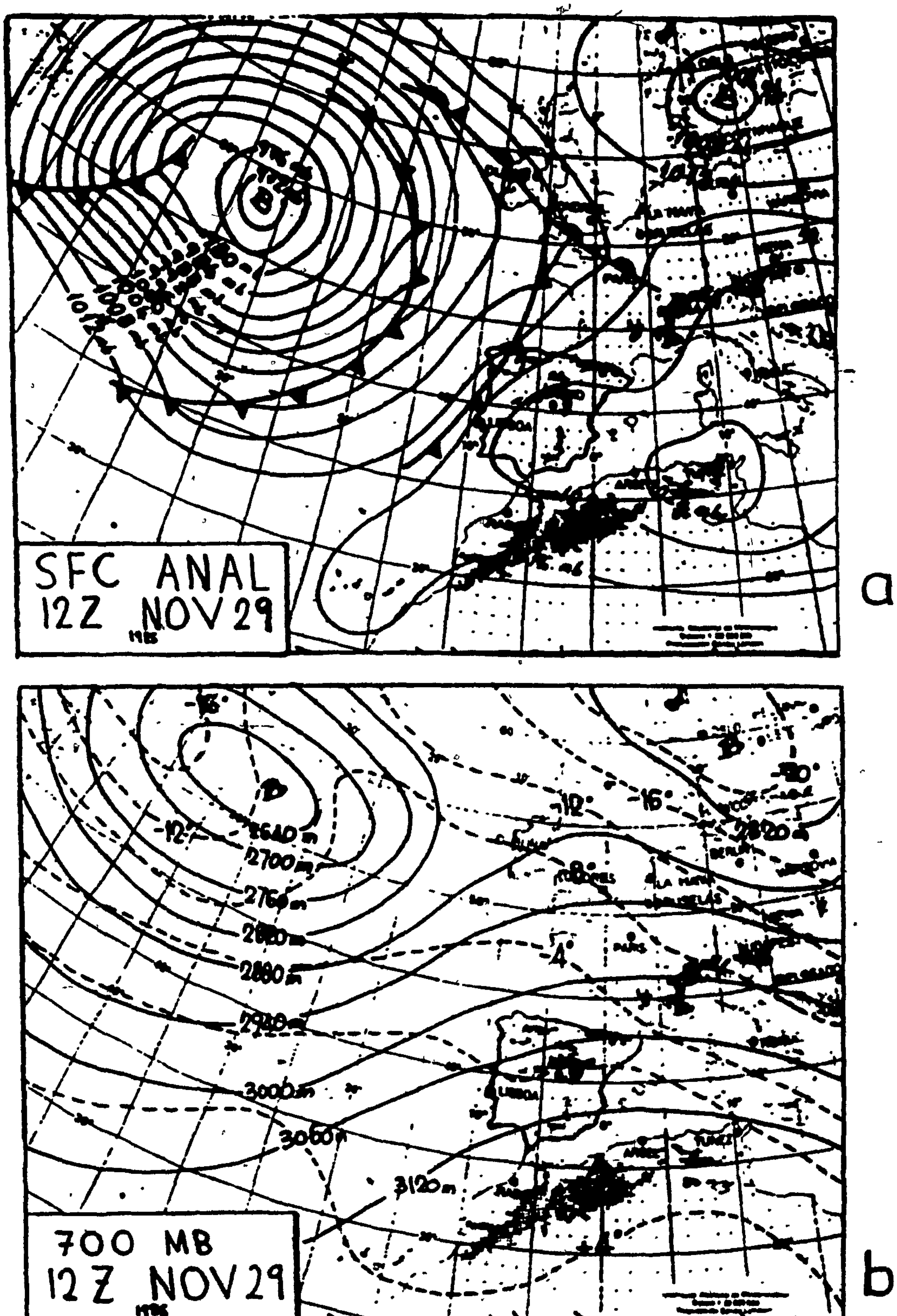

Figure 6.17. a) Surface analysis for case III
b) 700 mb chart for case III.

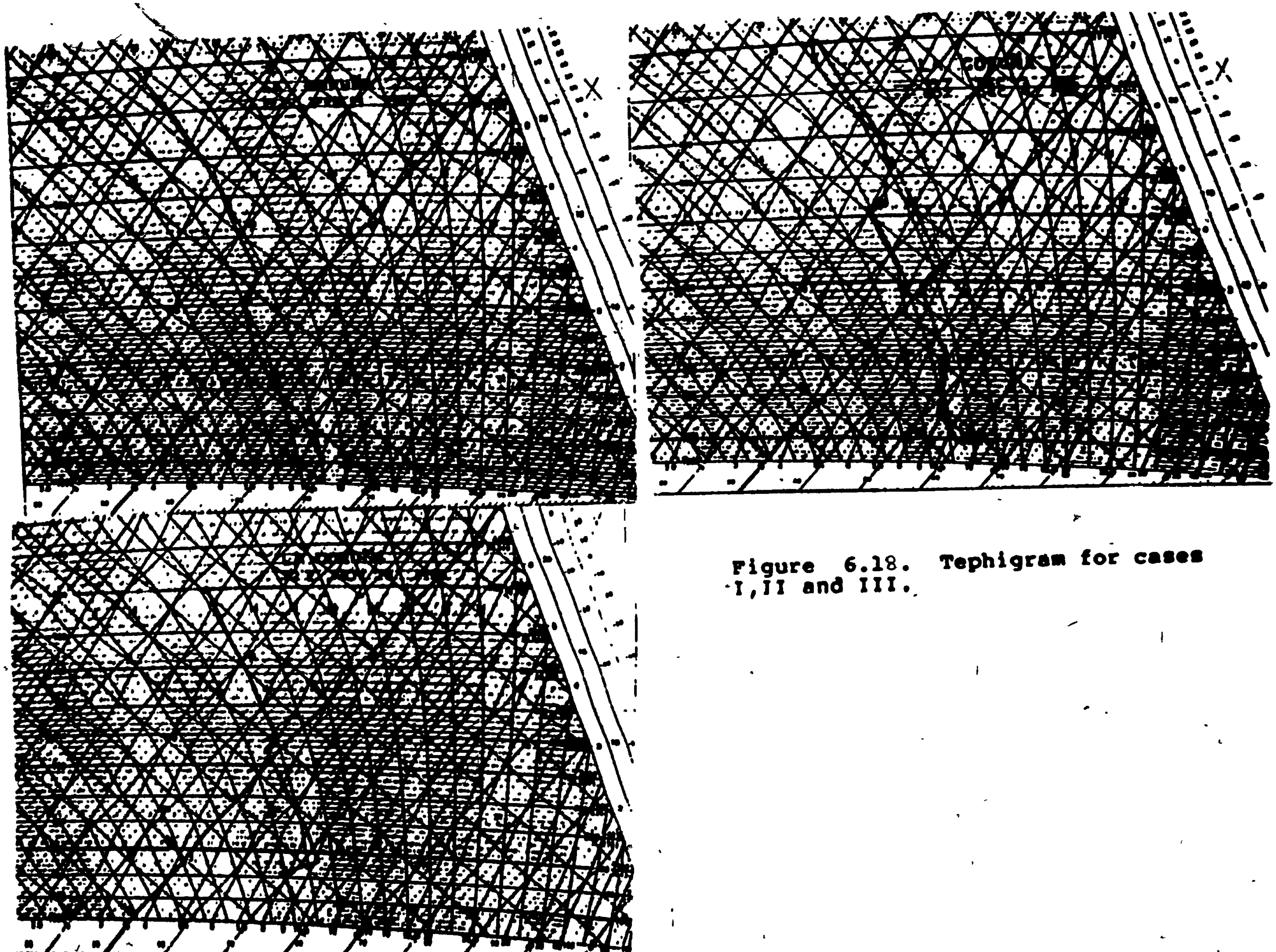

Figure 6.18. Tephigram for cases I,II and III.

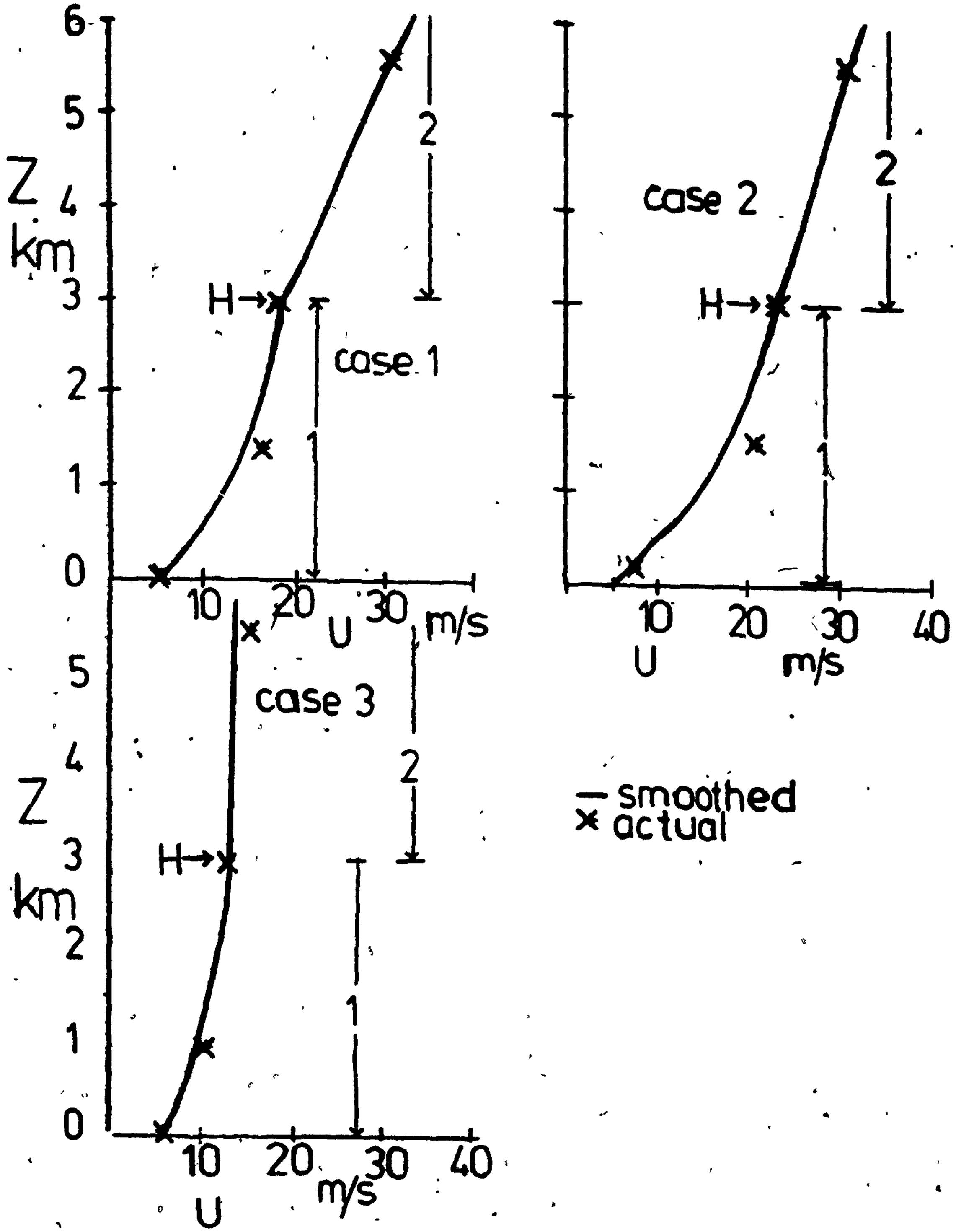

Figure 6.19. Input wind profile; smoothed vs actual for cases I,II,III.

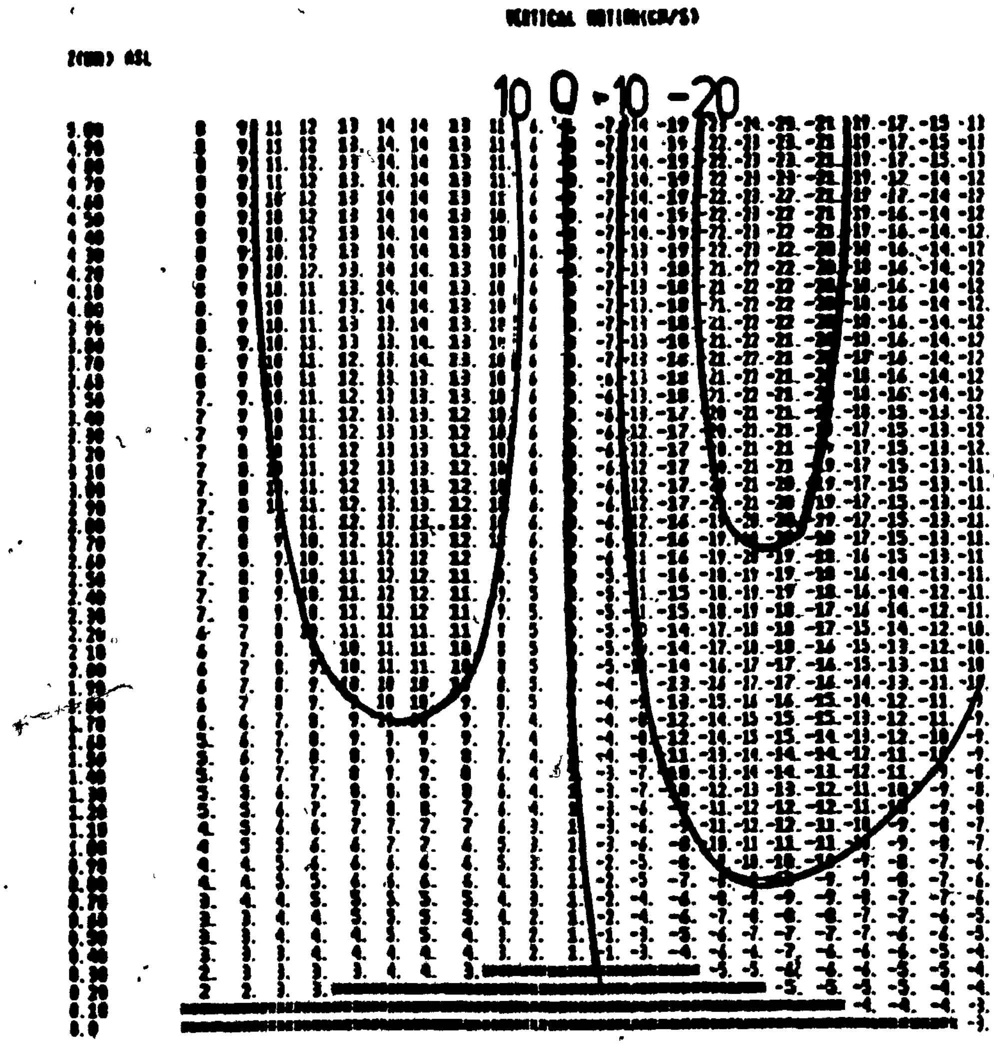

Figure 6.20. Computed vertical velocity distribution for case II.

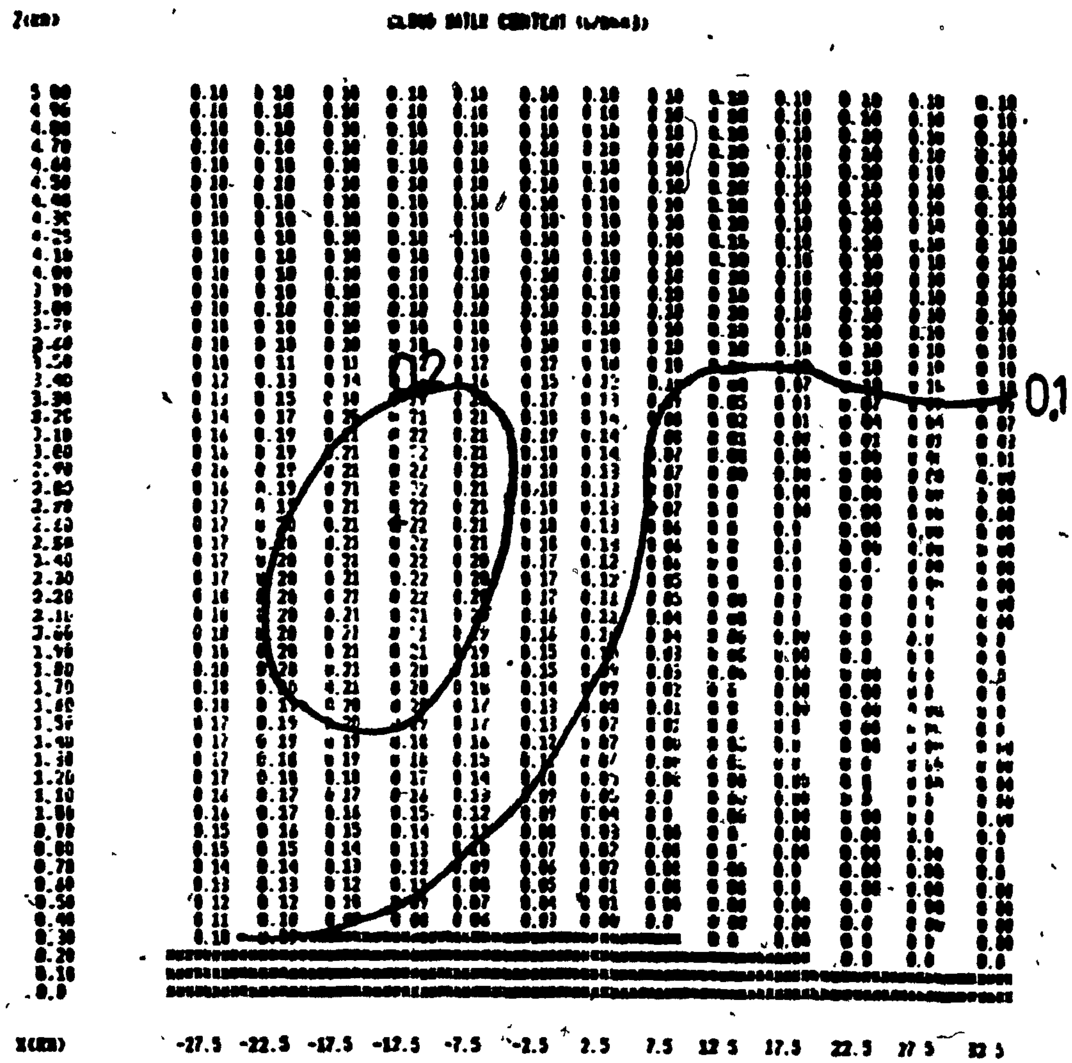

Figure 6.21 Computed cloud water content distribution for case II.

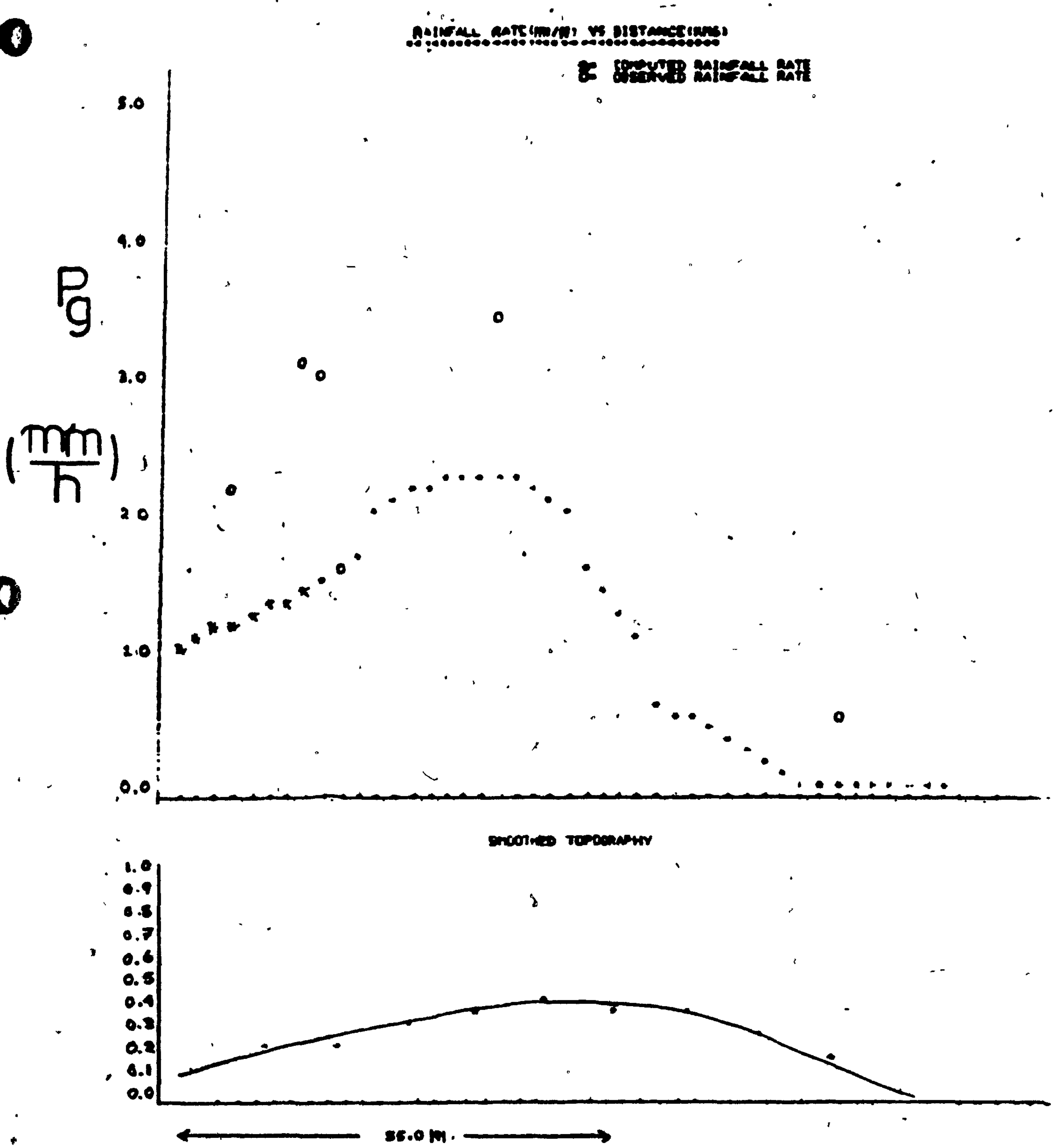

Figure 6.22. Surface rainfall rate distribution as a function of distance for case II.

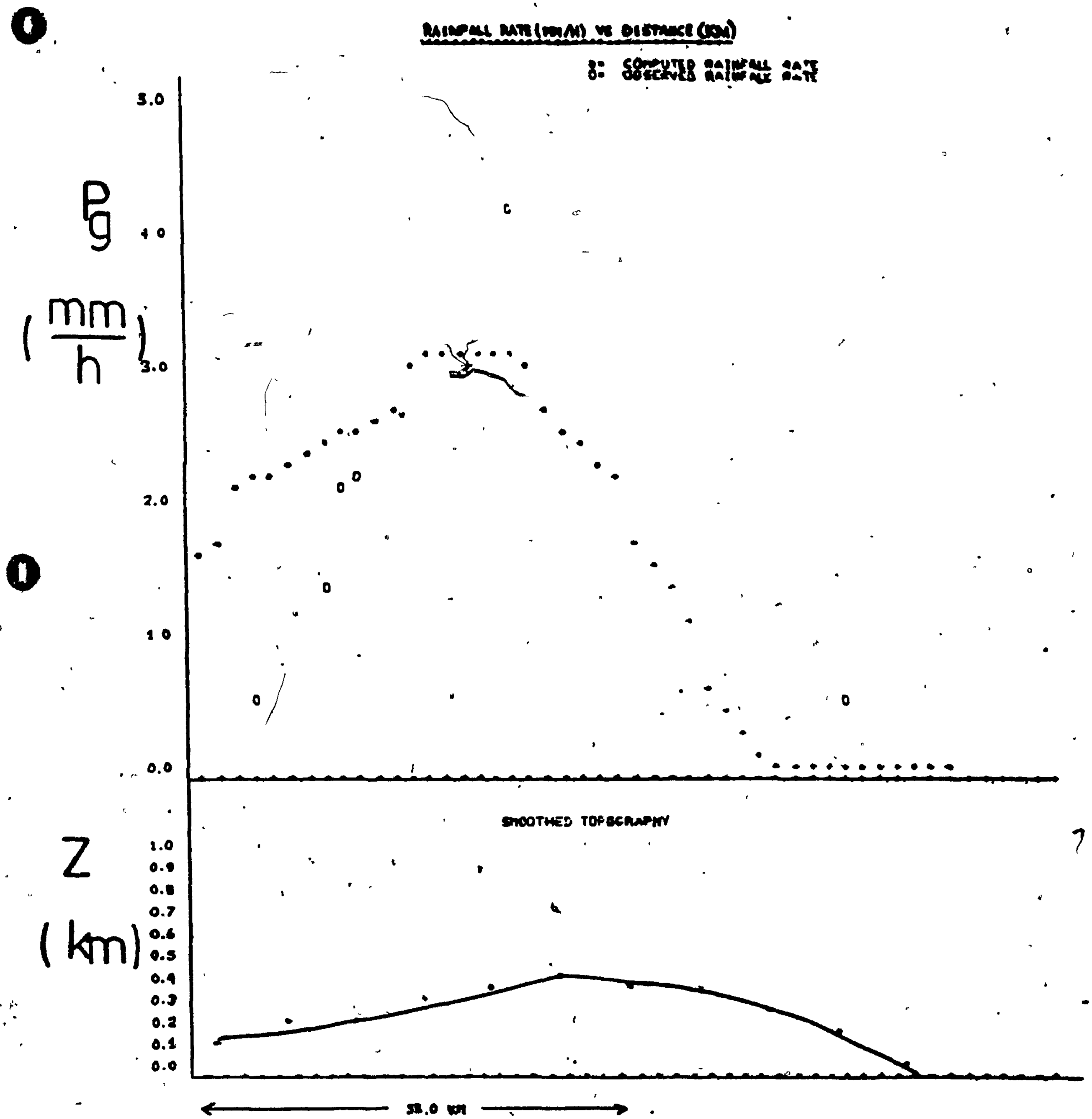

Figure 6.23. Same as figure 6.2 for case I.

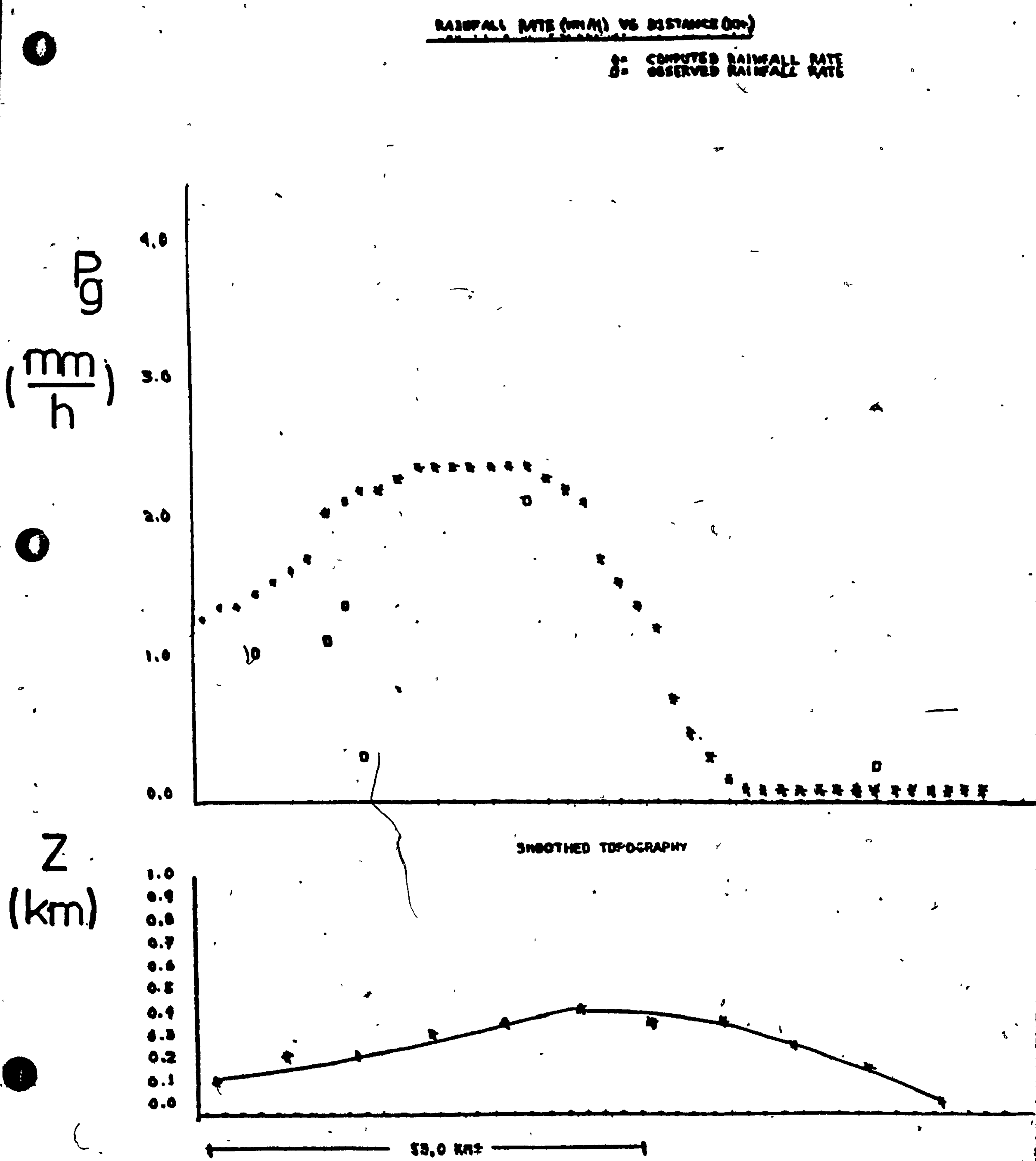

Figure 6.24. Same as figure 6.2 for case III.

provides upper air data in the vicinity and is located downwind of the hills. This is an inconvenient (especially for $T-T_d$ data) since the subsidence due to the hills themselves does modify the airflow and may not represent conditions at the larger scale. For this reason, the relative humidity on the upwind side of the hills are thought to be higher and will be taken as 100 percent for simplicity.

The soundings show that some part of the model domain is below 0°C where the warm rain parametrization is not appropriate. However, since the greatest part of the model domain lies within temperatures above 0°C, effects due to subfreezing precipitation processes were ignored.

The value taken for D_c in the numerical calculations is 3 km. This value is based on the discussion on the choice of a low-cloud thickness given in Bader and Roach (1977).

Synoptic setting for the case studies

case	I	II	III
Date	13/14 feb 1985	3/4 dec 1985	29/30 nov 1985
Period from to	18Z on 13th 18Z on 14th	06Z on 3rd 06Z on 4th	12Z on 29th
Data used from sounding at	12Z on 14th	12Z on 3rd 00Z on 4th	12Z on 29th
700 mb wind* speed (m/s)	18.6	23.0	13.0
l_1 (km^{-1})	0.42	0.436	0.362
l_2 (km^{-1})	0.0	0.0	0.0
H (km)	2.96	3.09	3.015
mean θ_w (°C)	12.5	15.0	14.0
P_0 (mm/h)	1.6	0.9	1.16

Table 6.4 Summary of rainfall cases.

* component perpendicular to the hill,e.g in the direction 203 degrees (line AB in figure 6.15).

Numerical results for the three cases are shown in table 6.5. It includes W max (maximum vertical velocity), ζ max (maximum vertical displacement), efficiency of precipitation (EFP), Q_c max (maximum value of cloud water content), rainfall rate at Santiago de Compostela (no. 428), R_s, and finally the 24 hours average rainfall rate registered at that station (R_o).

Case Date	I 13/14 Feb. 1985	II 3/4 Dec. 1985	III 29/30 Nov. 1985
W max (cm/s)	13	14	10
ζ max (m)	353	331	417
EFP (%)	0.74	0.54	0.75
Qc max (g/m^3)	0.15	0.22	0.15
R (mm/h)	3.0	2.4	2.5
R_o obs. (mm/h)	4.2	3.6	2.1

Table 6.5 Results of the case studies.

For case no.2, the vertical velocity profile and orographic cloud water content is displayed in figure 6.20 and 6.21 respectively while figure 6.22 through 6.24 depict the rainfall distribution along the orography for the three cases. For two out of the three cases, the model underestimates the rainfall rate. A possible explanation is that an airstream moving from the coast line running up the valley would find its windspeed increased by an effect of convergence into the valley across Santiago de

Compostela (funneling effect). The surface windspeed and accordingly the vertical motion and precipitation rate would then be increased. Such boundary layer effect is obviously not taken into account in the present model. There is also the possibility of release of potential instability which is not considered here.

6.3 Application in other countries

The concept of the seeder-feeder mechanism has been extensively used in Britain in explaining radar and raingauge observations in hilly regions. Bader and Roach (1977) and Hill et al. (1981), among others, have presented case studies of warm sector (or pre-frontal) situations somewhat similar to the Spain case study presented above.

A model of the seeder-feeder mechanism of orographic rain would certainly find its usefulness in other parts of the world under other synoptic situations (e.g. other than coastal regions of Western Europe in warm sectors of depressions). In fact, McGinn and Giles (1986) claimed that the apparent orographic enhancement of rainfall during persistent summer convective storms associated with occluding baroclinic disturbances along the Manitoba escarpement (Canada) can be explained by the seeder-feeder mechanism.

The case studies presented in this chapter are useful in that they illustrate the strong control of topography on rainfall. Moreover, through those, the response of the model in actual situations was tested and seems to give a reasonable first order approximation.

In general, discrepancies between observations and calculated orographic rainfall rate could be explained by the following reasons;

1) the model can only utilize a simplified smoothed profile for the terrain which in reality is not so

2) simple assumption made about the temperature and wind profile might not be entirely representative of the atmosphere (e.g. constant Scorer parameter in one given layer, temperature profile fit by θ_w etc.

3) potential instability can increase the mean rate of ascent and hence the rate of condensation and rate of precipitation over the hill

4) we have considered saturated air in both monsoon and Spain case studies while in reality it is not so

5) radiosonde data are not necessarily representative of the large scale and may be affected by the topography in the lower levels.

6) limitations of the raingauges network system.

Note that assumption 4) would contribute to an overestimation of the precipitation rate. In fact, most of the results show that the model precipitation rate is greater than the observed precipitation rate (upwind of the hill only).

CHAPTER 7: SUMMARY AND CONCLUSIONS

A two-dimensional model of the feeder-seeder mechanism of orographic rain has been presented. The basic equations of the model are the continuity equation, for both cloud water and rain water, and the differential equation for the vertical perturbation velocity. The first two equations are solved simultaneously using a "modified" forward scheme for the numerical integration and Kessler's parameterization for the microphysics. Boundary conditions needed for these two equations are set up in line with the seeder-feeder mechanism.

The dynamical part of the model is concerned with the differential equation for the vertical motion and streamline displacements (2-D mountain wave theory). Its solution is based on the hydrodynamical theory of internal, small adiabatic perturbations in a stratified atmosphere without friction. No feedback exists between the dynamical and the microphysical parts, a reasonable approximation for the orographic rain problem.

The numerical model is conceptually simple and inexpensive to run. It describes the orographic enhancement experienced by an airflow moving perpendicularly over a relatively small topographical ridge (width greater than 4 km and less than 50 km and maximum height less than 1 km). Only "warm rain" cases in non-frontal situations are examined (e.g. warm sector or pre-frontal orographic rain and monsoon cases).

The behaviour of the model was been found quite good (see chapter 5) and in agreement with many observational studies (Smith,1979, Hill et al. ,1981 and Bergeron ,1965 among others).

Moreover, comparisons with other models (Carruthers and Choularton, 1983, Bader and Roach, 1977 etc) reveals a similar behaviour and, in some respect, a better simulation of reality. For instance, the increase of the orographic enhancement as a function of windspeed is more sensitive in the model presented than in the two models mentioned above. The reason is probably related to a more appropriate treatment of the airflow, which depends more on the structure of the wind profile than on the temperature profile (as in Carruthers and Choularton's model).

One of the most important aims of this thesis was to determine how the orographic enhancement depends on the pre-existing rainfall rate. Concerning this point, the model behaviour is in line with Browning et al (1975). There is, however, a difference of opinion consisting in whether or not seeding rain needs to be present for orographic enhancement to happen. In fact, the above study leaves the impression that absence of seeding rain leads to no orographic enhancement for hills of all lenghts. But the model has shown that for large hills, when P_o is low, the cloud liquid water content can be high enough so that coalescence in the feeder cloud produces rain and consequently appreciable orographic enhancement (see figure 5.6, curve E and F).

On the other hand, the size of the hills determines whether the orographic rain will occur on the upwind slope, closer to the crest or slightly on the leeside. This fact seems to have been reproduced sucessfully by the present model (see table 5.7).

The dependence of P_o on the efficiency of precipitation (fig. 5.18) and/or on the orographic enhancement (figure 5.6) has led the author to the following classification for three regimes based on the hill half length;

hill half length	sensitivity of P_o on P_m and of P_o on EFP	importance of precipitation -drift.
a < 10 km	strong	strong
10 km < a < 20 km	moderate	weak to moderate
a > 20 km	weak	insignificant

The justification for this classification is that for large hills (a > 20 km), coalescence and autoconversion in the orographic cloud can be important because the mean cloud water content is generally higher than that for small hills. Also,precipitation drift effects can be neglected whereas for small hills (a < 10 km) , most of the hydrometeors exit the orographic cloud near the crest or on the downwind side where evaporation takes place. Moderate hills (a between 10 and 20 km) represent a transition region where the seeder-feeder mechanism and precipitaion drift may be significant. Note that when we varied the hill half length, the aspect ratio of the hill (height/half length) remained constant.

Although the above "classification" is of course not absolute, it is thought to clarify the various physical processes in connection with orographic enhancement. It also should be pointed out that even this classification follows Carruthers and Choularton's results as well as Smith (1979) it is not clearly demonstrated in those references the range in which the seeder-feeder mechanism is a major mechanism.

On the other hand, the importance of the seeder-feeder mechanism may be explicable in terms of the following non-dimensional number; $T_s \bar{U}/a$ (see chapter 2). A value equals to unity for this number represents a critical value over which the seeder-feeder mechanism may no longer be a major mechanism in orographic rain. That is for $a = T_s \bar{U}$ and with typical values for T_s and $\bar{U}$ (e.g T_s = 1200 sec and $\bar{U}$ = 15 m/s) we find a $\sim$ 18 km, in good agreement with the transition region (between 10 and 20 km) derived above from inspection of figure 5.6 and 5.21.

Another major conclusion of this thesis concerns the dynamical part of the model. Results of figure 5.10 and of table 5.2 show that the wind profile plays an important role in determining orographic enhancement; wind profiles having the structure of a low-level jet will theoretically give higher enhancement than with other wind profiles (everything else being the same). This favourable low-level jet structure is characterized by the presence of a strong increase of the windspeed up to low-level jet H, and by a very weak decrease of wind with altitude above this level (case A,B,E in figure 5.9). The prediction of the model is then in agreement with the observation that low-level jets are normally associated with heavy orographic rain.

On the other hand, the potential flow solution leads to a significant underestimation of the precipitation enhancement for wind profiles associated with a typical low-level jet. It is worth noting that Carruthers and Choularton (1983) claimed that a potential flow solution is sufficiently accurate to be used for hills of all lengths, and that the neglect of stratification would lead only to a slight overestimate in the enhancement over long hills. But the curvature effect of the wind profile was not taken into account in the Carruthers and Choularton's model. The latter effect has been demonstrated here to be quite important.

Other conclusions drawn from the model results are listed below:

1) sensitivity tests show that relative humidity is the most sensitive parameter in orographic enhancement followed by windspeed and wet bulb potential temperature. The background rainfall rate was found much less sensitive especially in the case of larger hills with P_o over 2.0 mm/h,

2) the efficiency of precipitation decreases as the windspeed is increased,

3) wind drift effects should not be neglected in a model of orographic rain (especially for small hills having their half length $a < D_c \bar{U}/\bar{V}$)

4) neglecting the effect of compressibility in the condensation rate expression leads to a significant underestimation of the computed orographic enhancement.

5) as the hill dimensions (both half length and height) are increased the location of maximum rainfall rate is moved upwind. The increase of the background rainfall rate also moves this location to the upwind side (see table 5.7).

The relevance of the model was also tested through case studies and found satisfactory. Hence, the formulation of the orographic problem by the seeder-feeder mechanism seems to be adequate, easy to understand and can be utilized in different regions of the world. Moreover, the above mechanism can be extended to the modelization of the orographic enhancement of snowfall (see Choularton and Perry, 1986).

Application to forecasting and climatology

Results of this thesis can help to explain the climatological seasonal peak of orographic rainfall enhancement in Western Europe. Nash and Browning (1977) and Bleasdale and Chan (1972) have both observed that orographic rainfall enhancement for the British Isles as a whole is intensified in the months November- February at the time of highest frequency of windspeed and LLJ when θ_w is relatively low (although still high for the time of the year). These situations are associated with saturated airmasses accompanying marine low pressure systems. Similar observations have been noted in Northwestern Spain in the winter months (Rivera,1986).

Tests performed on the present model are in line with these climatological observations; that is, the model predicts high orographic enhancement in cases of high windspeeds and high relative humidities even if θ_w is relatively low. This is due to its greater sensitivity with the first two parameters. Similarly, the extreme sensitivity of relative humidity of the upwind flow on the orographic enhancement (see fig. 5.4) may explain the relative larger importance of orographic enhancement in Western Europe as compared to Northeastern America. In fact, warm sectors of low pressure systems coming from the west are significantly drier (r.h. 80 per cent) when they cross hills or mountains of NE America whereas warm sectors of depressions over hills of Western Europe are wet (r.h. over 90 per cent) being associated with maritime airmasses.

On the other hand, it is thought that the results of the model and the background litterature accompanying this thesis, can give to the operational forecaster a better feeling for the relative importance of meteorological parameters in orographic enhancement.

The seeder-feeder mechanism seems a quite useful conceptual model which can be numerically implemented in an easy way despite some restrictions such as an obvious difficulty of defining a constant and unique value for the background rainfall rate. This is especially true in cases of passage of mesoscale rain areas due to the temporal and spatial variability of the showers associated.

Finally, another shortcoming of the theory is that the actual orographically induced condensation rate might extend higher than what is computed by the model (see figure 5.15). Such an " extra" condensation rate coming from higher levels would certainly increase the ground rainfall rate especially when there is release of potential instability.

APPENDIX A: LIST OF MAIN SYMBOLS

in the text	in the Fortran program	represents
a	XHALFa or A	hill mean width (bell-shaped ridge)
a'	APRIME	topography parameter
AUTOC	AC	autoconversion rate
-	AVGRH	average relative humidity
b	HTOP or B	hill height (bell-shaped ridge)
c	-	speed of sound
C_t	CT	rate of condensation per unit width perpendicular to the airflow in the orographic cloud.
COND	COND	condensation rate
C_p	CP	specific heat capacity of dry air
C_b	HUBCAG	height of upper boundary of the orographic cloud above the ground (at the left edge of the domain).
e_s	SATW	saturated vapor pressure with respect to water
EFP	EFP	efficiency of precipitation of an orographic cloud
EVAPC	EVPC	evaporation rate of cloud
EVAPR	EVPR	evaporation rate of rain
f	-	Coriolis force
g	G	acceleration of gravity
H	H	height of the upper layer in the dynamical part of the present model
	HLCL	height of the condensation level
h_o	HZERO	reference level in topography profile
k		wavelength of sinusoidal ground profile
k_1	K1	autoconversion paramater
k_2	K2	autoconversion threshold
l	L	vertical wavenumber or Scorer parameter
l_1	L1	vertical wavenumber in layers
l_2	L2	1,2 and 3(Scorer parameters).
l_3	L3	
L_v	LEV	latent heat of vaporization
m	CLWC	cloud liquid water content
M	RAINM	rain water content
	MTOP	model top; height of the 1st point of the domain of integration
P_g	RFRG	precipitation rate on the ground
P_o	BRAFR	background rainfall rate
p	P	pressure
p_s	PSLVL	sea-level pressure
P_m	-	maximum rate of precipitation
P_t	PT	total orographic component of rainfall rate per unit width
Q_c	QC	cloud water mixing ratio
Q_r	QR	rain water mixing ratio

Q_v	QV	water vapor mixing ratio
Q_{vs}	QVS	saturated water vapor mixing ratio
	QVSF	saturated water vapor mixing ratio modified after lee subsidence
r_s	RS	same as Q_{vs}
R	RAINFR	rainfall rate
R_d	R	gaz constant
R_v	RV	gaz constant
S	S	source or sink in the conservation equation
T	TO	temperature
T_d	TDO	dew point temperature
	TLCL	temperature at the lifting conden - sation level
$T-T_d$	DPD	dew point depression
U	U	windspeed
U_o	UO,UAVG	surface windspeed
U_m	UMAX	maximum windspeed
	URFRG	unfiltered ground rainfall rate
$\bar{V}$	VTBAR	raindrop mean terminal fallspeed
w	W	vertical motion
WASHOUT	WSHOUT	washout rate
x	X	horizontal coordinate
Z	Z	altitude
Z_g	ELEV	ground elevation
z_o	ZO	height of the middle layer in the dynamical part of the model
α	AA	constant of parametrization (rain - fall rate)
n	BB	constant of parametrization (rain - fall rate)
β		coefficient of static stability
Δx	DELTAX	numerical horizontal step
Δz	DELTAZ	numerical vertical step
ΔP		rain enhancement $(P_s - P_o)$
ΔP_m		maximum rain enhancement
ϵ		ratio of R_d/R_v
Γ	GAMAD	dry adiabatic lapse rate
Γ_s	GAMAS	moist adiabatic lapse rate
ζ	XKSI	vertical displacement
ρ_o	RO	air density
ρ_R		rainwater density
ψ		stream function
θ_w	THETAW	wet-bulb potential temperature
∇h	GRADX	gradient of the topography
ω		vertical motion in pressure units

APPENDIX B: SOLUTION OF THE WAVE EQUATION FOR A VARIABLE 1

Solution of vertical motion and streamline displacement for an asymetrical ridge and for a vertical variation of $l(z)$ is given in this appendix. The equation we are looking a solution from is

$$\frac{\partial^2 W}{\partial z^2} + \left(f(z) - k^2 \right) W = 0 \qquad \text{B1}$$

If the troposphere is divided into 3 layers where $f(z)$ is constant in each layer, that is

$$\begin{aligned} f(z) &= (l_1)^2 \quad \text{when } z \le z_0 \\ &= (l_2)^2 \quad \text{when } z_0 \le z \le H \\ &= (l_3)^2 \quad \text{when } z \ge H \end{aligned} \qquad \text{B2}$$

The solution in each layer denoted by subscript 1,2,3 are respectively (Sarker,1966);

$$\zeta_{1,2,3}(x,z) = \text{Real} < \left(\frac{\rho_0}{\rho_z}\right)^{1/2} \frac{U_0}{U_z} \frac{\Delta_{1,2,3}}{\Delta} \left[ab \frac{a+ix}{a^2+x^2} + a' \left(\tan^{-1}\frac{x}{a} + \frac{i}{2} \ln \frac{a^2+x^2}{a^2}\right)\right] > \qquad \text{B3}$$

$$w_{1,2,3}(x,z) = \text{Real} < \left(\frac{\rho_0}{\rho_z}\right)^{1/2} U(-h_0) \frac{\Delta_{1,2,3}}{\Delta} \frac{\partial}{\partial x} \left[ab \frac{a+ix}{a^2+x^2} + a' \left(\tan^{-1}\frac{x}{a} + \frac{i}{2} \ln \frac{a^2+x^2}{a^2}\right)\right] > \qquad \text{B4}$$

where the subscript $-h_0$ denotes the ground level and Δ given by;

$$\Delta = \cos l_1(h+z_0)\left[\cosh l_2(z_0 -H) + i\frac{l_3}{l_2}\sinh l_2(z_0 -H)\right]$$

$$-\frac{l_2}{l_1}\sin l_1(h+z_0)\left[\sinh l_2(z_0 - H) + i\frac{l_3}{l_2}\cosh l_2(z_0 -H)\right] \quad \text{B5.1}$$

$$\Delta_1(z,0) = \cos l_1(z-z_0)\left[\cosh l_2(z_0 -H) + i\frac{l_3}{l_2}\sinh l_2(z_0 -H)\right]$$

$$+\frac{l_2}{l_1}\sin l_1(z-z_0)\left[\sinh l_2(z_0 -H) + i\frac{l_3}{l_2}\cosh l_2(z_0 -H)\right] \quad \text{B5.2}$$

$$\Delta_2(z,0) = \cosh l_2(z-H) + i\frac{l_3}{l_2}\sinh l_2(z-H) \quad \text{B5.3}$$

$$\Delta_3(z,0) = \cos l_3(z-H) + i\sin l_3(z-H) \quad \text{B5.4}$$

In case of no middle layer where f(z) is negative (e.g l^2 is positive everywhere), Sarker's solution can be reduced to a two layer problem by setting $z_0 = H$ and $l_3=l_2$ in B5.1 through B5.4;

$$\Delta = \cos l_1(h+H) - i\frac{l_2}{l_1}\sin l_1(h+H) \quad \text{B6.1}$$

$$\Delta_1 = \cos l_1(z-H) + i\frac{l_2}{l_1}\sin l_1(z-H) \quad \text{B6.2}$$

$$\Delta_2 = \cos l_2(z-H) + i\sin l_2(z-H) \quad \text{B6.3}$$

where subscript 1 corresponds to the lower layer, subscript 2 to the upper layer and H represents the height of the first layer.

Finally, the result of equation (4.13) can be recovered from Sarker's solution by the following procedure. First, set

$$l=l_1=l_2=l_3 \quad \text{B7}$$

and $z_0 = H = 0$

in equation B5. This is then equivalent to a one layer model where l is constant. Also, set $a' = 0$ and $h = 0$ (to recover the bell-shaped profile) in equation B3. Equation B3 using B7 in B5 gives

$$\zeta(x,z) = \text{Real}\left[\left(\frac{\rho_0}{\rho_1}\right)^{1/2} \frac{U_0}{U_1} ab \left\{\frac{a+ix}{a^2+x^2}(\cos lz + i\sin lz)\right\}\right]$$

which is identical to 4.13 (after taking the real part). If l^2 is negative, a similar procedure could be done to recover equation 4.17 from Sarker's solution.

APPENDIX C

A SIMPLE FORMULA TO CALCULATE SURFACE RAINFALL RATE

Equation 2.1 can be written as

$$\mathrm{COND} = -\frac{d}{dt}(\rho_0 r_s) = -w\frac{d}{dz}(\rho_0 r_s)\bigg|_{ad} \qquad \mathrm{C1}$$

If precipitation-size particles can form immediately, from the cloud droplets, and if these hydrometeors fall vertically, then a simple approximation for the rate of precipitation at the ground is

$$R\left(\frac{kg}{m^2/s}\right) = \int_0^\infty \mathrm{COND}\ dz$$

$$= -\int_0^\infty \frac{d}{dz}(\rho_0 r_s)\bigg|_{ad} w\ dz \qquad \mathrm{C2}$$

If we assume that the environmental temperature T(z) lies along a moist adiabat, so that

$$\frac{d}{dz}(\rho_0 r_s)\bigg|_{ad} = \frac{d(\rho_0 r_s)}{dz} \qquad \mathrm{C3}$$

integrating, then gives (assuming a mean value for w);

$$R = -w\,\rho_0 r_s\bigg|_0^\infty$$

where w is the mean vertical velocity. As ρ_o and r_s tend to zero as z tends to infinity, the result expressed in mm/hr becomes

$$R_g(mm/hr) = \rho_o(0)r_s(0)\ w\ X\ 3600 \qquad C4$$

where $\rho_o(0)$ is the air density at the ground level (in kg/m^3) and $r_s(0)$ the saturated water vapor mixing ratio at the ground (g/g).

Moreover, an order of magnitude for w is $w = U \cdot \nabla h$ where ∇h is the gradient of topography and U the mean lower troposphere wind speed perpendicular to the ridge: the formula hence becomes

$$R_g(mm/hr) = U \cdot \nabla h\ \rho_o(0)r_s(0)\ X\ 3600 \qquad C5$$

Formula C.5 or C.4 are the most simple relationship for computing rainfall rate and is thought to give a first-order estimate of rainfall rate useful in operational forecasting.

APPENDIX D: SMOOTHING OPERATOR

The numerical solution contains short scale oscillations and it is desirable to smooth them. A very simple method of filtering is the " 3 point operator "; that is we define a new function $\overline{Z}_i$ which we want to be the smoothed version of Z_i . This new function will be a linear combination of Z_{i+1}, Z_i and Z_{i-1} , the subscripts i, $i-1, i+1$ refer to the function Z_i evaluated at horizontal points

$$x = i\Delta x$$
$$x_{i-1} = (i-1)\Delta x$$
$$x_{i+1} = (i+1)\Delta x$$

and/or vertical points

$$z = i\Delta z$$
$$z_{i-1} = (i-1)\Delta z$$
$$z_{i+1} = (i+1)\Delta z$$

The new function can be written as

$$\overline{Z}_i = Z_i + \nu(Z_{i-1} - 2Z_i - Z_{i+1}) \qquad \text{D1}$$

In the Fortran program, this operator was used to filter out short scales oscillations in the computed surface rainfall rate (in the horizontal) and the distribution of the cloud mixing ratio (in the vertical). The value of ν=0.5 was selected for the filter.

REFERENCES

Atlas climatico de España, Instituto Nacional de Meteorología de España, Madrid 1983.

Bader M.J. and Roach W.T.(1977). Orographic rainfall in warm sectors of depressions. Quart. J.R.Met.Soc 103,pp 269-280.

Bell R.S. (1978). The forecasting of orographically enhanced rain - fall accumulations using 10-level model data. Met. Magazine, 107 pp 113-124.

Bergeron T. (1949). The problem of artificial control of rainfall on the globe. II. The coastal orographic maxima of precipitation in autumn and winter. Tellus 1, #3 pp 15-31.

Bergeron T. (1960). Operation and results of ' Project Pluvius'.Physics of precipitation.

Bergeron T. (1965). On the low-level redistribution of atmospheric water caused by orography. Supp.Proc.Int.Conf.Cloud Physics.Tokyo ,May 1965, pp 96-100.

Best A.C.(1950). Empirical formulae for the terminal velocity of water drops falling through the atmosphere. Quart.J.R.Met.Soc. 76 , pp 302-311

Browning K.A. and Harrold, T.W. (1969). Air motion and precipitation growth in a wave depression. Quart.J.R.Met.Soc. 95, pp 288-309.

Browning K.A., Pardoe C.W. and Hill F.F (1975).The nature of orographic rain at wintertime cold fronts. Quart.J.R.Met.Soc.101.pp 333 -352.

Browning K.A.(1980) Structure, mechanism and prediction of orographically enhanced rain in Britain. In Orographic effects in Planetary flows. Garp Publications Series # 23 (ed. Hide and White).

Carruthers D.J. and Choularton T.W. (1982). Airflow over hills of moderate slope. Quart.J.R.Met.Soc. 108, pp 603-624.

Carruthers D.J. and Choularton T.W. (1983). A model of the seeder - feeder mechanism of orographic rain including stratification and wind-drift effects. Quart.J.R.Met.Soc. 109,pp 575,588.

Choularton T.W. and Perry S.J.(1986). A model of the orographic en - hancement of snowfall by the seeder-feeder mechanism. Quart.J.R. Met.Soc. 112 pp 335-345.

Chuan G.K. and Lockwood J.G. (1974). An assessment of topographic controls on the distribution of rainfall in the Central Pennies. Met. Magazine 103. pp 275-287.

Collier C.G. (1975). A representation of the effects of topography on surface rainfall within moving baroclinic disturbances.Quart. J.R.Met.Soc. 101, pp 407-422.

Colton D.E.(1976). Numerical simulation of the orographically induced precipitation for use in hydrological analysis. J.of Applied Meteorology 15, pp 1241-1251.

Douglas C.K. and Glasspoole J.(1947). Meteorological conditions in orographic rainfall in the British Isles. Quart.J.R.Met.Soc. 73 pp 11-38.

Elliot R.D and Hovind E.L. (1964). The water balance of orographic clouds.Journal of Applied Meteorology. 3 pp 235-239.

Gill A.E.(1982) Atmospheric-Ocean Dynamics. Academic Press.vol. 30.

Gocho Y.(1978). Numerical experiment of orographic heavy rainfall due to a stratiform cloud. J.of Met.Soc.of Japan 56,pp 405,422.

Hill F.F. and Browning K.A.(1980). Radar and raingauge observations of orographic rainfall over South Wales.Met.Office Radar Research Laboratory. Research report # 20. Malvern,England.

Hill F.F.,Browning K.A. and Bader M.J. (1981). Radar and raingauge observations of orographic rain over South Wales. Quart.J.R.Met. Soc. 107, pp 643-670.

Hobbs P.V., Honze R.Jr. and Matejka T.(1975). The dynamical and microphysical structure of an occluded frontal system and its momodification by orography. Journal of Atmospheric Science. 32 pp 1542-1562.

Holgate H.T.D. (1973). Rainfall forecasting for river authorities. Met. Magazine 102, pp 33-48.

Iribarne J.V. and Godson W.L.(1973). Atmospheric Thermodynamics. D.Reidel Publishing Company.

Kelkar V.N (1959). Size distribution of raindrops, part 1, Indian J. of Met. and Geophysics, vol.10. no.2.

Kessler E.(1969). On the distribution and continuity of water substance in atmospheric circulations. Vol 10 no. 32. Met.Monographs.

Ludlam F.H.(1956) The structure of rainclouds. Weather 11 pp 187-196

McGinn R.A. and A.C.Giles (1986). Low-relief topography and apparent orographic enhancement of storm rainfall totals along the Manitoba escarpement. 20th Annual Congress of Canadian Met. and Oceanography Soc. Regina, Canada.

Myers V.A.(1962). Airflow on the windward side of a ridge.J.Geophys. Res. 67 pp 4267-4291.

Nash J. and Browning K.A.(1977). Structure of the lower atmosphere associated with heavy falls of orographic rain in South Wales. Unpublished Meteorological Office Radar Research Laboratory report # 7. Dec 1977.

Pedgeley D.E. (1970). Heavy rainfalls over Snowdonia. Weather 25 pp 340-350.

Pruppacher H.R. and Klett J.D.(1980). Microphysics of clouds and precipitation. D.Reidel Publishing Company.

Queney P. (1948). The problem of air-flow over mountains. A summary of theoritical studies. Bull of American Met.Soc. pp 16-25.

Rivera A. (1986) Director of the forecasting centre. Madrid.Spain. Private communication.

Ryden B.E. (1972). On the problem of vertical distribution of precipitation especially in areas with great height differences.In " Distribution of precipitation in mountainous areas '. pp 362-369. Vol II WMO report # 326.

Sarker R.P.(1966) A dynamical model of orographic rainfall. Monthly Weather Review. 94 pp 555-572.

Sawyer J.S.(1956). The physical and dynamical problems of orographic rain. Weather, 11, pp 375,381.

Scorer R.S.(1949).Theory of waves in the lee of mountains. Quart.J.R Met.Soc. 75 pp 41-56.

Smith R.B.(1979). The influence of mountains on the atmosphere. Advances in Geophysics 21 pp 87-230 Academic Press, New-York.

Spinnangr F. and Johansen H.(1955). On the influence of the orography in southern Norway. Meteorol. Ann. 4 , pp 17-35.

Storebo P.B. (1976).Small scale topographical influences on precipitation. Tellus, 28, pp 45-59.

Storr D. and Ferguson H.L.(1972). The distribution of precipitation in some mountainous Canadian watersheds.In " Distribution of precipitation in mountainous areas " vol II WMO 3 326.

Wexler R. and Atlas D. (1958). Moisture and supply and growth of stratiform precipitation. J. of Met. Vol pp 531-538.

Williams P. and Peck E.L.(1962). Terrain influences on precipitation in the intermountain west as related to synoptic situations. Journal of Appl. Met. 1 pp 343-347.

Young K.C.(1974). A numerical simulation of wintertime orographic precipitation. Part I. Description of model microphysics and numerical technique. J. of Atmospheric Science 31. pp 1735-1748.

Woodcock A.H. (1975). Anomalous orographic rain in Hawaii. Monthly Weather Review 103, pp 334-343.